الجمهورية الجزائرية الديموقراطية الشعبية
*People's Democratic Republic of Algeria*
وزارة التعليم العالي والبحث العلمي
*Ministry of Higher Education and Scientific Research*
جامعة الشهيد حمه لخضر – الوادي
*University of Echahid Hamma Lakhdar – Eloued*
كلية العلوم الطبيعية والحياة
*Faculty of Nature and Life Sciences*
قسم البيولوجيا الخلوية والجزيئية
*Department of Cellular and Molecular Biology*

# MASTER THESIS

**In partial fulfilment of the requirements for the degree of Master**

**Major:** Biological Sciences

**Speciality:** Applied Biochemistry

## THEME

Structure–Activity Relationships of Ferrocenyl Acetylaniline Derivatives as Dual Inhibitors of Carbohydrate-Hydrolysing Enzymes and Inflammatory Processes: Combined Experimental and Computational Insights

**Presented by:**

**AMIRAT Asma**

**MEBAREK Hadil**

**MECHERI Kheira Yousra**

**Jury Members:**

| | | |
|---|---|---|
| Chairman | **SAADI Hamza** | **El-Oued University** |
| Supervisor | **LANEZ Elhafnaoui (M.C.A.)** | **El-Oued University** |
| Co-Supervisor | **BENAMOR Mohammed Larbi** | **El-Oued University** |
| Examiner | **CHELLALBA Imane** | **El-Oued University** |

**Academic Year: 2025 – 2026**


بسم الله الرحمن الرحيم

# الإهداء

**الحمد لله أولًا، الذي أنار دربي ووفقني ومنحني القوة والصبر لإتمام هذا العمل والوصول إلى هذه اللحظة التي أحمده عليها بكل امتنان، لولا فضل الله وتوفيقه لما وصلت إلى هذه المرحلة ولا تحقق هذا الإنجاز.**

أهدي ثمرة جهدي وتخرجي إلى :أمي الحبيبة، أعظم نعمة في حياتي، وصاحبة الفضل الأكبر بعد الله في كل خطوة وصلت إليها .إلى من كانت دعواتها سندي، وصبرها قوتي، وحنانها ملجئي في كل الأوقات .شكرًا لكل تضحية قدمتها من أجلي، ولكل مرة منحتِني فيها الأمل والقوة والدعم .مهما كتبت فلن أوفيك حقك، فهذا النجاح يحمل اسمك بقدر ما يحمل اسمي.

إلى والدي، وإلى من كان لي أبًا، شكرًا لكل ما قدمتموه لي، سواء بدعوة صادقة، أو موقفٍ طيب، أو نصيحة وإرشاد كان لها أثر جميل في مسيرتي .أسأل الله أن يديمكم نعمةً وسندًا.

إخوتي رمزي وإسلام، لأن وجود الإخوة يبقى دائمًا مصدر أمان وقوة، شكرًا لكم على دعمكم الصادق وعلى كل لحظة جميلة خففتم بها عني صعوبة الطريق.

لكل من دعمني وكان جزءًا من هذه الرحلة، سواء بكلمة طيبة، أو دعاء صادق، أو دعم صامت لا يُنسى .فهناك أشخاص يتركون أثرًا جميلًا دون أن يطلبوا شيئًا بالمقابل.

وإلى نفسي التي استودعني الله إياها، تلك الروح التي أكرمني الله بحملها، فكان عليّ أن أصونها بالأمل، وأقودها بالصبر، وأسعى بها في طريق العلم والمعرفة بكل ما أملك من إيمان وطموح، وأمنحها حقها من الفخر بعد هذا الطريق الطويل.

فالحمد لله الذي أعانها حتى وصلت.

وهكذا تنتهي الكلمات ...ويبقى أثر أصحابها خالدًا في القلب.

**يسرى**

# الإهداء

**أولًا، الحمد لله رب العالمين، الذي وفقني وأعانني ومنحني القوة والصبر، وفتح لي أبواب التيسير حتى أصل إلى هذه اللحظة التي طالما حلمت بها .الحمد لله على فضله الذي لا يُحصى، وعلى نعمه الظاهرة والباطنة، وعلى توفيقه الذي رافقني في كل خطوة من هذا الطريق.**

بكل امتنانٍ وفخر، أهدي هذا العمل إلى:

**أمي** الحبيبة، نبض حياتي، والسبب الخفي وراء كل نجاح أصل إليه .إلى المرأة التي مهدت لي الطريق بدعواتها، وساندتني بصبرها اللامحدود، وألهمتني دائمًا لأطمح إلى الأفضل .كل إنجاز أحققه ما هو إلا انعكاس لحنانك وعظيم عطائك.

**أبي**، إلى من كان لي سندًا وعونًا في مسيرتي، شكرًا لكل ما قدمته من دعمٍ ونصيحةٍ وكلمةٍ طيبة كان لها أثر جميل في حياتي.

**إخوتي وأخواتي** الأعزاء :**عبد الجليل، مريم، زهية، طه نور الإسلام**، سندي الدائم ورفقاء العمر وأجمل ما أهدتني الحياة .شكرًا لوجودكم، ولمحبتكم، ولدعمكم الذي ملأ رحلتي دفئًا وطمأنينة.

وفي الختام، أسأل الله أن يجعل هذا العمل خالصًا لوجهه الكريم، وأن ينفعني به في الدنيا والآخرة، وأن يجعله بدايةً لما هو أعظم وأجمل، وأن يبارك في كل من كان جزءًا من هذه الرحلة.

**أسماء**

# الإهداء

**الحمد لله أولًا وأخيرًا، الحمد لله الذي بنعمته تتم الصالحات، والذي وفقني وأعانني ومنحني القوة والصبر، ويسّر لي الطريق رغم ما فيه من صعوبات، وفتح لي أبواب العلم حتى أتم هذا العمل وأصل إلى هذه اللحظة التي أحمده عليها بكل امتنان وشكر .الحمد لله عدد ما كان، وعدد ما يكون، وعدد الحركات والسكون، على فضله العظيم وتوفيقه الذي لا يُعد ولا يُحصى.**

بكل فرحٍ عميق واحترامٍ كبير، أهدي هذا العمل إلى:

**ابي** العزيز سندي في هذه الحياة، الى **أمي** الحبيبة، مرتكز روحي ومصدر أملي الدائم .من مهدت بصمتها الطريق أمامي، وكانت تضحياتها الخفية نورًا رافقني في كل خطوة، وإيمانها بي لم يتزعزع رغم كل التحديات .حبكِ غير المشروط هو أساس كل ما أنا عليه اليوم، وهذا الإنجاز هو أقل تعبير عن امتنان قلبي لكِ.

**إخوتي** الأعزاء، **يوسف وتوفيق**، درعي وفخري وسندي الأقرب .شكرًا لوقوفكم الدائم بجانبي، ولدعمكم وتشجيعكم الذي جعل هذه الرحلة أسهل وأجمل بوجودكم.

**أختي** الصغيرة الحبيبة، أجمل ما في البيت وبهجة أيامه، ضحكتكِ وبراءتكِ كانتا مصدر دفءٍ لي في أكثر لحظات الدراسة تعبًا، وأنتِ دائمًا فرحتي الصغيرة الثابتة.

لكل من كان له أثر في هذه الرحلة، خاصة صديقتي واختي **وصال**

شكرًا لكل من قدّم لي كلمة طيبة، أو دعاءً صادقًا، أو دعمًا صامتًا لا يُنسى .فبعض الأثر لا يُرى لكنه يبقى في القلب طويلًا، ولا يُنسى مهما مرّ الزمن.

**هديل**

## *Acknowledgements*

**We would like to express our sincere gratitude to Professor** Elhafnaoui Lanez**, supervisor of this dissertation, for his invaluable guidance, encouragement, and continuous support throughout this work.**

We also extend our appreciation to all the professors and teachers of the Department of **Cellular and Molecular Biology** at University of El Oued, especially Professor **Aicha Adaika** and Professor **Marwa Jarallah**, for their support and scientific guidance. Special thanks are also addressed to Professor **Zaater Abdelmalek**, Dean of the Faculty, and Professor **Omar Farhati**, Director of the University, for their efforts and encouragement.

Our thanks also go to the **VTRS Laboratory** and the **CRAPC Center** for providing the facilities and research environment necessary for this study.

Finally, we express our deepest gratitude to our families, colleagues, and friends for their unconditional support, encouragement, and motivation throughout this journey.

## ABSTRACT

This thesis reports the design, synthesis, physicochemical characterization, and biological evaluation of three **ferrocenyl acetylaniline derivatives**, namely FcMe2Ac, FcMe3Ac, and FcMe4Ac, with the aim of exploring their potential as dual **antidiabetic** and anti-inflammatory agents. The compounds were synthesized through a nucleophilic substitution approach, affording moderate to high yields **(48–80%)**. Their structures were confirmed by FT-IR, UV–Visible, and one- and two-dimensional NMR spectroscopy, which verified the successful incorporation of both **ferrocenyl** and **acetylaniline** moieties. Electrochemical studies using **cyclic voltammetry** revealed quasi-reversible Fe**(II)**/Fe**(III) redox** behavior for all **derivatives**, highlighting the influence of substitution patterns on electron-transfer properties. Biological assays demonstrated significant inhibition of the **carbohydrate**-hydrolyzing enzymes α-**amylase** and α-glucosidase, with $IC_{50}$ values ranging from 8.06 to 10.39 $\mu g \cdot mL^{-1}$. Among the tested compounds, FcMe4Ac exhibited the strongest **antidiabetic** activity, outperforming the reference drug acarbose. The **derivatives** also displayed notable anti-**inflammatory activity** through inhibition of bovine serum albumin denaturation, with $IC_{50}$ values between 4.22 and 7.29 $\mu g \cdot mL^{-1}$, where FcMe4Ac again showed superior efficacy compared with diclofenac. Density functional theory **(DFT)** calculations provided insight into the electronic properties of the molecules, indicating moderate stability and favorable reactivity. Molecular **docking** studies revealed strong binding affinities toward α-**amylase** and α-glucosidase, supported by hydrophobic interactions, hydrogen bonding, and π–π contacts within the active sites. Molecular dynamics simulations confirmed the stability of the **ligand**–enzyme **complexes** over time. Furthermore, **ADMET** predictions suggested favorable pharmacokinetic and safety profiles, including high gastrointestinal absorption, balanced lipophilicity, and low predicted toxicity. Overall, the results identify FcMe4Ac as a promising lead compound for the development of multifunctional agents targeting diabetes and inflammation.



**Keywords:** Ferrocenyl **acetylaniline derivatives**; Antidiabetic activity; Anti-**inflammatory activity**; α-Amylase inhibition; Molecular **docking**; **ADMET** prediction.

**RÉSUMÉ**

Cette thèse présente la conception, la synthèse, la caractérisation physicochimique et l'évaluation biologique de trois dérivés **ferrocenyl**-acétylaniline, à savoir FcMe2Ac, FcMe3Ac et FcMe4Ac, dans le but d'explorer leur potentiel en tant qu'agents à double activité antidiabétique et anti-inflammatoire. Les composés ont été synthétisés par une stratégie de substitution nucléophile, permettant d'obtenir des rendements modérés à élevés **(48–80 %)**. Leurs structures ont été confirmées par les techniques spectroscopiques FT-IR, UV–Visible et RMN mono- et bidimensionnelle, démontrant l'incorporation réussie des fragments **ferrocenyl**e et acétylaniline. Les études électrochimiques réalisées par voltammétrie cyclique ont révélé un comportement rédox quasi réversible Fe**(II)**/Fe**(III)** pour l'ensemble des dérivés, mettant en évidence l'influence du mode de substitution sur les propriétés de transfert électronique. Les essais biologiques ont montré une inhibition significative des enzymes α-**amylase** et α-glucosidase, avec des valeurs d'$IC_{50}$ comprises entre 8,06 et 10,39 $\mu g \cdot mL^{-1}$. Parmi les composés étudiés, FcMe4Ac a présenté l'activité antidiabétique la plus élevée, surpassant l'acarbose utilisé comme référence. Les dérivés ont également manifesté une activité anti-inflammatoire notable par inhibition de la dénaturation de l'albumine sérique bovine, avec des valeurs d'$IC_{50}$ comprises entre 4,22 et 7,29 $\mu g \cdot mL^{-1}$, FcMe4Ac montrant une efficacité supérieure à celle du diclofénac. Les calculs basés sur la théorie de la fonctionnelle de la densité **(DFT)** ont permis de mieux comprendre les propriétés électroniques des molécules, indiquant une stabilité modérée et une réactivité favorable. Les études de **docking** moléculaire ont révélé de fortes affinités de liaison envers l'α-**amylase** et l'α-glucosidase, soutenues par des interactions hydrophobes, des liaisons hydrogène et des contacts π–π au sein des sites actifs. Les simulations de dynamique moléculaire ont confirmé la stabilité des **complexes ligand**–enzyme au cours du temps. De plus, les prédictions **ADMET** ont mis en évidence des profils pharmacocinétiques et toxicologiques favorables, caractérisés par une absorption gastro-intestinale élevée, une lipophilie équilibrée et une faible toxicité prédite. Dans l'ensemble, les résultats désignent FcMe4Ac comme un composé chef de file prometteur pour le développement de nouveaux agents multifonctionnels destinés à la prise en charge du diabète et de l'inflammation.

**Mots-clés :** Dérivés **ferrocenyl**-acétylaniline ; Activité antidiabétique ; Activité anti-inflammatoire ; Inhibition de l'α-**amylase** ; Docking moléculaire ; Prédiction **ADMET**.

**الملخص**

تتناول هذه الأطروحة تصميم وتخليق وتوصيف الخصائص الفيزيائية والكيميائية، إضافة إلى التقييم البيولوجي لثلاثة مشتقات من الفيروسينيل أسيتيل أنيلين، وهي FcMe2Ac و FcMe3Ac و FcMe4Ac، بهدف استكشاف إمكاناتها كعوامل علاجية مزدوجة مضادة للسكري ومضادة للالتهاب. تم تحضير هذه المركبات باستعمال استراتيجية الاستبدال النيوكليوفيلي، محققة مردودات تراوحت بين 48 و80%، وتم تأكيد تراكيبها الكيميائية باستخدام تقنيات FT-IR و UV–Visible والرنين المغناطيسي النووي أحادي وثنائي الأبعاد، مما أثبت نجاح دمج وحدتي الفيروسينيل والأسيتيل أنيلين ضمن بنيتها الجزيئية. أظهرت الدراسات الكهروكيميائية بواسطة الفولتمترية الدورية سلوكاً أكسدة-اختزالياً شبه عكوس لزوج الحديد **(III**Fe/Fe**(II)**)، مما أبرز تأثير نمط الاستبدال على خصائص انتقال الإلكترونات. كما بينت الاختبارات البيولوجية فعالية ملحوظة في تثبيط إنزيمي **amylase**-α وglucosidase-α، حيث تراوحت قيم $IC_{50}$ بين 8.06 و10.39 ميكروغرام/مل، مع تسجيل المركب FcMe4Ac أعلى نشاط مضاد للسكري متفوقاً على الأكاربوز. كذلك أظهرت المركبات نشاطاً مضاداً للالتهاب من خلال تثبيط تمسخ ألبومين مصل الأبقار بقيم $IC_{50}$ تراوحت بين 4.22 و7.29 ميكروغرام/مل، مع تفوق FcMe4Ac على الديكلوفيناك. وقد وفرت حسابات **DFT** فهماً أعمق للخصائص الإلكترونية للمركبات، بينما كشفت دراسات الالتحام الجزيئي عن ألفة ارتباط قوية تجاه الإنزيمين المستهدفين، وأكدت محاكاة الديناميكا الجزيئية استقرار معقدات الليغاند–الإنزيم. كما أظهرت تنبؤات **ADMET** خصائص دوائية واعدة شملت امتصاصاً معوياً مرتفعاً وليبوفيلية متوازنة وانخفاض السمية المتوقعة. وبصورة عامة، تشير النتائج إلى أن المركب FcMe4Ac يمثل مرشحاً واعداً لتطوير عوامل علاجية متعددة الوظائف تستهدف داء السكري والالتهابات.

**الكلمات المفتاحية:** مشتقات الفيروسينيل أسيتيل أنيلين؛ النشاط المضاد للسكري؛ النشاط المضاد للالتهاب؛ تثبيط إنزيم-α أميلاز؛ الالتحام الجزيئي؛ تنبؤات.**ADMET**

# Content

# Content

## List of figures

**List of tables**

## List of abbreviations

DFT: Density Functional Theory

FT-IR: Fourier Transform Infrared Spectroscopy

NMR: Nuclear Magnetic Resonance

MD: Molecular Dynamics

ADMET: Absorption, Distribution, Metabolism, Excretion and Toxicity

SAR: Structure–Activity Relationship

# General Introduction

# General introduction

Ferrocene **derivatives** have recently attracted considerable attention in modern medicinal chemistry due to their remarkable structural stability, reversible **redox** properties, and diverse biological activities. In addition, organometallic systems containing **ferrocene** are under continuous investigation because the presence of the iron atom within the structure can modify the physical and chemical properties, as well as the pharmacological activity, of organic compounds. **(Patra, Gasser, 2017)**.

The organometallic compound **ferrocene** consists of an iron atom sandwiched between two cyclopentadienyl rings, which gives it a highly stable aromatic structure. Since its discovery, **ferrocene** has become one of the most extensively studied metallocene compounds due to its remarkable thermal stability, its ability to undergo reversible **redox** reactions, its lipophilic nature, and its excellent electron-transfer capability. **(Togni, Hayashi, 1995)**. These unique properties make **ferrocenyl derivatives** attractive candidates in several scientific fields, including catalysis, electrochemistry, materials science, and pharmaceutical research.

In medicinal chemistry, **ferrocenyl** groups have been introduced into different biologically active molecules to obtain compounds with interesting pharmacological effects. Several **ferrocenyl derivatives** were reported to show antimicrobial, anticancer, antimalarial, anti-inflammatory, and **antidiabetic** activities **(Jaouen, Vessières, Top, 2015)**. Their activity is mainly linked to their **redox** properties and to their ability to interact with biological macromolecules through hydrophobic interactions, hydrogen bonds, and π–π interactions. The lipophilic nature of the **ferrocenyl** moiety may also help these compounds cross biological membranes more easily and interact with enzyme active sites.

Diabetes mellitus is among the most common metabolic disorders and is characterised by long-term hyperglycaemia caused by insufficient insulin secretion or insulin resistance. One method used to reduce postprandial hyperglycaemia is the inhibition of **carbohydrate**-digesting enzymes such as α-**amylase** and α-glucosidase **(Saleem et al., 2021)**. These enzymes are involved in the breakdown of **carbohydrate**s and the release of glucose. Their inhibition can therefore slow glucose absorption and contribute to better control of blood sugar levels.

Inflammation is another important process associated with several pathological conditions, including cardiovascular diseases, metabolic disorders, and chronic degenerative diseases. Oxidative stress and protein denaturation are known to contribute to inflammatory damage. Because of this, many studies have focused on the development of compounds able to stabilise proteins and reduce oxidative processes linked to inflammation **(Vessières, Top, Beck, Hillard, Jaouen, 2006)**.

Computational chemistry is now widely used in the study of biologically active compounds. Techniques such as Density Functional Theory **(DFT)**, **molecular docking**, **molecular** dynamics simulations, and **ADMET** prediction can provide useful information about **molecular** geometry, electronic distribution, chemical reactivity, **ligand**–protein interactions, and pharmacokinetic behaviour **(Cramer, 2013)**. These methods are often used together with experimental studies to better understand structure–activity relationships.

The present work deals with the synthesis, structural characterisation, biological evaluation, and computational study of new **ferrocenyl acetylaniline derivatives**. The aim was to examine how **molecular** structure and electronic properties may influence biological activity using both experimental and theoretical methods. The synthesised compounds were characterised using FT-IR, UV–Visible spectroscopy, and one- and two-dimensional NMR analyses. Their biological activity was evaluated by α-**amylase** and α-glucosidase inhibition assays together with bovine serum albumin **(BSA)** denaturation tests. **DFT** calculations, **molecular docking**, **molecular** dynamics simulations, MM-PBSA analysis, and **ADMET** prediction were also carried out to support the experimental results and identify the derivative showing the best activity.

Despite the promising biological properties of **ferrocenyl derivatives**, the relationship between their structural and electronic characteristics and their **antidiabetic** and anti-inflammatory activities remains not yet fully understood, particularly in terms of how substitution patterns influence **redox** behaviour, **enzyme inhibition**, and overall pharmacological performance. This raises the question of whether **ferrocenyl acetylaniline derivatives** can act as effective dual **antidiabetic** and anti-inflammatory agents and how their biological behaviour can be rationalized through combined experimental and computational approaches.

This combined experimental and computational study gives additional information about the behaviour of **ferrocenyl derivatives** and suggests that these compounds may have potential in the treatment of metabolic and inflammatory disorders.

# Part I: Bibliographic Study

# CHAPTER I:

## Ferrocene Derivatives:

## Structure, Reactivity and Applications

## I.1. Overview

Organometallic chemistry has become a very active area at the boundary between inorganic and organic chemistry with numerous applications in catalysis, material science and medicinal chemistry. Of all types of organometallic compounds, **ferrocene** is particularly remarkable and extensively investigated system due to greatly stability, unique electronic structure, and broad chemical reactivity **(Togni & Hayashi, 1995)**.

Since **ferrocene** was serendipitously discovered in 1951, it has been a central compound in the evolution of modern organometallic chemistry. Its unique structure and related bonding, an iron atom sandwiched between two cyclopentadienyl rings, posed problems to classical bonding theories and stimulated development of new concepts like metal–**ligand** π-interactions and electron delocalisation **(Kealy & Pauson, 1951)**.

Over the past years, the use of **ferrocene** with biologically active compounds has raised new hopes or perspectives in medicinal chemistry. Ferrocenyl **derivatives** were found to exhibit numerous biological activities such as anticancer, antimicrobial, antimalarial, anti-inflammatory and **antidiabetic** activities **(Patra & Gasser, 2017)**. The addition of the **ferrocenyl** group to organic frameworks increases lipophilicity of the conjugates, improves membrane permeability and promotes strong interactions with biological targets, for example enzymes and proteins. In addition, the **redox** active **ferrocene** can also take part in electron transfer processes, which are largely a part of biological processes including oxidative stress metabolism and **enzyme inhibition**. This is particularly important for the development of drugs for treatment of metabolic and inflammatory diseases where the **redox** balance serves as a key factor **(Astruc, 2011)**.

## I.2. Structural and Electronic Properties of Ferrocene

### I.2.1. Molecular Structure and Bonding

Ferrocene is an arene complex in which a Fe**(II)** cation lies between two Cp rings. Since the two Cp rings each contribute five π-electrons, the Fe atom has 18 valence electrons **(8 from Fe plus 5 π-electrons from each Cp ring)**, fulfilling the 18-electron rule which makes the molecule highly stable **(Togni, Hayashi, 1995)**.

The metal–arene interactions involve delocalised π-bonding, resulting in a highly symmetric structure with exceptional thermal and chemical stability. The Fe–Cp interaction is strongly covalent due to the efficient overlap between Fe d-orbitals and **ligand** π-orbitals **(Astruc, 2007)**.

### I.2.2. Electrochemical and Redox Properties

One of the most important properties of **ferrocene** is its reversible Fe**(II)**/Fe**(III) redox** behaviour, which explains its wide use in electrochemistry and contributes to its biological activity, especially in antioxidant and **enzyme inhibition** processes **(Bard, Faulkner, 2001)**.

The electronic properties of **ferrocenyl derivatives** are strongly affected by the nature of their substituents. Electron-donating groups increase electron density and lower oxidation potentials, while electron-withdrawing groups produce the opposite effect. These modifications influence both electrochemical behaviour and biological activity, as illustrated in Figure 1.1.

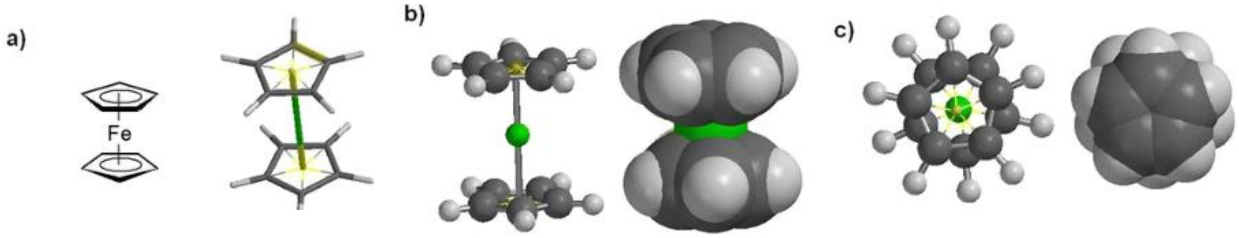


***Figure I.1:*** *Structural representations of* ***ferrocene****: a) Formula and tube structure; b) ball-and-stick* ***(left)*** *and space-filling* ***(right)*** *side views; c) ball-and-stick* ***(left)*** *and space-filling* ***(right)*** *top views. Adapted from* ***(Holub et al., 2022)****.*

## I.3. synthesis and functionalisation of ferrocenyl derivatives

### I.3.1. Synthetic Approaches for Ferrocenyl Derivatives

The preparation of **ferrocenyl derivatives** is accessible via a multitude of routes, such as electrophilic substitution, nucleophilic substitution, and cross-coupling reactions. Among them, nucleophilic substitutions of **ferrocenyl**methyl intermediates are especially significant because of their generality and efficiency **(Stepnicka, 2008)**, as illustrated in Figure 1.2.

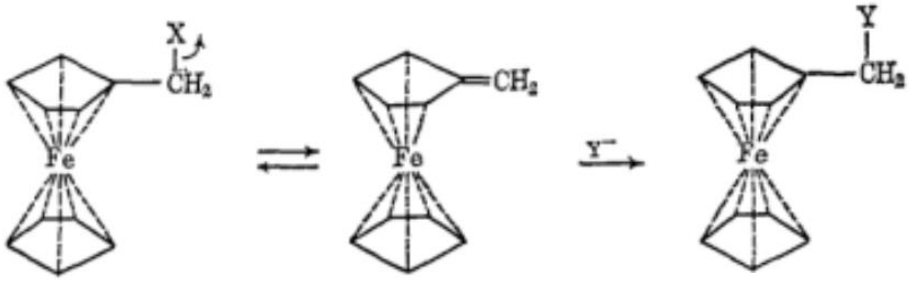


***Figure I.2:*** *General pathways for the nucleophilic substitution of* ***ferrocenyl****methyl intermediates. Adapted from* ***(Zubair et al., 2023)****.*

### I.3.2. Nucleophilic Substitution Mechanism of Ferrocenylmethyl Intermediates

Ferrocenylmethyl **derivatives** act as reactive intermediates capable of undergoing SN2-type reactions, in which a nucleophile attacks an electrophilic carbon atom. This strategy allows the introduction of a wide variety of functional groups, including pharmacologically active moieties **(Togni, 1995)**, as presented in Figure 1.3.

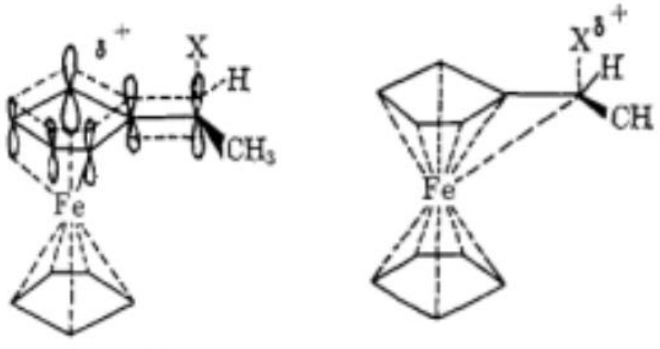


***Figure I.3:*** *Structural representation and transition states of* ***ferrocenyl derivatives****. Adapted from* ***(Zubair et al., 2023)****.*

The efficiency of such reactions depends on several factors, including steric hindrance, electronic effects, and the nature of the leaving group. In general, reactions involving primary carbon centres and good leaving groups proceed more readily, resulting in high yields and selectivity **(see Figure 1.3.3 for examples of core structures)**.

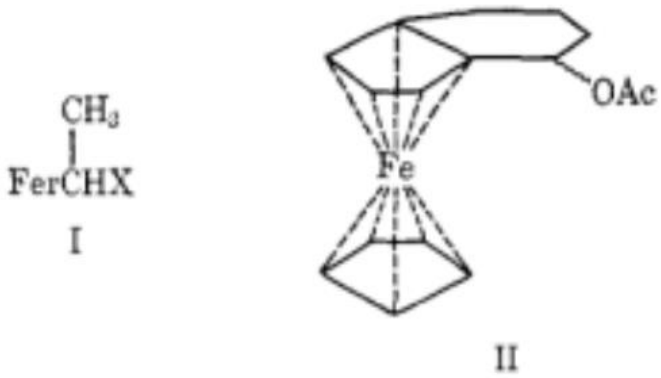


***Figure I.4:*** *Chemical structures of core* ***ferrocenyl derivatives (I and II)****. Adapted from* ***(Zubair et al., 2023)****.*

### I.3.3. Functionalisation and Biological Relevance of Ferrocenyl Derivatives

Functionalisation of **ferrocene** is of particular importance in medicinal chemistry, as it enables the fine-tuning of physicochemical properties such as lipophilicity, polarity, and electronic distribution. These modifications directly influence biological activity and pharmacokinetic behaviour **(Patra & Gasser, 2017)**, as depicted in the reaction mechanism in **Figure I.5.**

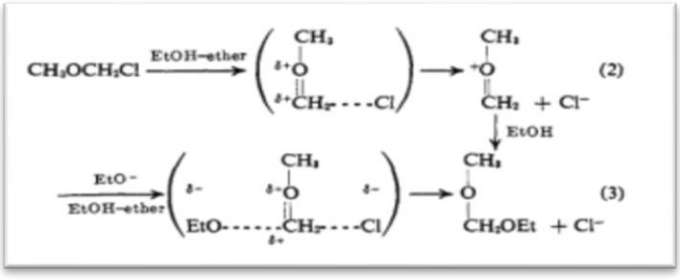


***Figure I.5:*** *Proposed mechanism for the functionalization and ether formation of* ***ferrocene derivatives****. Adapted from* ***(Zubair et al., 2023)****.*

## I.4 Electrochemical Behaviour of Ferrocene Compounds

### I.4.1. Cyclic Voltammetry of Ferrocene Derivatives

The electrochemical properties of **ferrocene derivatives** are among their most distinctive features. These properties are typically studied using **cyclic voltammetry**, which provides valuable information about **redox** potentials, electron transfer kinetics, and reversibility of electrochemical processes **(Bard, Faulkner, 2001)** as representative cyclic voltammograms are illustrated in **Figure I.6.**

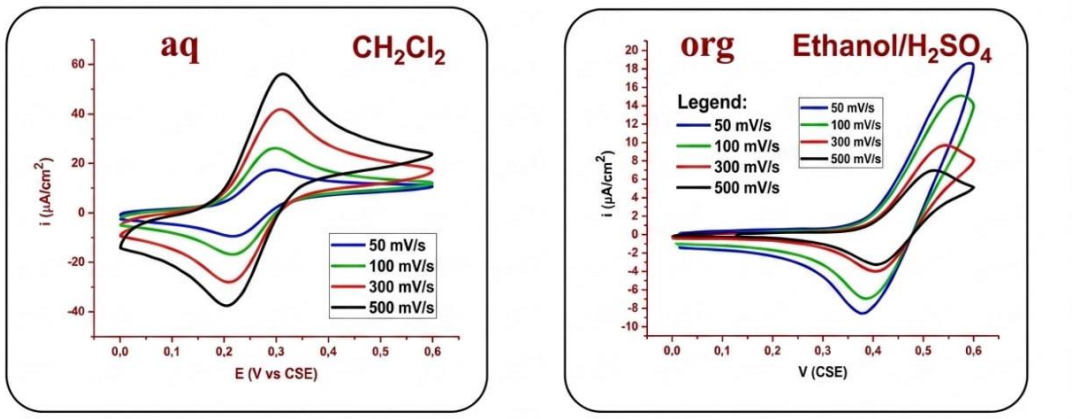


***Figure I.6:*** *Representative cyclic voltammograms illustrating the quasi-reversible Fe**(II)**/Fe**(III)** **redox** behavior of **ferrocene derivatives** at different scan rates. Adapted from **(Bouterfit et al., 2013)**.*

### I.4.2. Redox Behaviour and Electronic Effects

Ferrocene shows a well-defined and reversible Fe**(II)**/Fe**(III)** **redox** process, characterized by narrow peak separation and high reproducibility, which makes it a standard reference in electrochemical studies. Substituents on the cyclopentadienyl rings significantly influence this **redox** behaviour, where electron-donating groups lower oxidation potentials and electron-

withdrawing groups increase them, reflecting changes in electron density and **molecular** structure **(Astruc, 2007)**.

### I.4.3. Biological Relevance of Redox Activity

The **redox** activity of **ferrocene** is closely linked to its biological properties. In particular, it can contribute to antioxidant activity by participating in electron transfer processes that neutralise reactive oxygen species. Additionally, **redox** behaviour may influence interactions with enzymes and proteins, affecting binding affinity and biological efficacy **(Astruc, 2011)**.

The voltammograms display oxidation and reduction peaks associated with the reversible electron-transfer process between **ferrocene** and ferrocenium species. This electrochemical behaviour reflects the remarkable **redox** stability and electronic properties of **ferrocenyl** compounds **(Bard & Faulkner, 2001)**.

## I.5 Biological and Pharmacological Relevance of Ferrocene Derivatives

### I.5.1. Biological Importance of Ferrocenyl Derivatives

Ferrocenyl **derivatives** have gained significant interest in medicinal chemistry due to their broad biological activities. They are known to interact with various biological targets such as enzymes, proteins, and nucleic acids, resulting in diverse pharmacological effects **(Patra, Gasser, 2017)**.

### I.5.2. Enzyme Inhibition and Antidiabetic Activity

One of the most important applications of **ferrocenyl derivatives** is in the inhibition of enzymes involved in metabolic processes. In particular, α-**amylase** and α-glucosidase are key enzymes responsible for the breakdown of **carbohydrate**s into glucose. Inhibition of these enzymes is an effective strategy for controlling postprandial hyperglycaemia in diabetic patients **(Kim et al., 2005)**, as visually demonstrated by the **molecular docking** interactions in **Figure I.7.**

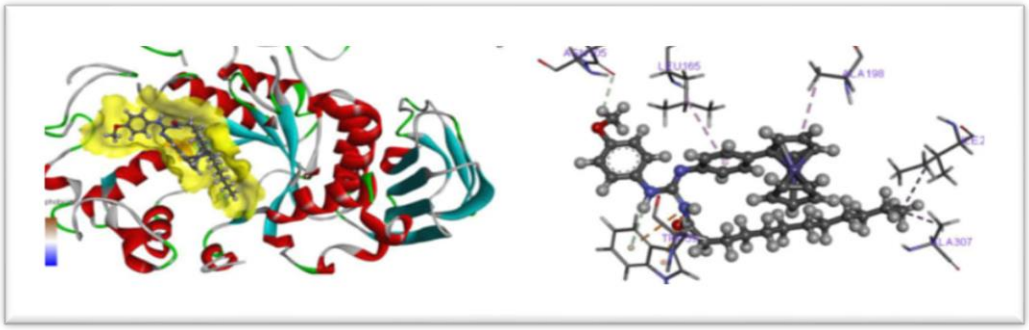

***Figure I.7:*** *Three-dimensional* ***(3D)*** *representation illustrating the* ***docking*** *conformation and stability of the* ***ferrocene*** *derivative within the active site pocket of the α-****amylase*** *enzyme.* *Adapted from* ***(McDougall et al., 2005)****.*

### I.5.3. Interaction Mechanisms with Biological Targets

Ferrocenyl **derivatives** have demonstrated strong inhibitory activity against these enzymes, often exhibiting lower $IC_{50}$ values compared to conventional drugs. This enhanced activity is attributed to multiple interaction mechanisms, including hydrogen bonding, hydrophobic interactions, and π–π stacking with amino acid residues in the enzyme active sites **(McDougall et al., 2005)**.

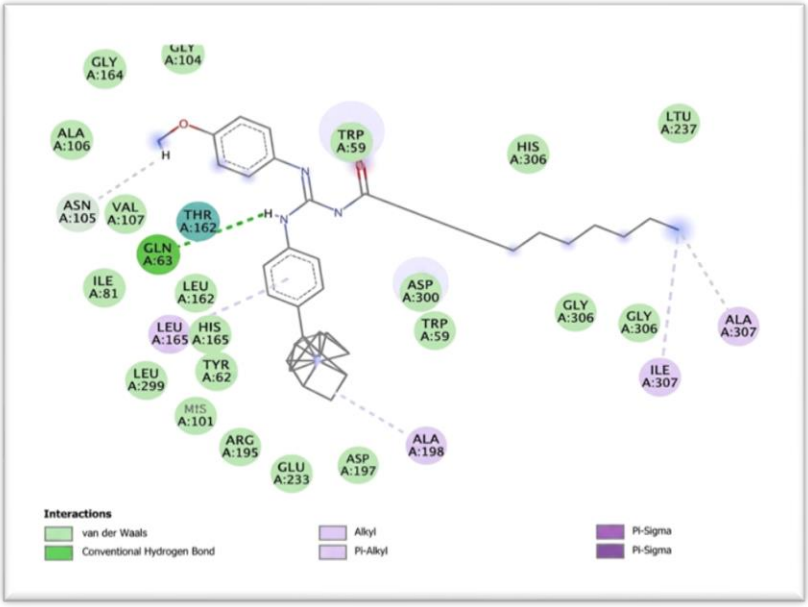


***Figure I.8:*** *Two-dimensional* ***(2D)*** *interaction map showing the types of interactions* ***(hydrogen bonds and π–π interactions)*** *between the* ***ferrocene*** *derivative and amino acid residues of the target metabolic enzyme, adapted from* ***(Bouterfit et al., 2013)****.*

### I.5.4. Anti-Inflammatory Properties of Ferrocenyl Compounds

In addition to **antidiabetic** activity, **ferrocenyl** compounds have shown promising anti-inflammatory properties. These properties are commonly evaluated using protein denaturation assays, such as bovine serum albumin **(BSA)**. In these assays, compounds that stabilise protein structure and prevent denaturation are considered to have anti-inflammatory potential **(Mizushima, Kobayashi, 1968)**.

## I.5.5. Structure–Activity Relationships of Ferrocenyl Derivatives

The biological activity of **ferrocenyl derivatives** is strongly influenced by their **molecular** structure. Factors such as substituent position, electronic distribution, and steric effects play a crucial role in determining interaction strength and selectivity toward biological targets. This relationship is often described in terms of structure–activity relationships **(SAR)**, which provide valuable insights for drug design and optimisation **(Patra, Gasser, 2017)** as illustrated by the calculated energy profiles in **Figure I.9.**

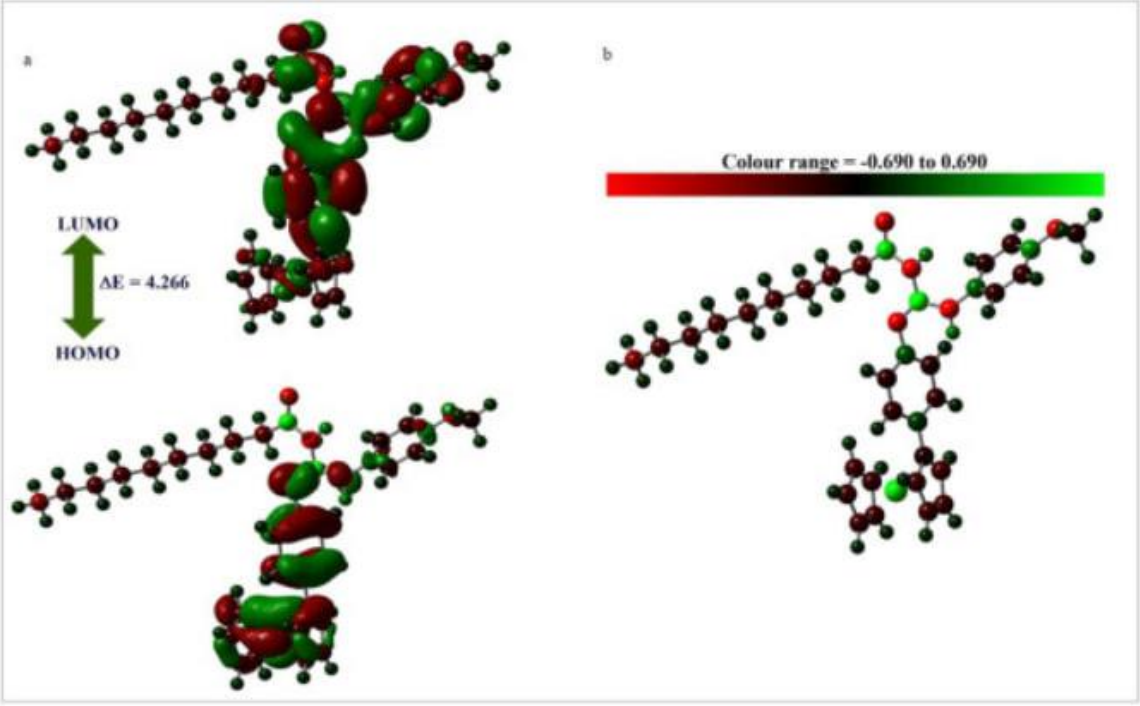


***Figure I.9:*** *Electronic distribution of the* ***molecular*** *orbitals* ***(HOMO–LUMO)*** *of the* ***ferrocene*** *derivative, illustrating the electron cloud density and its potential biological reactivity. Adapted from* ***(Patra & Gasser, 2017)****.*

# CHAPTER II:

# Computational Approaches in Molecular

## II.1 Overview

Metabolic diseases, such as diabetes mellitus, and inflammatory disorders represent some of the most significant health challenges facing humanity in the modern era **(World Health Organization, 2016; Hotamisligil, 2006)**. This necessitates an urgent need to develop pharmaceutical compounds that are more effective and possess fewer side effects. Ferrocene emerges as a unique chemical scaffold due to its exceptional chemical stability and distinctive electronic properties, making it an ideal candidate for developing organometallic derivatives with enhanced biological activity. **(Biot & Dive, 2010; Gasser et al., 2011)**

This study aims to design and synthesize a series of ferrocenyl acetylaniline derivatives(**Kamiński et al., 2022),** accompanied by a rigorous investigation of their physical and chemical properties. This thesis transcends traditional laboratory boundaries by adopting an "in silico to in vitro" methodology**(Sliwoski et al., 2014).** By integrating Density Functional Theory (DFT) calculations, molecular docking, and molecular dynamics (MD) simulations, we aim to elucidate how these molecules interact with target enzymes at the atomic level. Such an approach opens new horizons in the design of innovative drugs for the management of diabetes and inflammation.

## II.2. Density Functional Theory (DFT) and Electronic Descriptors

### II.2.1. Theoretical Foundations of DFT

DFT is extremely helpful in explaining the electronic structure of atoms and molecules. It considers electron density as the most important quantity. Due to the work of Hohenberg, Kohn, and Sham, DFT easily handles complex many-electron systems with reduced computational effort, and therefore is widely popular amongst the computational chemists. The applications of DFT, as the name suggests, are used for the prediction of structures. Due to the development of electronic descriptors in DFT, it is also used to assess chemical reactivity and understand it in a more analytical sense**(Geerlings et al., 2003; Chatwaraj, 2009)**

### .II.2.2. Conceptual DFT and Global Reactivity Descriptors

In conceptual DFT, many electronic descriptors are defined. Among the most important are chemical hardness (η) and softness (S) as well as electronegativity (χ). Electronic descriptors assess systems based on the attractiveness of systems to receive more electrons, and therefore, can be used to assess the hardness of a system with respect to a change in electron density. Systems with high chemical hardness are less polarizable and thus less reactive, while those with high softness are easier to reorganize. Soft systems are more reactive due to the lower hardness and thus, the lower resistance to polarizability.Such descriptors are relevant to practical cases, specifically when energies for the Highest Occupied and the Lowest Unoccupied Molecular Orbital are used**(Zhan et al., 2003).** In this sense, the energy for the Highest Occupied Molecular Orbital is a measure of the ability for the system to donate electrons while the energy for the LUMO is a measure of the ability to accept them.The energy gap in these orbitals can be a very first approximation of the kinetic stability and reactivity of the molecular system **(Mendez et al., 2003).** However, it can be misleading if analyzed in a more general sense as it neglects a number of environmental and dynamic factors, as visually exemplified by the calculated molecular orbital profiles **in Figure 2.1**

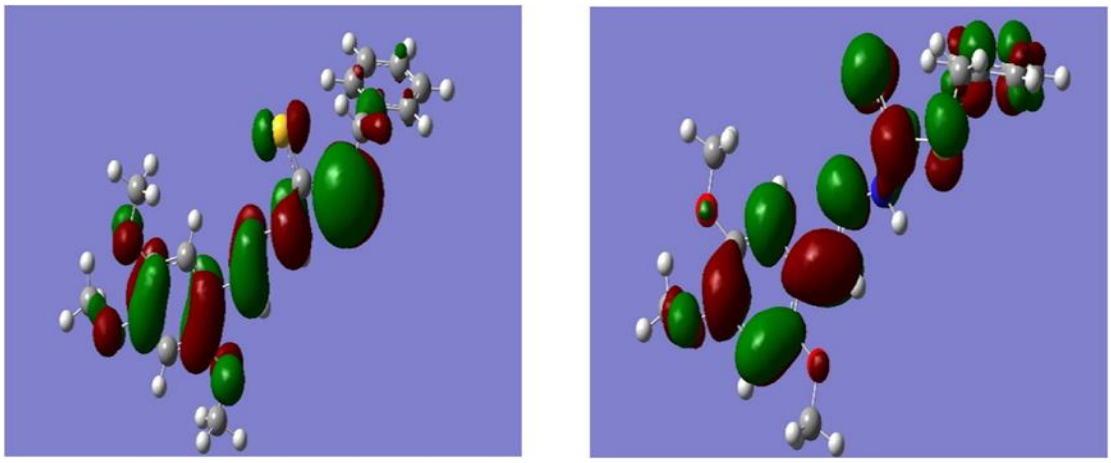

***Figure II.1:*** *Spatial distribution of the Highest Occupied Molecular Orbital (HOMO) and the Lowest Unoccupied Molecular Orbital (LUMO) of the ferrocenyl derivatives, illustrating the orbital symmetries and energy gap. Adapted from* ***(El-Sayed et al., 2022).***

### II.2.3. Local Reactivity Indicators and Fukui Functions

In addition to global descriptors, DFT provides local reactivity indicators such as the Fukui function, which describes changes in electron density upon electron gain or loss. It is used to identify the molecular regions most susceptible to nucleophilic or electrophilic attack, especially in complex systems with uneven reactivity distribution. **(Roy et al., 2006)**

### II.2.4. Molecular Electrostatic Potential (MEP) Mapping

The molecular electrostatic potential (MEP) map is widely used to visualize charge distribution and polarity within a molecule. It highlights electron-rich (nucleophilic) and electron-deficient (electrophilic) regions, helping to predict chemical reactivity and interactions with biological targets. In Figure 2.2, red regions represent electron-rich sites, while blue regions indicate electron-deficient sites. **( El-Sayed et al., 2022).**

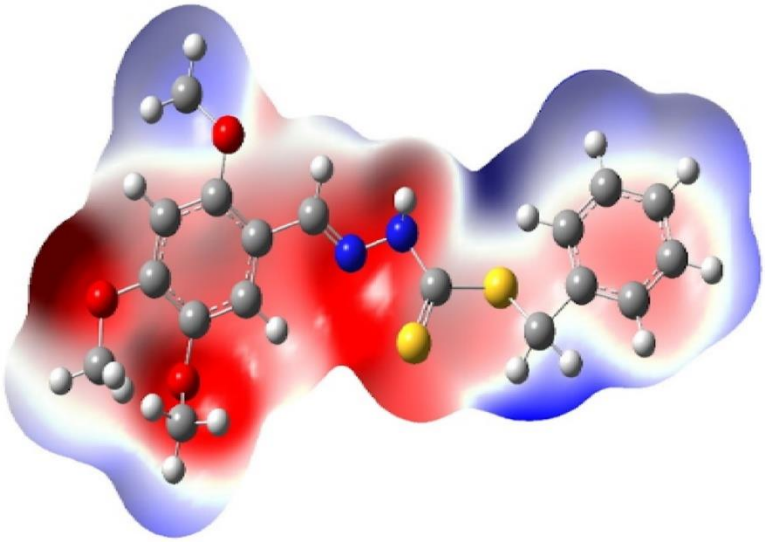

***Figure II.2:*** *Molecular electrostatic potential (MEP) map of the synthesized derivative, illustrating the relative polarity, nucleophilic (red), and electrophilic (blue) regions. Adapted from* ***(El-Sayed et al., 2022).***

### II.2.5. Applications in Computer-Aided Drug Design (CADD)

Total DFT combined with all of its electronic, software and molecular descriptors advance reasoning by combining electronic structure and molecular reactivity and are especially promising for the design of new compounds in medicinal chemistry (drugs) and in materials design **(El-Sayed et al., 2022).**

## II.3. Molecular Docking and Ligand–Protein Interactions

### II.3.1. Fundamental Principles of Computational Docking

Molecular docking is an in silico technique used to predict the binding orientation and conformation of small molecules within the active site of macromolecular receptors. It provides valuable information about ligand positioning, binding affinity, and molecular recognition, supporting structure-based drug design. **(Parr & Yang, 1984).**

### II.3.2. Conformational Sampling and Scoring Functions

During docking, different ligand conformations and orientations are explored within the receptor active site. Scoring functions estimate the binding free energy, and the lowest-energy conformation is generally considered the most stable and biologically relevant binding mode. **(Langenaeker et al., 1995).**

### II.3.3. Intermolecular Driving Forces and Complex Stabilization

Ligand–protein complex stability is mainly governed by non-covalent interactions, particularly hydrogen bonds and hydrophobic contacts. Electrostatic and van der Waals interactions may also contribute depending on the molecular system, as illustrated in Figure 2.3.

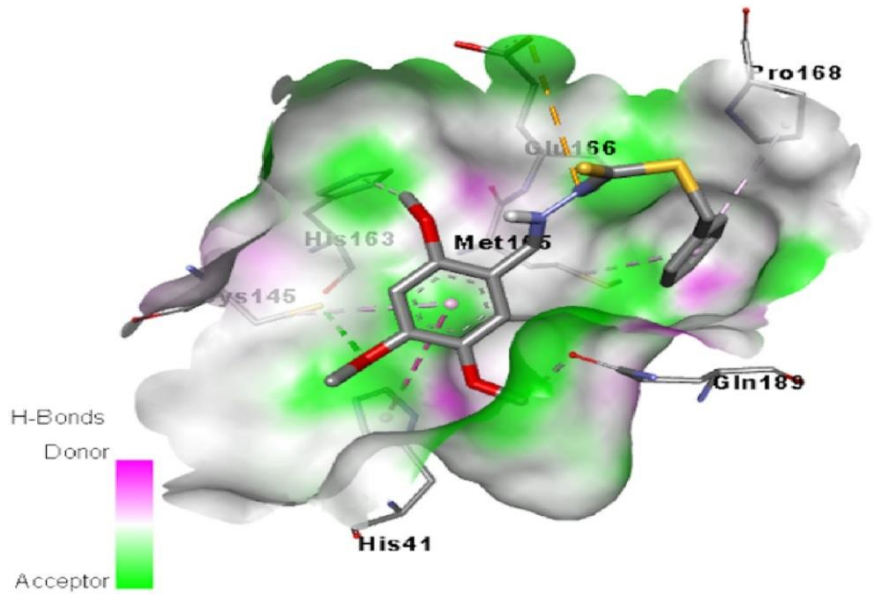


***Figure II.3:*** *Three-dimensional (3D) binding pose of the synthesized compound within the active site of the target enzyme, showing key hydrogen bonds and hydrophobic interactions with catalytic residues.* ***Dennington, R., Keith, T., & Millam, J. (2016).***

The 3D docking conformation presented in Figure 2.3 details the stabilization of the ligand-protein complex through specific non-covalent interactions, such as hydrogen bonding

with key catalytic residues and hydrophobic contacts, as visually demonstrated by the dual conformation profiles in **Figure II.4.**

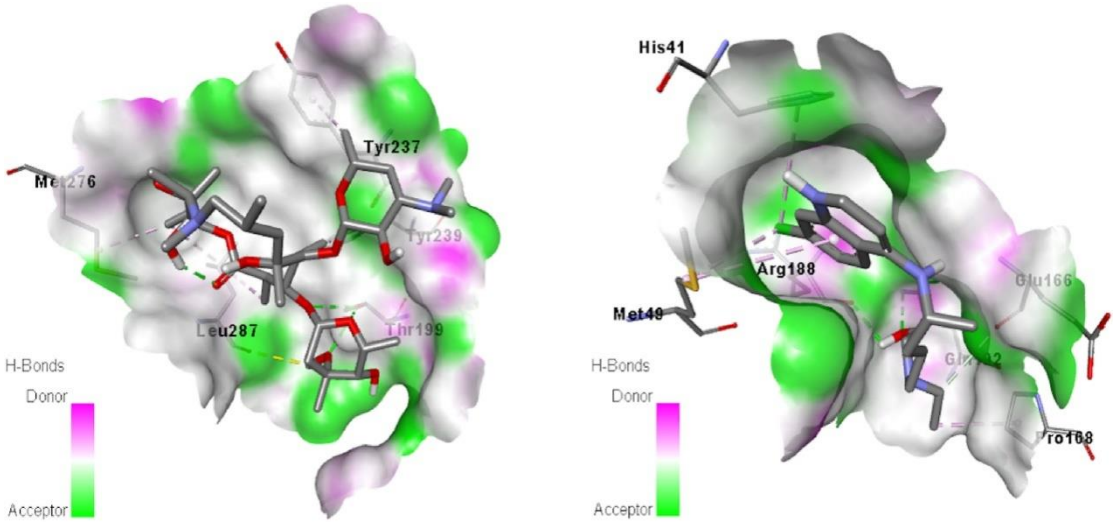


***Figure II.4:*** *A comparative visualization of different ligand conformations and derivatives within the active binding pocket, illustrating the variations in binding affinity and structural features.* ***Lu, T., & Chen, F. (2012)***

The comparative analysis presented in **Figure II.4** evaluates the binding affinity and identifies the structural features that contribute to the superior inhibitory activity of the most potent candidates.

### II.3.4. Three-Dimensional (3D) Spatial Configurations of Enzyme–Ligand Complexes

To gain a deeper insight into the site-specific binding modes, the three-dimensional (3D) spatial orientations of the synthesized ligands within the catalytic pockets of all target systems (Enzyme 1–8 complexes) are systematically displayed **in Figure 2.5**

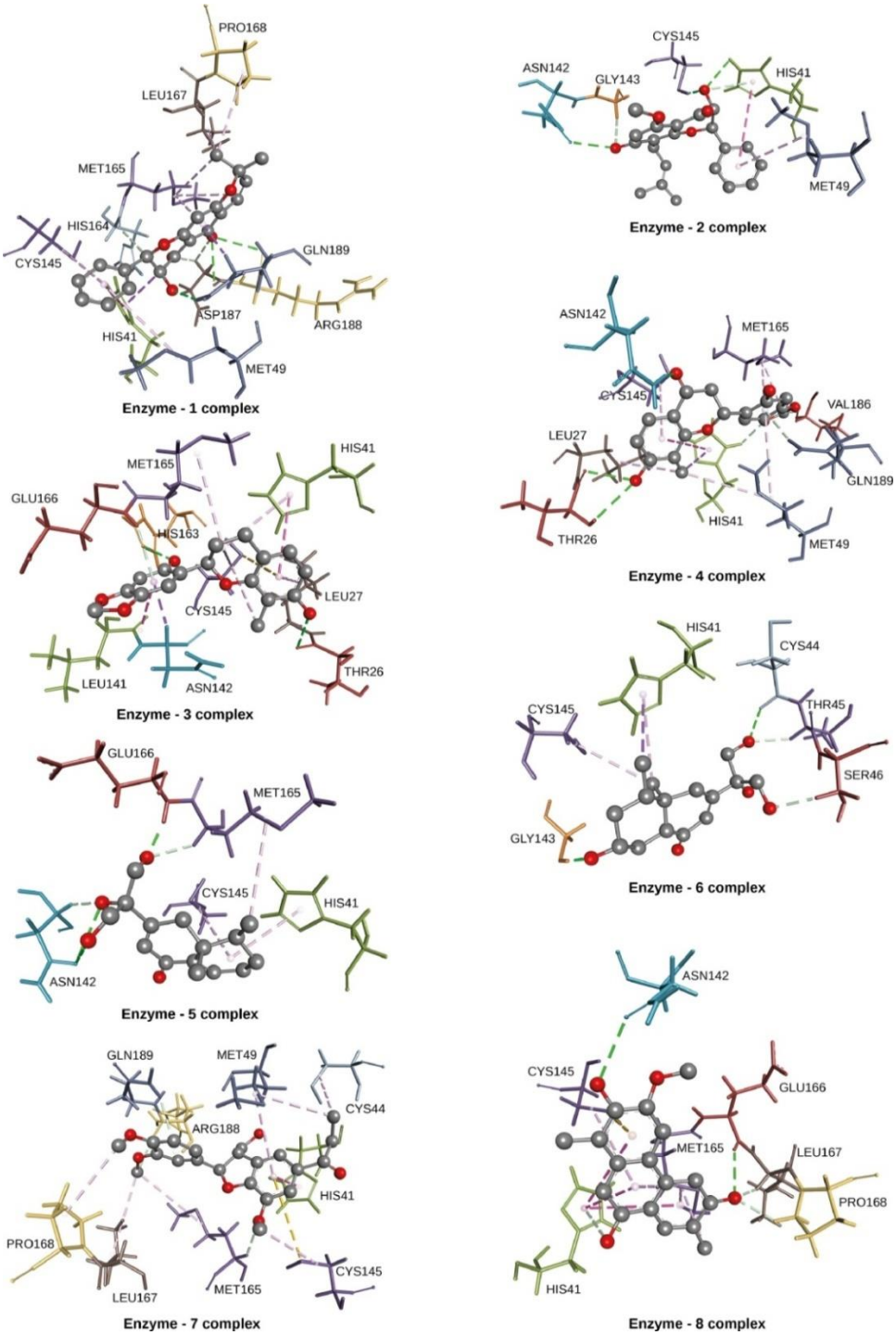


***Figure II.5:*** *Three-dimensional (3D) visualization of the docking configurations for Enzyme 1–8 complexes, showing the spatial orientation of the ligand within the catalytic pockets and*

*emphasizing the close proximity to key residues required for enzyme inhibition.* ***. Lu, T., & Chen, F. (2012).***

To complement the 3D conformational analysis, the 2D binding interactions of all synthesized compounds with the enzyme complexes were systematically illustrated in Figure II.6.

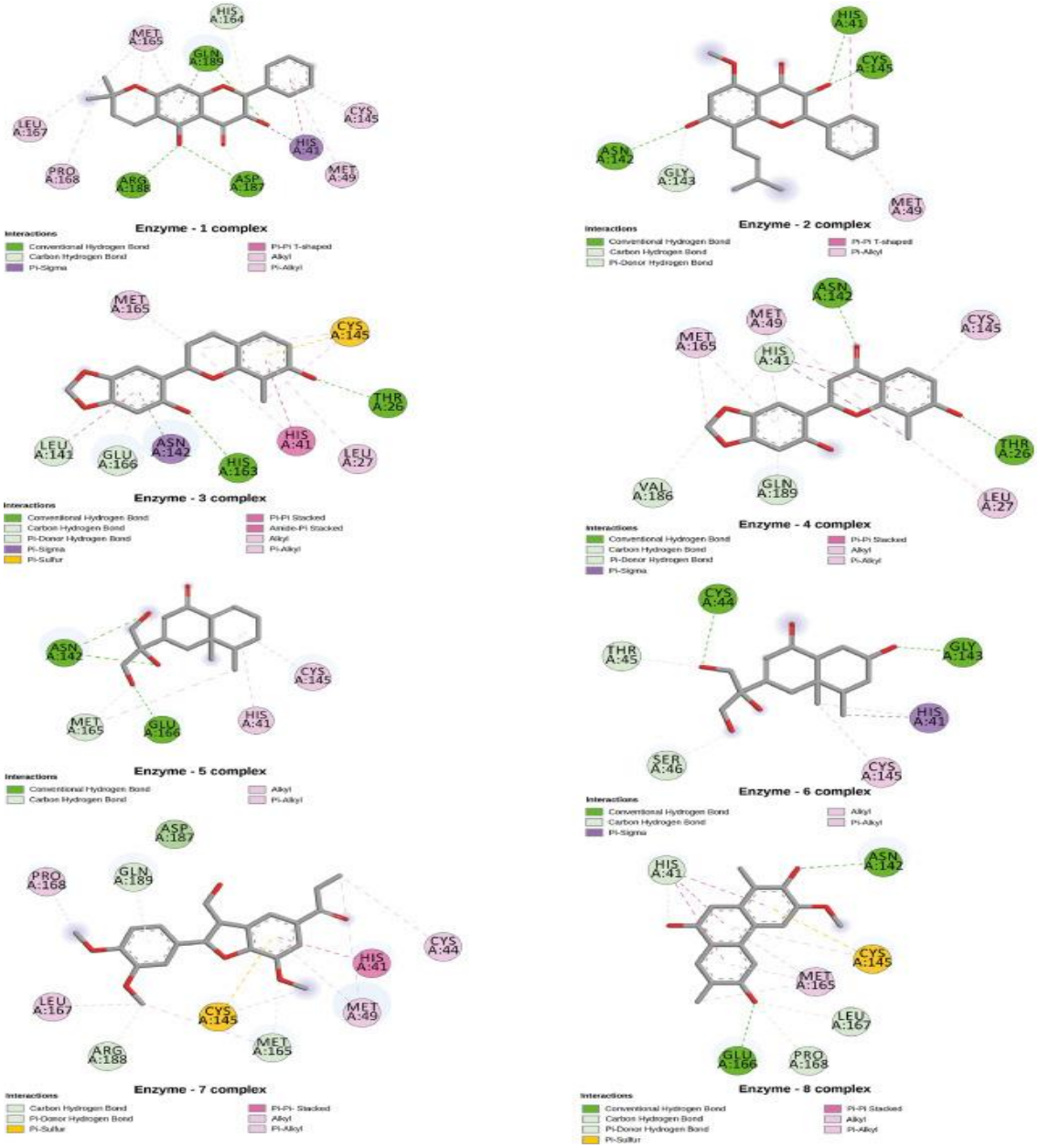

***Figure II.6:*** *Two-dimensional (2D) binding site interaction diagrams of the Enzyme 1–8 complexes, illustrating the specific hydrogen bonds, hydrophobic interactions, and amino acid residues involved in stabilizing the synthesized derivatives. .* ***Lu, T., & Chen, F. (2012).***

The 2D interaction plots presented in Figure 2.6 detail the precise non-covalent networks, highlighting the key amino acid residues and close contacts that govern the binding affinities observed across all synthesized candidate complexes.

## II.4. Molecular Dynamics Simulation

### II.4.1. Theoretical Principles and Governing Mechanics

Molecular Dynamics (MD) simulation is a computational technique used to study the time-dependent behavior and structural evolution of macromolecular systems in a simulated biological environment. Unlike molecular docking, which provides a static binding model, MD simulations describe atomic movements and conformational changes over time. Atomic trajectories are calculated using Newton's equations of motion, while molecular interactions are governed by empirical force fields, including bonded and non-bonded interactions such as electrostatic and van der Waals forces. **Raza, S., et al. (2023)**

### II.4.2. Post-Docking Validation and Structural Convergence

MD simulations are widely used to validate the stability of ligand–protein complexes after molecular docking. By monitoring nanosecond-scale trajectories, it is possible to determine whether the ligand remains stably bound within the active site. **Hospital, A., et al. (2015)** Structural stability and convergence are commonly evaluated using Root-Mean-Square Deviation (RMSD) profiles, as illustrated in Figure 2.7 for the eight enzyme–ligand complexes during the 30 ns simulation.

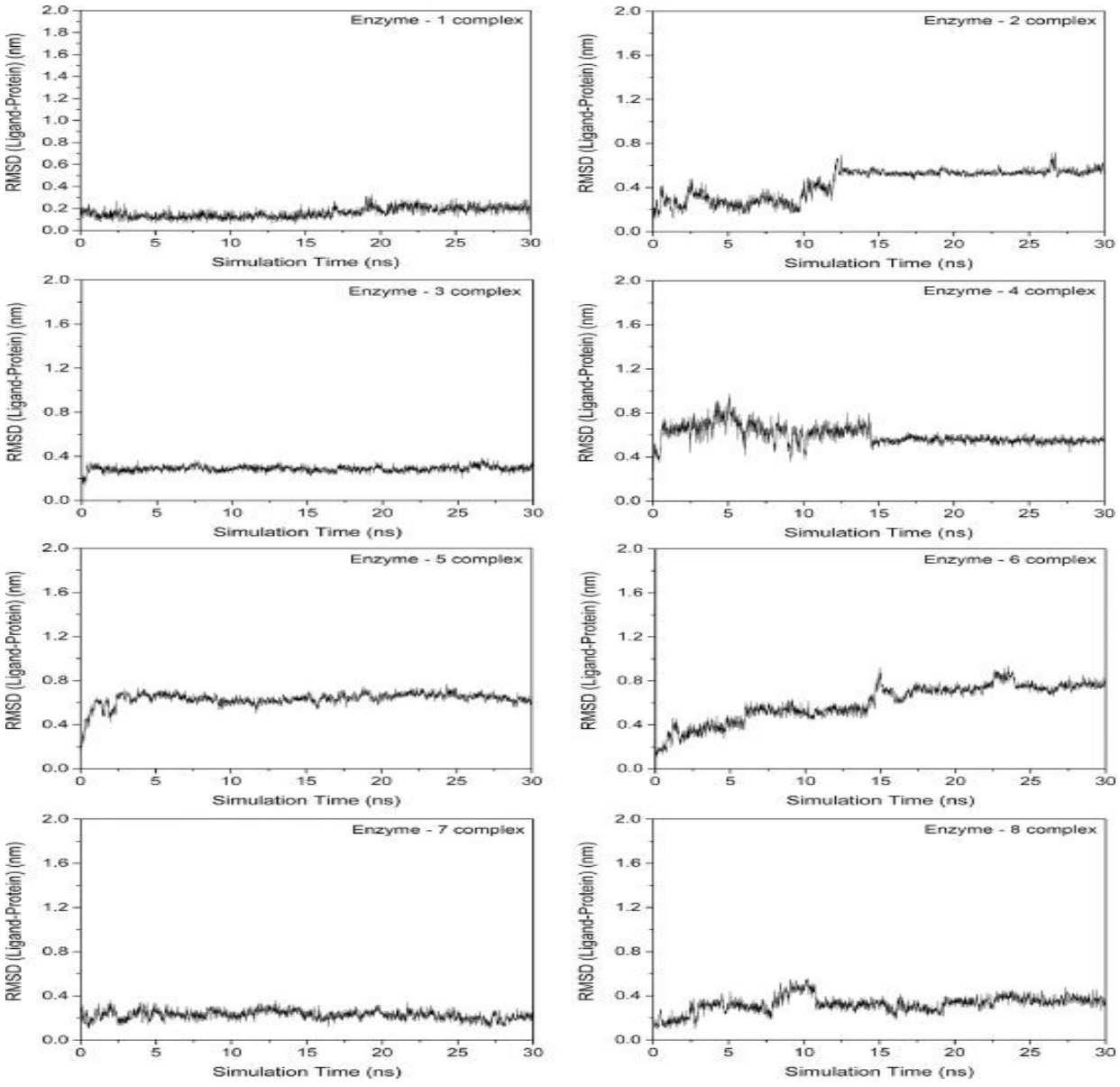


***Figure II.7:*** *Root-Mean-Square Deviation (RMSD) profiles for the eight enzyme–ligand complexes recorded over a 30 ns molecular dynamics simulation trajectory.* ***Schrödinger, LLC. (2020).***

The RMSD trajectories presented in Figure 2.7 demonstrate that the molecular systems achieved steady-state equilibrium and structural convergence, confirming that the ligands remained securely docked within the catalytic pockets throughout the simulation period.

The RMSD plots of the eight enzyme–ligand complexes over the 30 ns simulation were used to evaluate structural stability and convergence, confirming stable ligand binding within the catalytic pockets. In addition, the Radius of Gyration (Rg) was calculated to investigate protein compactness and structural integrity during the simulation, as shown in Figure 2.8.

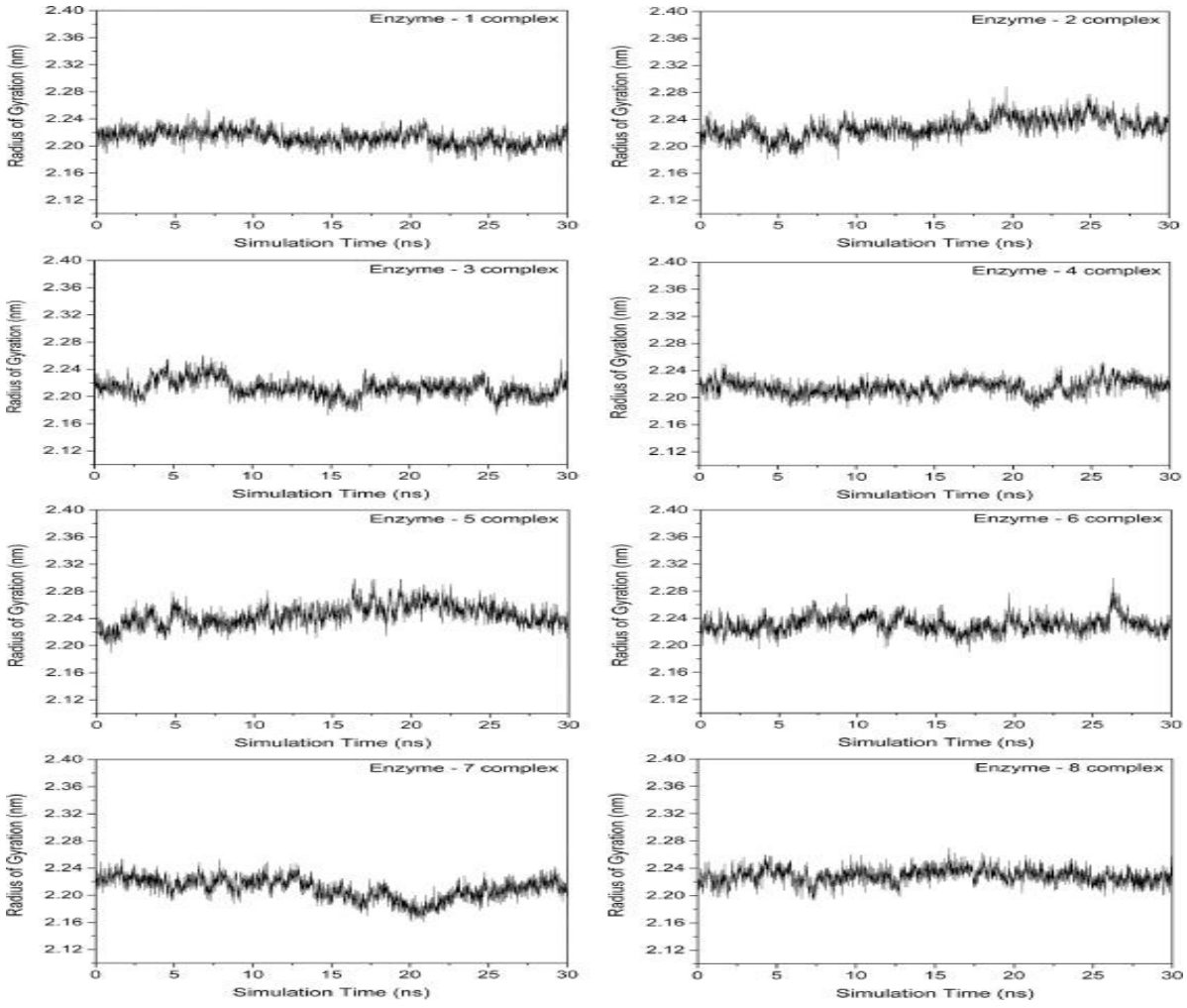


Figure II.8: *Radius of Gyration (Rg) profiles for the eight enzyme–ligand complexes plotted as a function of the 30 ns simulation time.* ***Raza, S., et al. (2023).***

The Radius of Gyration (Rg) profiles compiled in Figure 2.8 represent the structural compactness and folding integrity of the proteins during the interaction with the ligands. The highly steady and unfluctuating nature of these plots indicates that the host protein structures did not undergo significant conformational distortions or unfolding throughout the 30 ns simulation window.

Despite its advantages, MD simulation requires significantly higher computational resources and longer simulation times compared to molecular docking. For this reason, MD is generally used as a complementary approach to validate and refine docking results rather than as a standalone method. **(Roy et al., 2006)**

## II.5. ADMET Prediction and Drug-Likeness Evaluation

### II.5.1. Pharmacokinetic Profiling in Drug Discovery

After evaluating binding affinity, ADMET profiling (Absorption, Distribution, Metabolism, Excretion, and Toxicity) becomes an essential step in drug discovery. It provides important information about the pharmacokinetic behavior and potential toxicity of candidate molecules. Early in silico ADMET screening helps eliminate compounds with unfavorable properties, allowing only promising drug candidates to proceed to further experimental studies. **(Pearson, 1993).**

### II.5.2. Model Applicability Domains and Physicochemical Space

To ensure the reliability of the computational models and define the structural limitations of candidate selection, a comprehensive applicability domain analysis was performed, as illustrated in Figure 2.9.

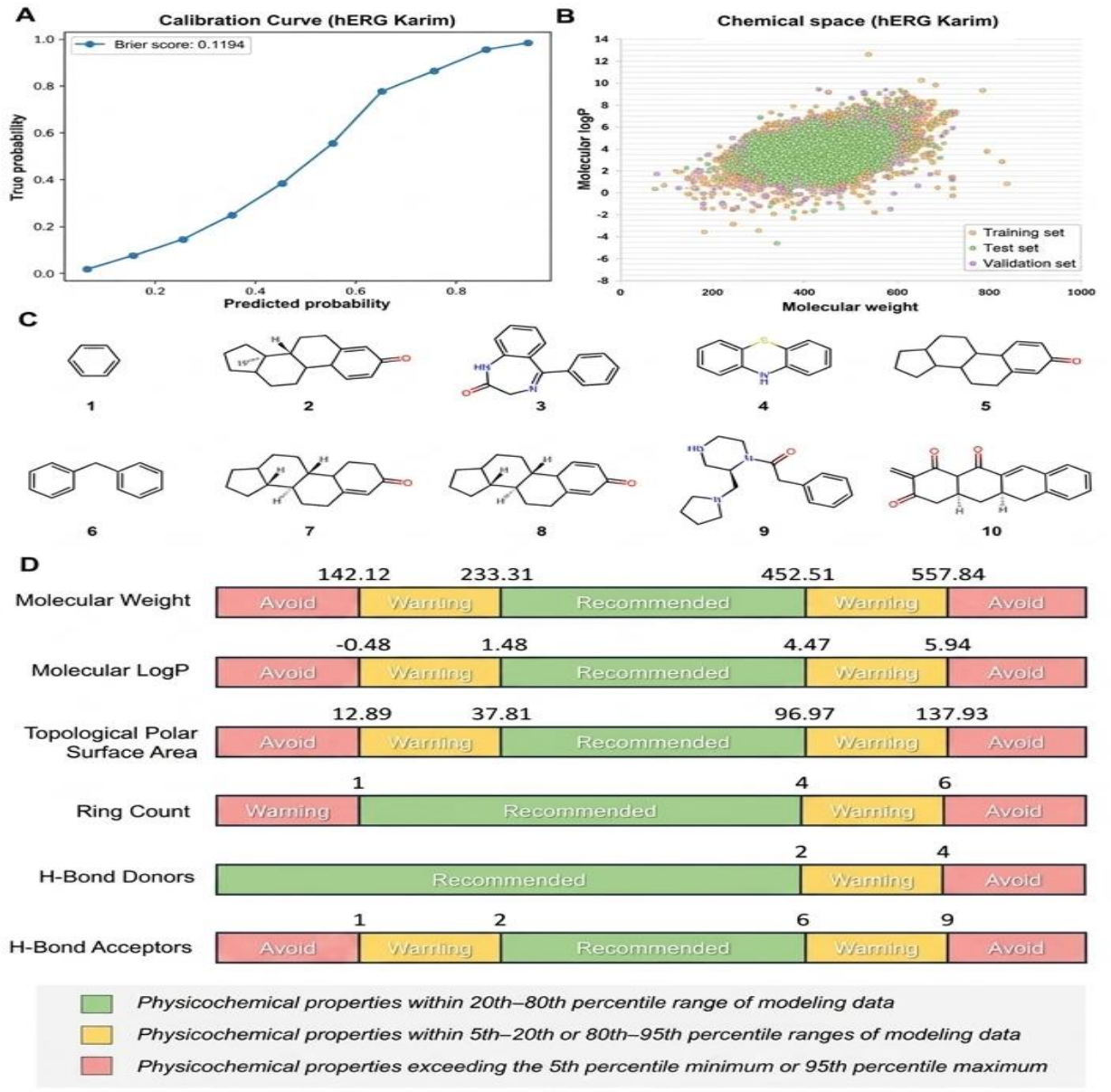


***Figure II.9:*** *Model Applicability Domains, Physicochemical Space Distributions, and Structural Rule Evaluations****(Humphrey, W., Dalke, A., & Schulten, K. (1996).***

- **Calibration Curve**: Validates the predictive accuracy of the hERG toxicity model, correlating predicted probabilities against empirical toxicity datasets
- **Chemical Space Visualization**: Two-dimensional scatter plot documenting the distribution of the training, test, and validation sets mapped against Molecular Weight and Lipophilicity (Log P)
- **Prevalent Scaffolds:** Structural representation of the top 10 chemical scaffolds identified within the Blood-Brain Barrier Penetration (BBBP) modeling dataset
- **Applicability Domain Mapping (ADMETPred)**: Comprehensive color-coded distribution of critical drug-likeness parameters, including
- Molecular Weight: Highlighting the ideal "Recommended" chemical range versus restricted "Avoid" zones.
- **Molecular Log P:** Defining the lipophilicity boundaries required for optimal membrane permeability.
- **Topological Polar Surface Area (TPSA):** Calculating parameters critical for oral bioavailability and passive Blood-Brain Barrier (BBB) permeation.
- **Structural Rule Constraints:** Quantification of ring counts, hydrogen-bond donors (HBD), and hydrogen-bond acceptors (HBA) in strict compliance with Lipinski's Rule of Five and associated structural heuristics.
- Computational ADMET evaluation meticulously analyzes individual phase boundaries:
- **Absorption:** Focuses on the passive or active transport of the compound across cellular and intestinal membranes.
- **Distribution:** Details how the compound is transported through the systemic circulation, including its specific binding affinity to plasma proteins and its capacity to cross restrictive biological barriers such as the Blood-Brain Barrier (BBB).
- **Metabolism:** Determines the biotransformation pathways of the core scaffold, evaluating its interaction with metabolic enzymes, primarily the hepatic Cytochrome P450 (CYP) isoenzymes.

- **Excretion:** Evaluates the clearance pathways of the parent drug and its hydrophilic metabolites from the systemic circulation, typically via renal filtration or biliary clearance.
- **Toxicity:** Predicts critical safety endpoints, managing hazards such as hepatotoxicity, mutagenicity (Ames test), and acute cardiac toxicity (hERG channel inhibition).

Concurrently with ADMET profiling, global drug-likeness evaluations match the structural and physicochemical traits of novel candidates against established benchmarks of successful commercial therapeutics. Lipinski's Rule of Five serves as a foundational heuristic rule, setting specific thresholds for molecular weight (≤500 Da), lipophilicity (Log P≤5) , hydrogen-bond donors (≤5) , and hydrogen-bond acceptors (≤10).

Chemical entities that adhere to these parameters generally exhibit superior oral bioavailability and predictable pharmacokinetic behavior. Nonetheless, these guidelines are applied flexibly as bounding heuristics to optimize early-stage structural refinement.

In summary, the in silico prediction of ADMET networks and drug-likeness parameters acts as a high-efficiency filter. By eliminating structurally flawed candidates prior to resource-intensive experimental and clinical trials, this digital validation fundamentally improves the overall efficiency of the drug discovery process**(Zhan et al., 2003).**

# PART II: EXPERIMENTAL

# CHAPTER I:

## Materials & Methods

## 1. General Introduction

This chapter outlines the experimental protocols and computational strategies adopted for the synthesis, structural elucidation, in vitro biological evaluation, and in silico investigation of **ferrocenyl acetylaniline derivatives**. The overall methodology integrates synthetic organometallic chemistry with advanced spectroscopic, electrochemical, biological, and **molecular** modelling techniques in order to establish a comprehensive correlation between **molecular** structure, electronic properties, and biological activity, particularly in relation to anti-inflammatory and **antidiabetic** potential.

The synthesis of the target compounds was carried out at the Laboratory of Valorisation and Technology of Saharian Resources **(VTRS)**, Faculty of Technology, University of El Oued, under controlled laboratory conditions. The same research facility was used to perform all computational investigations, including density functional theory **(DFT)** calculations, **molecular docking**, **molecular** dynamics simulations, and MM-PBSA analyses, thereby ensuring methodological consistency between experimental and theoretical results.

Spectroscopic characterisation was conducted in collaboration with the Centre de Recherche Scientifique et Technique en Analyses Physico-Chimiques **(CRAPC)**, University of Ouargla. A combination of FT-IR, UV–Visible spectroscopy, and one- and two-dimensional NMR techniques was employed to confirm the **molecular** structures of the synthesised **derivatives**. In addition, **cyclic voltammetry** was used to explore the **redox** properties of the **ferrocenyl** core, which are directly related to its electronic behaviour and potential antioxidant contribution to biological activity.

The biological potential of the synthesised compounds was evaluated through in vitro assays targeting inflammation and glucose metabolism. The anti-**inflammatory activity** was assessed using the bovine serum albumin **(BSA)** denaturation method, which reflects the ability of the compounds to inhibit protein denaturation associated with inflammatory processes. The **antidiabetic activity** was investigated through α-**amylase** and α-glucosidase inhibition assays, which are key enzymes involved in **carbohydrate** digestion and glucose release.

In parallel, computational investigations were conducted to support and rationalise the experimental findings. Molecular **docking** and **molecular** dynamics simulations were performed to explore the interaction of the synthesised compounds with relevant biological targets associated with inflammation **(COX-2)** and diabetes **(α-amylase and α-glucosidase)**, providing insight into binding affinity, interaction mechanisms, and stability of the **ligand**–protein **complexes**.

Furthermore, in silico **ADMET** predictions were carried out to assess pharmacokinetic properties, drug-likeness, and potential toxicity, enabling a preliminary evaluation of the suitability of the synthesised compounds as bioactive agents.

Overall, this integrated approach, combining synthesis, in vitro biological evaluation, and advanced computational modelling, provides a robust framework for understanding the structure–activity relationships of **ferrocenyl derivatives** and highlights their potential as promising candidates for the development of novel anti-inflammatory and **antidiabetic** agents.

Despite the comprehensive nature of the adopted methodology, a key challenge remains in fully correlating subtle structural variations within **ferrocenyl acetylaniline derivatives** with their observed biological activities, particularly in terms of enzyme selectivity, **redox** behaviour, and binding stability. This raises an important question regarding how effectively combined experimental and computational approaches can predict and rationalize the bioactivity of these organometallic systems.

## 2. Chemicals and Reagents

All reagents and solvents used in this study were of analytical grade and employed without further purification unless otherwise specified. The selection of chemicals was guided by their suitability for organometallic synthesis, spectroscopic and electrochemical characterisation, as well as their compatibility with subsequent in vitro anti-inflammatory and **antidiabetic** assays.

Ferrocene **(Fc, 99%)** and orthophosphoric acid **(85%)** were obtained from Alfa Aesar. The o-, m-, and p-aminoacetophenone isomers **(99%)**, together with tetrabutylammonium tetrafluoroborate **($Bu_4NBF_4$, electrochemical grade, 99%)** used as supporting electrolyte, were purchased from Sigma-Aldrich. Iodomethane and anhydrous magnesium sulfate **(97%)** were supplied by Acros Organics, while acetic acid **(99–100%)** and ethanol **(95%)** were provided by Biochem Chemopharma.

For the anti-inflammatory evaluation, bovine serum albumin **(BSA)** and diclofenac sodium **(reference drug)** were procured from Sigma-Aldrich. Phosphate buffer solutions were prepared using sodium dihydrogen phosphate and disodium hydrogen phosphate in double-distilled water, with pH adjusted according to assay requirements. **(Lanez & Henni, 2025)**

For the **antidiabetic** studies, human pancreatic α-**amylase** and α-glucosidase **(from *Saccharomyces cerevisiae*)** were obtained from Sigma-Aldrich and used without further purification. Acarbose was employed as the reference inhibitor in both enzyme assays. Soluble starch was used as substrate for the α-**amylase** assay, while p-nitrophenyl-α-D-glucopyranoside **(pNPG)** was used for the α-glucosidase assay. The α-**amylase** reaction was terminated using 3,5-dinitrosalicylic acid **(DNS)** reagent. **(Laraoui et al., 2023)**

The **ferrocenyl**methyl quaternary ammonium intermediate was synthesised according to previously reported procedures and used directly without additional purification. **(Khand et al. 1989)** All aqueous solutions were prepared using double-distilled water, and solvents used for analytical and biological measurements were of appropriate purity to ensure reproducibility.

Stock solutions of the synthesised compounds were freshly prepared, stored under controlled conditions **(4 °C when required)**, and used within a limited time frame to prevent degradation. All experimental procedures were conducted under standard laboratory conditions to ensure reliability and consistency of the obtained results.

# 3. Instrumentation and Experimental Conditions

## 3.1. Spectroscopic Analysis

### 3.1.1. FT-IR Spectroscopy

Fourier-transform infrared **(FT-IR)** spectra were recorded using a Shimadzu 8000S spectrophotometer over the spectral range of 4000–400 $cm^{-1}$. Solid samples were prepared as KBr pellets under standard conditions.

This technique enabled the identification of characteristic functional groups, including N–H stretching vibrations, carbonyl **(C=O)** bands, and aromatic C–H modes, thereby confirming the successful formation of the **ferrocenyl acetylaniline** framework. In addition, the observed vibrational features provided insight into inter**molecular** interactions, such as hydrogen bonding, which are relevant to protein–**ligand** interactions in anti-inflammatory assays and enzyme binding in **antidiabetic** systems. **(Lanez et al., 2020)**

### 3.1.2. UV–Visible Spectroscopy

Electronic absorption spectra were recorded using a Shimadzu UV-1800 spectrophotometer within the wavelength range of 200–900 nm. Measurements were performed in dimethyl sulfoxide **(DMSO)** using quartz cuvettes with a 1 cm optical path length.

The spectra provided information on the electronic transitions of the compounds, including π–π*, n–π* and metal-centred transitions, reflecting the degree of conjugation between the **ferrocenyl** core and the substituted aromatic system.

Furthermore, UV–visible spectroscopy was employed in biological interaction studies, including:

- monitoring compound–protein interactions in the BSA denaturation assay **(anti-inflammatory activity)**,
- evaluating compound–enzyme binding with α-**amylase** and α-glucosidase **(antidiabetic activity)**,

allowing determination of binding constants and thermodynamic parameters. **(Lanez et al., 2020)**

## 3.2. Nuclear Magnetic Resonance (NMR)

### 3.2.1. $^{1}$H NMR Analysis

$^{1}$H NMR spectra were recorded on a Bruker ARX-500 spectrometer operating at 400 MHz using DMSO-$d_6$ as solvent. Chemical shifts **(δ)** are reported in parts per million **(ppm)** relative to tetramethylsilane **(TMS)** as internal reference.

The spectra enabled precise identification of proton environments corresponding to the **ferrocenyl** rings, aromatic moiety, methylene bridge, and acetyl group, thereby confirming the expected **molecular** structures and substitution patterns. **(Lanez et al., 2023)**

### 3.2.2. $^{13}$C NMR Analysis

$^{13}$C NMR spectra were obtained under similar experimental conditions, allowing detailed assignment of carbon environments, including carbonyl carbons, aromatic carbons, cyclopentadienyl carbons, and methylene carbons.

These data provided further confirmation of the successful functionalisation of the **ferrocenyl** scaffold and contributed to the validation of the **molecular** architecture. **(Benamara et al., 2020)**

### 3.2.3. Two-Dimensional NMR (HSQC/HMBC)

Two-dimensional NMR experiments, including HSQC and HMBC, were performed to establish proton–carbon correlations and confirm structural connectivity.

HSQC spectra provided direct one-bond correlations between protons and carbons, whereas HMBC experiments revealed long-range interactions, enabling unambiguous assignment of substitution patterns and verification of the linkage between the **ferrocenyl**methyl fragment and the **acetylaniline** moiety. **(Lanez et al., 2019)**

## 3.3. Electrochemical Measurements (Cyclic Voltammetry)

Electrochemical characterisation was carried out using a PGZ301 potentiostat/galvanostat **(Radiometer Analytical, France)** in dimethyl sulfoxide **(DMSO)** under an inert nitrogen atmosphere at 298 K.

A conventional three-electrode system was employed, consisting of a glassy carbon working electrode **(0.013 cm$^2$)**, a platinum wire counter electrode **(0.05 cm$^2$)**, and a saturated $Hg/Hg_2Cl_2$ reference electrode. Tetrabutylammonium tetrafluoroborate **(0.1 M)** was used as the supporting electrolyte.

Prior to each measurement, the solution was purged with nitrogen to remove dissolved oxygen and ensure stable electrochemical conditions.

Cyclic voltammetry experiments were conducted within an appropriate potential window to investigate the Fe**(II)**/Fe**(III) redox** behaviour of the **ferrocenyl derivatives**. The resulting electrochemical parameters, including formal potentials, peak separations, and current ratios, provided valuable insight into electron-transfer kinetics and intrinsic electronic properties.

Importantly, these electrochemical characteristics are closely related to the **redox**-active nature of the **ferrocenyl** core, which may contribute to biological activity, particularly through modulation of oxidative processes involved in inflammatory pathways and metabolic enzyme function. **(Lanez et al., 2020)**

## 4. synthesis of Ferrocenyl Acetylaniline Derivatives

This section describes the synthetic strategy employed for the preparation of **ferrocenyl acetylaniline derivatives**, designed as potential bioactive compounds for anti-inflammatory and **antidiabetic** applications. The adopted methodology is based on a nucleophilic substitution reaction involving a **ferrocenyl**methyl quaternary ammonium intermediate, enabling efficient formation of the C–N bond under mild and environmentally compatible conditions.

This synthetic approach offers high selectivity, operational simplicity and reproducibility, while allowing structural modulation through positional substitution on the aromatic ring, which is expected to influence **enzyme inhibition** capacity and protein interaction behaviour.

The overall synthetic pathway is illustrated in **Figure 1**, highlighting the formation of the **ferrocenyl**methyl intermediate followed by its coupling with the corresponding aminoacetophenone isomers.

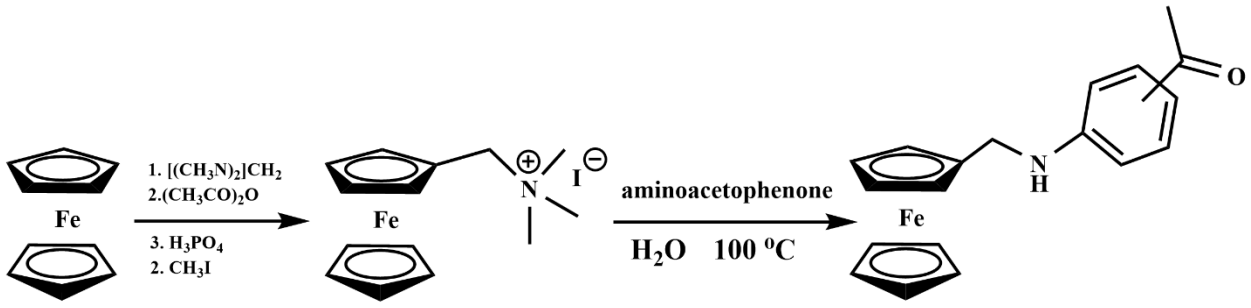


***Figure I.1.*** *Synthetic route for the preparation of N-[****(ferrocenyl)****methyl]****acetylaniline derivatives (FcMe2Ac, FcMe3Ac and FcMe4Ac)****.*

## 4.1. General Synthetic Procedure

The target compounds were synthesised via a nucleophilic substitution reaction between trimethyl**ferrocenyl**methylammonium iodide and the corresponding aminoacetophenone isomers **(ortho, meta and para)**, as presented in Figure 1.

In a typical procedure, aminoacetophenone **(3.84 mmol)** was gradually added to a stirred aqueous solution of trimethyl**ferrocenyl**methylammonium iodide **(2.56 mmol)** dissolved in distilled water **(60 mL)**. The reaction mixture was maintained under reflux for 4 h to ensure complete conversion.

After cooling to room temperature, a precipitate formed and was isolated by vacuum filtration. The crude product was thoroughly washed with distilled water to remove residual salts and unreacted species.

Purification was achieved by recrystallisation from a 90% ethanol/water mixture. In the case of the meta derivative, additional purification by column chromatography **(chloroform/methanol, 99:1 v/v)** was required to obtain analytically pure material.

The use of an aqueous medium, combined with mild reaction conditions, represents a sustainable and efficient synthetic protocol. Moreover, this approach yields compounds with appropriate purity and structural integrity suitable for subsequent biological evaluation, including **enzyme inhibition (α-amylase and α-glucosidase)** and protein denaturation assays **(BSA)**. **(Lanez et al. 2019b)**

## 4.2. synthesis of Individual Compounds

### 4.2.1. N-[(ferrocenyl)methyl]-2-acetylaniline (FcMe2Ac)

- **Yield:** 650 mg **(77%)**.
- **Appearance:** Yellow crystalline solid.
- **Melting point:** 148–150 °C.
- **$^{1}$H NMR (500 MHz, DMSO-$d_6$):** δ 2.60 **(3H, m, $CH_3$)**, 3.40 **(2H, t, α-$C_5H_4$)**, 4.05 **(2H, t, β-$C_5H_4$)**, 4.15 **(5H, s, $C_5H_5$)**, 4.30 **(2H, d, $CH_2N$)**, 6.62 **(1H, m, Ar-H)**, 6.84 **(1H, d, Ar-H)**, 7.40 **(1H, m, Ar-H)**, 7.85 **(1H, d, Ar-H)**, 9.01 **(1H, s, NH)**.
- **$^{13}$C NMR (500 MHz, DMSO-$d_6$):** δ 29 **($CH_3$)**, 42 **($CH_2N$)**, 67, 68 **($C_5H_4$)**, 69 **($C_5H_5$)**, 87 **(ipso-C)**, 112, 116, 118, 134, 138, 150 **(aromatic carbons)**, 210 **(C=O)**.

- **FT-IR (KBr, ν, cm⁻¹):** 3426, 3291 **(N–H)**, 3082 **(Ar–C–H)**, 1647 **(C=O)**, 1566, 1516 **(C=C)**, 1454, 1416, 1146, 1003, 617.
- **UV–Vis (DMSO):** λmax = 259 nm **(π–π*)**, 380 nm **(d–d)**.
- Cyclic voltammetry **(DMSO, $Fc^+$/Fc)**: Ipa = 29.13 μA, Ipc = −28.52 μA, Epa = 2.17 mV, Epc = −85.60 mV, ΔE = 87.8 mV, E° = 43.9 mV, Ipa/Ipc = 1.02.

### 4.2.2. N-[(ferrocenyl)methyl]-3-acetylaniline (FcMe3Ac)

- **Yield**: 480 mg **(48%)**.
- Appearance: Yellow–orange crystalline solid.
- **Melting point:** 138–140 °C.
- **$^1$H NMR (500 MHz, DMSO-$d_6$):** δ 2.45 **(3H, s, $CH_3$)**, 3.42 **(2H, t, α-$C_5H_4$)**, 4.08 **(2H, t, β-$C_5H_4$)**, 4.18 **(5H, s, $C_5H_5$)**, 4.32 **(2H, d, $CH_2N$)**, 6.70–7.20 **(3H, m, Ar-H)**, 7.65 **(1H, d, Ar-H)**, 8.95 **(1H, s, NH)**.
- **$^{13}$C NMR (500 MHz, DMSO-$d_6$):** δ 28 **($CH_3$)**, 43 **($CH_2N$)**, 66, 68 **($C_5H_4$)**, 69 **($C_5H_5$)**, 86 **(ipso-C)**, 114, 118, 125, 131, 136, 152 **(aromatic carbons)**, 205 **(C=O)**.
- **FT-IR (KBr, ν, cm⁻¹):** 3432, 3338 **(N–H)**, 2925, 1650 **(C=O)**, 1582, 1510, 1450, 1365, 1170, 820.
- **UV–Vis (DMSO):** λmax = 268 nm, 402 nm.
- **Cyclic voltammetry (DMSO, $Fc^+$/Fc):** Ipa = 52.4 μA, Ipc = −51.9 μA, Epa = 10 mV, Epc = −92 mV, ΔE = 102 mV, E° = 51.0 mV, Ipa/Ipc = 1.01.

### 4.2.3. N-[(ferrocenyl)methyl]-4-acetylaniline (FcMe4Ac)

- **Yield**: 690 mg **(80%)**.
- **Appearance**: Deep yellow crystalline solid.
- **Melting point:** 162–164 °C.
- **$^1$H NMR (500 MHz, DMSO-$d_6$):** δ 2.35 **(3H, m, $CH_3$)**, 3.41 **(2H, t, α-$C_5H_4$)**, 4.10 **(2H, t, β-$C_5H_4$)**, 4.20 **(5H, s, $C_5H_5$)**, 4.31 **(2H, d, $CH_2N$)**, 6.65 **(2H, d, Ar-H)**, 6.78 **(1H, t, NH)**, 7.76 **(2H, d, Ar-H)**.
- **$^{13}$C NMR (500 MHz, DMSO-$d_6$):** δ 28 **($CH_3$)**, 43 **($CH_2N$)**, 66 **($C_5H_4$)**, 68 **($C_5H_5$)**, 87 **(ipso-C)**, 112, 125, 132, 154 **(aromatic carbons)**, 194 **(C=O)**.
- **FT-IR (KBr, ν, cm⁻¹):** 3445, 3345 **(N–H)**, 2932, 1651 **(C=O)**, 1589, 1562, 1369, 1281, 1173, 822.

- **UV–Vis (DMSO):** λmax = 432 nm.
- **Cyclic voltammetry (DMSO, $Fc^{+}$/Fc):** Ipa = 71.07 μA, Ipc = −71.66 μA, Epa = 16 mV, Epc = −99 mV, ΔE = 115 mV, E° = 57.5 mV, Ipa/Ipc = 0.99.

## 5. Computational Methodology

Computational investigations were conducted to elucidate the electronic properties and interaction potential of the synthesised **ferrocenyl acetylaniline derivatives** in relation to their anti-inflammatory and **antidiabetic** activities. The adopted in silico framework integrates density functional theory **(DFT)**, **molecular docking**, **molecular** dynamics **(MD)** simulations, and MM-PBSA free energy calculations, complemented by **ADMET** prediction tools.

This integrated approach enables the establishment of correlations between **molecular** structure, electronic distribution, and binding behaviour towards biologically relevant targets, particularly α-**amylase** and α-glucosidase enzymes, as well as proteins involved in inflammatory processes. These analyses provide mechanistic insight into **ligand**–protein recognition, **enzyme inhibition**, and stability of the formed **complexes**.

### 5.1. Electronic Structure Calculations (DFT)

Quantum chemical calculations were performed using Gaussian 16 **(Frisch et al., 2009)** to investigate the electronic properties of FcMe2Ac, FcMe3Ac and FcMe4Ac.

Geometry optimisation was carried out at the B3LYP level of theory using the 6-311++G**(d,p)** basis set for light atoms **(C, H, N and O)**, while the Stuttgart–Dresden **(SDD)** effective core potential was applied to the iron centre **(Andersson & Uvdal, 2005)**. Frequency calculations were performed at the same level to confirm that all optimised structures correspond to true minima, characterised by the absence of imaginary frequencies.

The optimised geometries were subsequently used to determine frontier **molecular** orbitals **(HOMO and LUMO)**, energy gaps and global reactivity descriptors, including electronegativity **(χ)**, chemical hardness **(η)**, softness **(S)** and electrophilicity index **(ω)**. These parameters provide valuable insight into the reactivity and interaction potential of the compounds with biological targets such as digestive enzymes and inflammatory proteins.

In addition, **molecular** electrostatic potential **(MEP)**, electron localisation function **(ELF)**, localised orbital locator **(LOL)** and reduced density gradient **(RDG)** analyses were performed to characterise charge distribution, reactive sites and weak intra**molecular** interactions. These

descriptors are particularly relevant for understanding hydrogen bonding, electrostatic interactions and van der Waals contributions involved in **enzyme inhibition** and protein stabilisation mechanisms.

Visualisation and analysis of the calculated properties were carried out using GaussView and Multiwfn software. **(Lu & Chen, 2012)**.

## 5.2. Molecular Docking Simulations

Molecular **docking** simulations were carried out to investigate the binding affinity and interaction mechanisms of the synthesised **ferrocenyl acetylaniline derivatives** toward key enzymes involved in **antidiabetic** and anti-inflammatory activities. In particular, the study focused on α-**amylase (PDB ID: 1HNY)** and α-glucosidase **(PDB ID: 3TOP)**, which are well-established targets in the management of postprandial hyperglycaemia. These enzymes play a crucial role in **carbohydrate** digestion, making them relevant biological targets for **enzyme inhibition** studies.

### 5.2.1. Receptor Preparation

The three-dimensional structures of the selected enzymatic targets are illustrated in **Figure I.2**, highlighting the structural organisation of their catalytic domains and active sites.

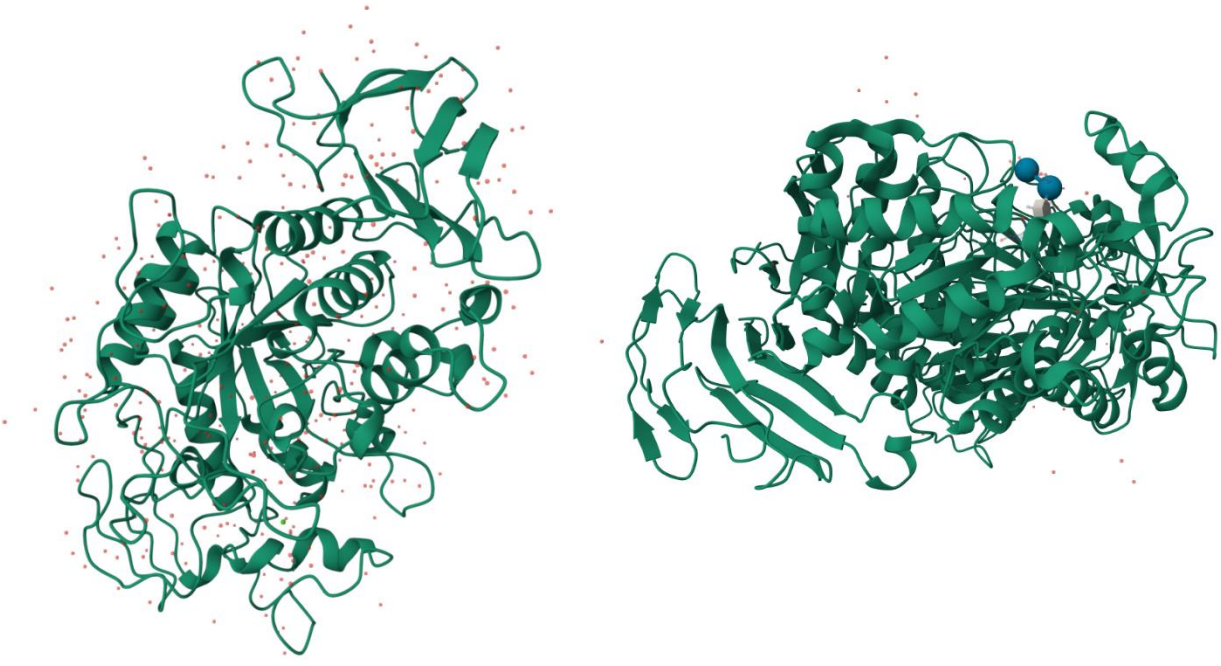

***Figure I.2.*** *Three-dimensional structures of target enzymes used in* ***docking*** *studies:* ***(a)*** *α-**amylase (PDB ID: 1HNY)** and* ***(b)*** *α-glucosidase* ***(PDB ID: 3TOP)****.*

The crystallographic structures were retrieved from the Protein Data Bank (https://www.rcsb.org/) **(Rose et al., 2017)** and prepared using AutoDock Tools **(ADT 1.5.7)**. **(Steffen et al., 2010)** All crystallographic water molecules, co-crystallised **ligand**s, and non-essential heteroatoms were removed to avoid interference with **ligand** binding. Polar hydrogen atoms were added, and Kollman charges were assigned. The prepared receptors were then converted into PDBQT format.

### 5.2.2. Ligand Preparation

The optimised geometries of FcMe2Ac, FcMe3Ac, and FcMe4Ac were used as input structures **Figure I.3.**

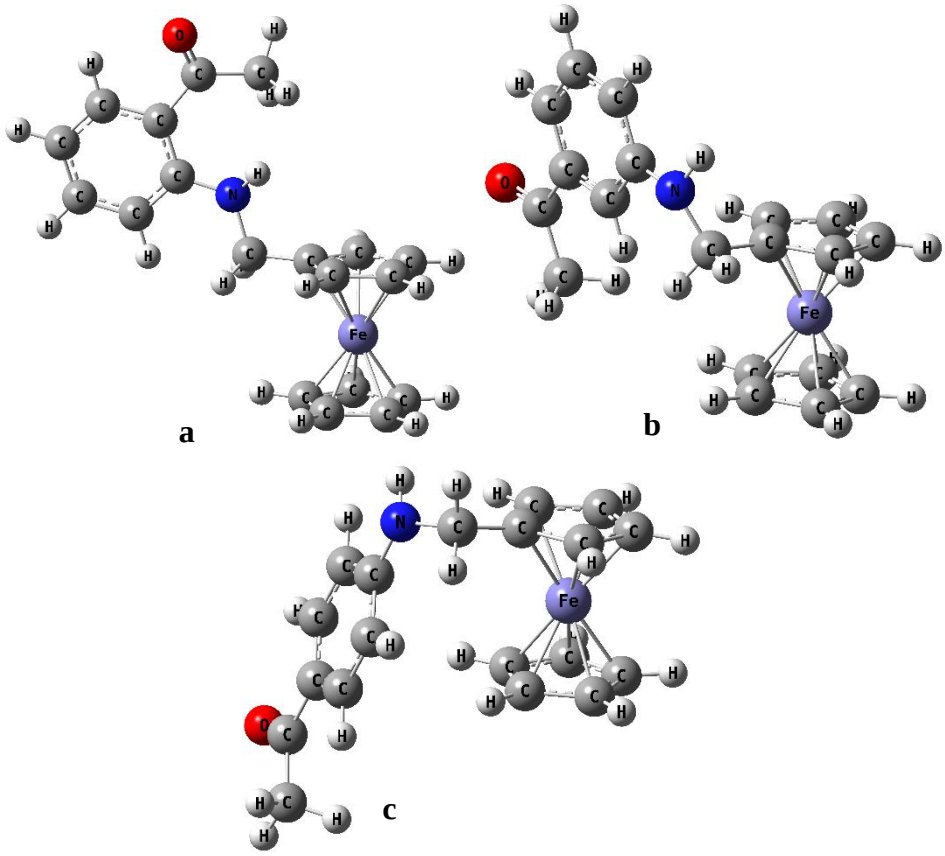


***Figure I.3.*** *Optimised* ***molecular*** *structures of* ***ferrocenyl derivatives*** *used as* ***ligand****s: FcMe2Ac* ***(a)****, FcMe3Ac* ***(b)****, and FcMe4Ac* ***(c)****.*

Ligands were prepared using AutoDock Tools by assigning Gasteiger charges and defining rotatable bonds, followed by conversion into PDBQT format.

### 5.2.3. Docking Protocol and Validation

The **docking** workflow is presented in **Figure I.4**, summarising receptor preparation, **ligand** preparation, grid generation and **docking** analysis.

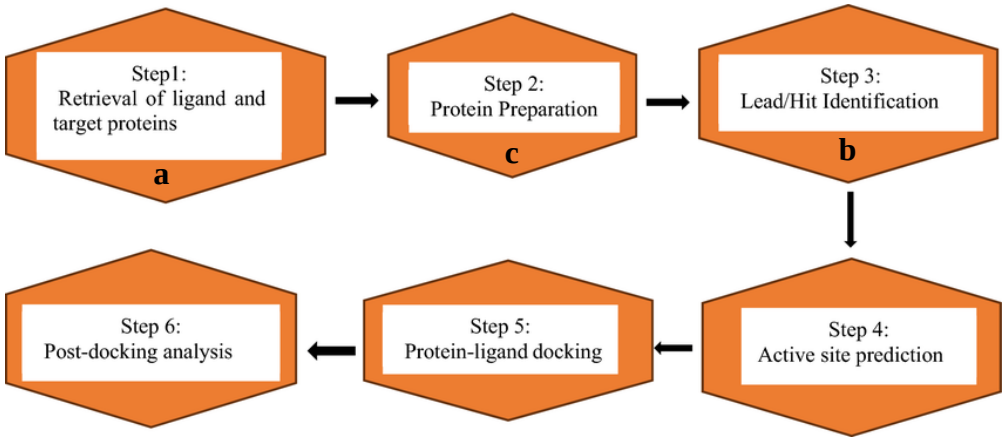


***Figure I.4.*** *Molecular* ***docking*** *workflow illustrating protein and* ***ligand*** *preparation, grid generation,* ***docking*** *execution and interaction analysis.*

Docking simulations were performed using AutoDock 4.2 with the Lamarckian genetic algorithm. A grid box of 60 × 60 × 60 Å with a spacing of 0.375 Å was centred on the catalytic active sites of the enzymes, encompassing key residues responsible for substrate recognition and catalysis.

For each **ligand**–target system, 100 independent **docking** runs were carried out. The most stable binding conformation was selected based on the lowest binding energy and the highest cluster population.

Validation of the **docking** protocol was performed by re**docking** the co-crystallised **ligand** into the active site of each enzyme. The accuracy of the **docking** procedure was assessed by calculating the root-mean-square deviation **(RMSD)** between the crystallographic and predicted conformations. RMSD values below 2.0 Å confirmed the reliability and robustness of the adopted **docking** parameters and ensured the validity of subsequent interaction analyses. **(Lanez et al., 2024)**

## 5.3. Molecular Dynamics (MD) Simulations

Molecular dynamics **(MD)** simulations were performed to evaluate the stability and dynamic behaviour of the selected **ligand**–enzyme **complexes** involving α-**amylase** and α-

glucosidase, which are key targets in **antidiabetic** activity, as well as their relevance in inflammation-related metabolic pathways. Simulations were carried out using GROMACS. **(Lanez et al., 2023)**

### 5.3.1. System Setup and Solvation

The solvated systems are illustrated in **Figure I.5**, showing the enzyme–**ligand complexes** embedded in an explicit aqueous environment.

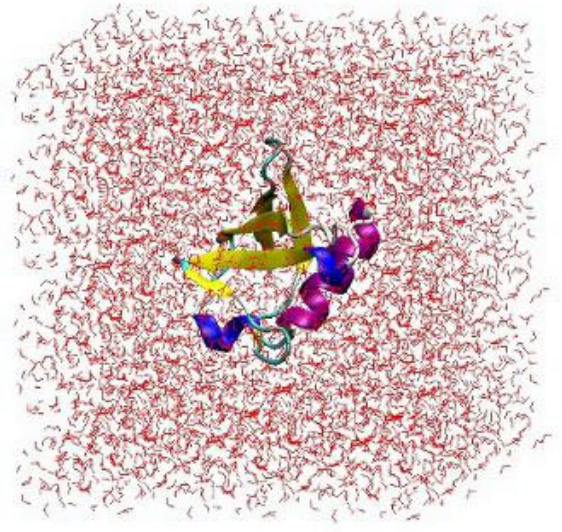

***Figure I.5.*** *Solvated protein–**ligand** complex showing the explicit water box used for **molecular** dynamics simulations.*

The CHARMM36 force field was employed for protein parameterisation, **(Huang & Mackerell, 2013)** while **ligand** parameters were generated using the CGenFF protocol **(Vanommeslaeghe & MacKerell, 2012)**. Each system was placed in a cubic simulation box with a minimum distance of 10 Å between the protein surface and the box boundary and solvated using the TIP3P water model. Counter ions were added to neutralise the system and ensure electrostatic stability.

### 5.3.2. Energy Minimisation and Equilibration

The general **molecular** dynamics simulation protocol, including minimisation, equilibration, and production stages, is summarised in **Figure I.6.**

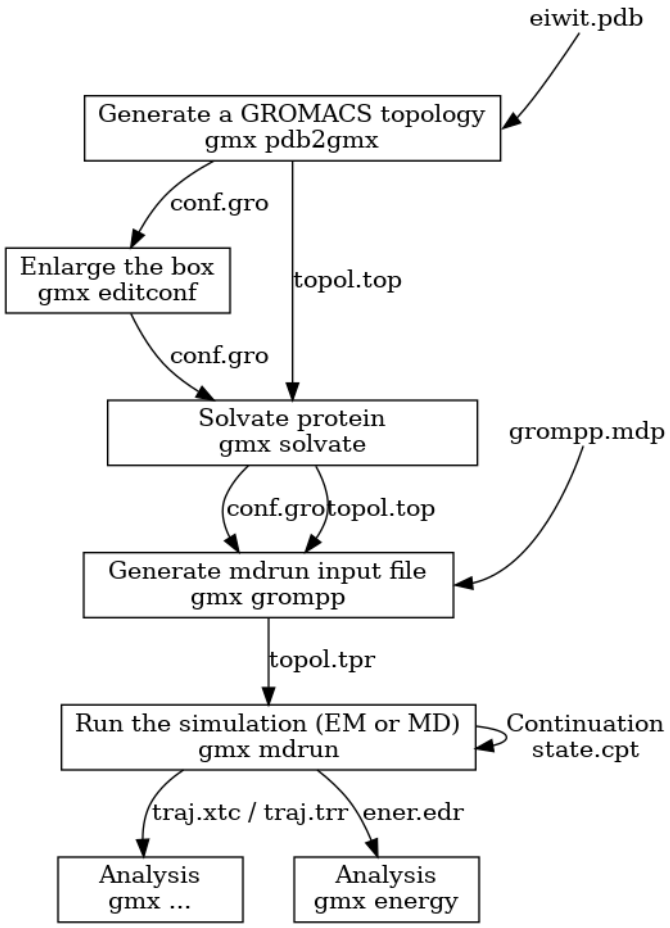


***Figure I.6.*** *Molecular dynamics simulation workflow including system preparation, energy minimisation, equilibration and production phases.*

Energy minimisation was performed using the steepest descent algorithm to eliminate steric clashes and optimise the system geometry. The system was subsequently equilibrated under NVT conditions **(300 K, 500 ps)**, followed by NPT conditions **(1 atm, 500 ps)**, using the V-rescale thermostat and Parrinello–Rahman barostat.

### 5.3.3. Production Run Parameters

Production simulations were conducted for 100 ns with a time step of 2 fs. Periodic boundary conditions were applied in all directions, and long-range electrostatic interactions were treated using the Particle Mesh Ewald **(PME)** method. Covalent bonds involving hydrogen atoms were constrained using the LINCS algorithm.

Trajectory analyses were carried out using GROMACS built-in tools, including RMSD, RMSF, radius of gyration **(Rg)**, and solvent surface accessibility area **(SASA)**.

## 5.4. MM-PBSA Binding Free Energy Calculations

Binding free energy calculations were performed using the g_mmpbsa tool. **(Kumari et al., 2014)** Snapshots extracted from the last 20 ns of equilibrated trajectories were used.

The total binding free energy **(ΔG_bind)** was estimated as the sum of van der Waals, electrostatic, polar solvation and non-polar solvation contributions.

## 5.5. ADMET Prediction

Pharmacokinetic and toxicity properties were predicted using **ADMET**lab 2.0 **(Dong et al., 2018)** and ProTox-II **(Banerjee et al., 2018)** to evaluate the drug-likeness and safety profile of the synthesised compounds.

The assessed parameters included:

- gastrointestinal absorption
- blood–brain barrier permeability
- cytochrome P450 interactions
- plasma protein binding
- toxicity indicators **(hepatotoxicity, mutagenicity, and $LD_{50}$)**

These predictions provide an initial evaluation of the suitability of the compounds as potential **antidiabetic** and anti-inflammatory agents, ensuring that favourable biological activity is not compromised by poor pharmacokinetic behaviour or toxicity risks.

# CHAPTER II:

## Results & Discussion

## General Introduction

This chapter presents a detailed analysis of the experimental and computational results obtained for the synthesised **ferrocenyl acetylaniline derivatives**, with particular emphasis on their anti-inflammatory and **antidiabetic** activities. The primary objective is to establish clear correlations between **molecular** structure, electronic properties, and biological behaviour through the integration of in vitro assays and in silico investigations.

The discussion begins with an evaluation of the synthetic outcomes, including reaction efficiency, yield variation, and the influence of substitution pattern. This is followed by comprehensive structural characterisation using FT-IR, UV–visible spectroscopy, nuclear magnetic resonance **($^{1}$H, $^{13}$C and 2D NMR)**, and **cyclic voltammetry**. These complementary techniques provide reliable confirmation of **molecular** structures and offer insight into the electronic features of the **ferrocenyl** core, which are closely related to its **redox** activity and potential biological performance.

Subsequently, the in vitro biological results are presented and discussed in detail. The anti-**inflammatory activity** is assessed through protein denaturation inhibition assays, while the **antidiabetic** potential is evaluated via α-**amylase** and α-glucosidase inhibition studies. These experimental findings allow the identification of the most active derivative and provide initial structure–activity relationships.

To further rationalise these observations, computational investigations are conducted. Density functional theory calculations are employed to analyse electronic descriptors and reactive sites, while **molecular docking** and **molecular** dynamics simulations are used to explore the interaction mechanisms of the synthesised compounds with relevant enzymatic targets. In addition, MM-PBSA calculations and **ADMET** predictions are discussed to evaluate binding stability, interaction energetics, and pharmacokinetic suitability.

Overall, this integrated experimental–computational approach enables a comprehensive understanding of the behaviour of **ferrocenyl derivatives** and highlights the interplay between **molecular** design and biological activity.

Despite the strong agreement between experimental and computational findings, certain discrepancies and limitations remain, particularly regarding the precise contribution of electronic effects and substitution patterns to binding affinity and inhibitory potency. These aspects suggest that further investigation is required to fully elucidate the structure–activity relationships governing the observed biological effects.

## 1. synthesis of Ferrocenyl Acetylaniline Derivatives

The **ferrocenyl acetylaniline derivatives (FcMe2Ac, FcMe3Ac and FcMe4Ac)** were successfully obtained through a nucleophilic substitution strategy involving a **ferrocenyl**methyl quaternary ammonium intermediate and the corresponding aminoacetophenone isomers. The adopted synthetic route demonstrated high reliability and reproducibility, affording the desired products as yellow to orange crystalline solids under relatively mild experimental conditions.

The reaction pathway is depicted in **Figure II.7**, which outlines the key mechanistic steps leading to the formation of the C–N bond at the **ferrocenyl**methyl position.

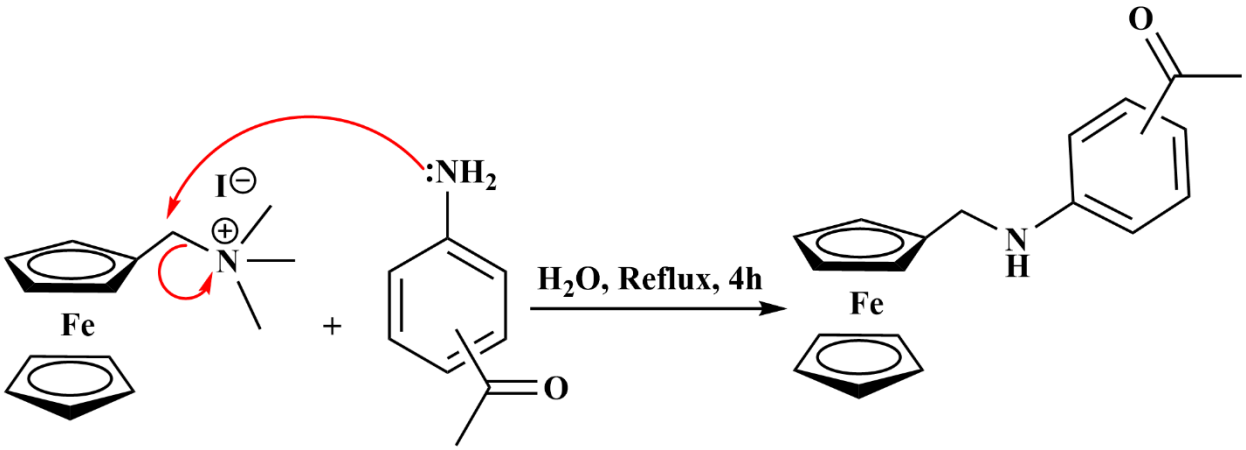


***Figure II.7.*** *Proposed reaction mechanism for the formation of N-[**(ferrocenyl)**methyl]**acetylaniline derivatives** via nucleophilic substitution.*

As illustrated in **Figure II.7**, the transformation proceeds via a bi**molecular** nucleophilic substitution **(SN2)** mechanism, where the lone pair of the amino group attacks the electrophilic methylene carbon bonded to the quaternary ammonium centre. This process results in the displacement of trimethylamine as a leaving group and the formation of the **ferrocenyl**methylamine linkage **(Ouennoughi et al., 2017)**.

The efficiency of this reaction can be rationalised by both electronic and structural factors. The **ferrocenyl** moiety exhibits electron-donating properties, which facilitate stabilisation of the transition state and enhance the reactivity of the methylene carbon **(Chebbah et al., n.d)**. In parallel, the quaternary ammonium group acts as an excellent leaving group, enabling smooth bond cleavage under aqueous conditions. Such behaviour is consistent with previously reported reactivity patterns of **ferrocenyl**methyl **derivatives**, where favourable electronic delocalisation

and structural flexibility promote nucleophilic substitution processes**. (Hanane et al., 2023Adaika et al., 2025)**

The chemical structures of the obtained compounds are presented in **Figure II.8**, highlighting the positional variation of the acetyl substituent on the aromatic ring.

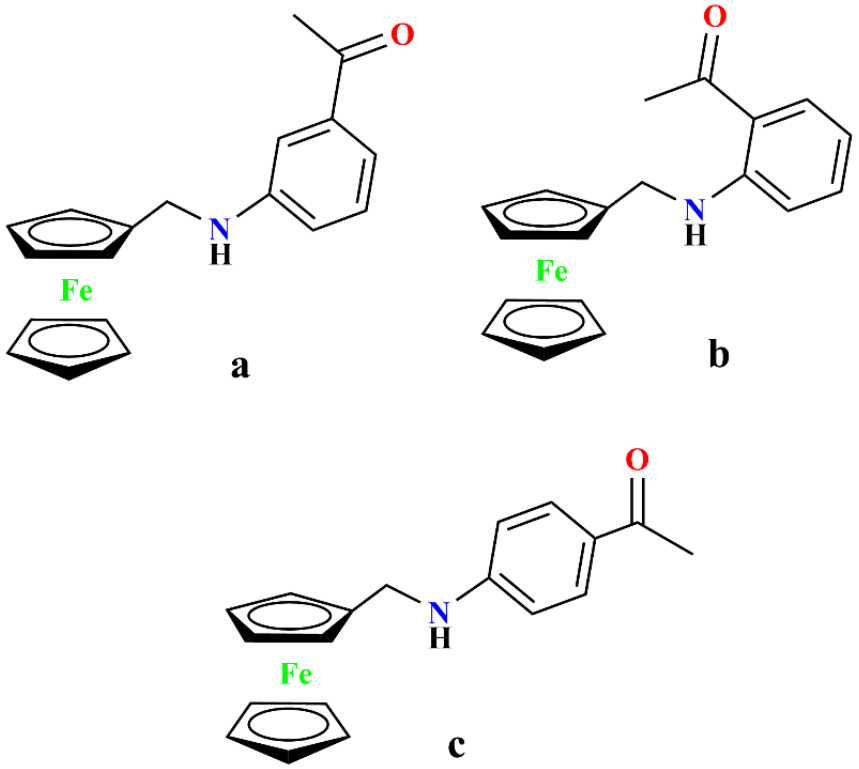


***Figure II.8.*** *Chemical structures of the synthesised* ***ferrocenyl acetylaniline derivatives****: **(a)** FcMe2Ac **(ortho)**, **(b)** FcMe3Ac **(meta)**, and **(c)** FcMe4Ac **(para)**.*

As shown in **Figure II.8**, the three **derivatives** differ solely by the position of the acetyl group, which significantly influences steric accessibility and electronic distribution within the molecule. These factors are known to play a critical role in modulating the nucleophilicity of the amino group and, consequently, the efficiency of the substitution reaction**. (Lanez et al., 2025)**

To further evaluate the synthetic performance, the yields and physical characteristics of the obtained compounds are summarised in **Table 1**.

**Table 1.** Yields and physical properties of the synthesised **ferrocenyl acetylaniline derivatives**.

| **Compound** | **Substituent Position** | **Yield (%)** | **Appearance** | **Melting Point (°C)** |
|---|---|---|---|---|

| | | | | |
|---|---|---|---|---|
| **FcMe2Ac** | Ortho | 77 | Yellow crystalline solid | 148–150 |
| **FcMe3Ac** | Meta | 48 | Yellow–orange solid | 138–140 |
| **FcMe4Ac** | Para | 80 | Deep yellow solid | 162–164 |

As shown in **Table 1**, the reaction yields follow the order: FcMe4Ac > FcMe2Ac > FcMe3Ac

This trend can be rationalised by considering both steric and electronic effects, which are known to govern nucleophilic substitution reactions in aromatic amines. The para-substituted derivative **(FcMe4Ac)** exhibited the highest yield **(80%)**, reflecting minimal steric hindrance and favourable resonance interaction between the acetyl group and the amino functionality. This electronic delocalisation enhances the nucleophilicity of the amine, thereby facilitating the substitution process. **(Lanez et al., 2025)**

In contrast, the meta derivative **(FcMe3Ac)** showed a significantly lower yield **(48%)**, which can be attributed to the absence of resonance interaction between the substituents. In the meta position, the acetyl group exerts mainly an inductive electron-withdrawing effect, reducing the electron density on the amino group and consequently its nucleophilicity.

The ortho derivative **(FcMe2Ac)** presented intermediate behaviour **(77%)**, where steric hindrance between adjacent substituents partially limits the accessibility of the nucleophilic site, despite favourable electronic effects.

These observations are in good agreement with previously reported studies on substituted aniline **derivatives**, where both steric congestion and electronic factors significantly influence reactivity. Furthermore, the results confirm that the adopted synthetic strategy is robust and well adapted for the preparation of **ferrocenyl derivatives** with controlled structural variation. **(Benine et al., 2025)**

## 2. FT-IR Spectral Analysis

The structural features of the synthesised **ferrocenyl acetylaniline derivatives** were initially investigated by Fourier-transform infrared **(FT-IR)** spectroscopy. The recorded spectra for FcMe2Ac, FcMe3Ac and FcMe4Ac are presented in **Figure II.9**, while the principal absorption bands and their corresponding assignments are summarised in **Table 2**.

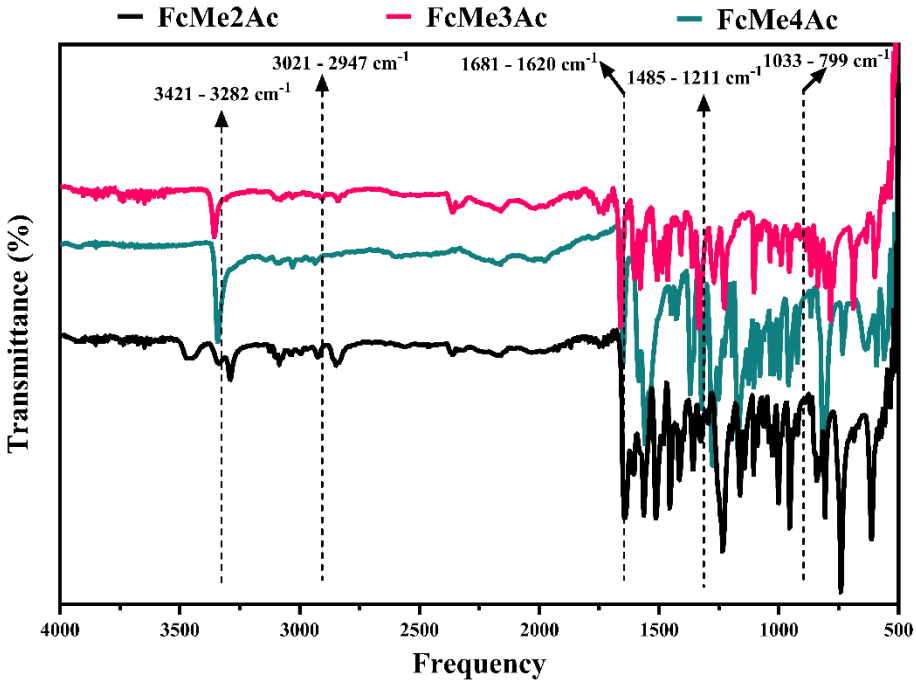


***Figure II.9.*** *FT-IR spectra of the synthesised* ***ferrocenyl acetylaniline derivatives****.*

**Table 2.** Characteristic FT-IR absorption bands **($cm^{-1}$)** and their assignments for the synthesised compounds.

| Assignment | FcMe2Ac ($cm^{-1}$) | FcMe3Ac ($cm^{-1}$) | FcMe4Ac ($cm^{-1}$) | Description |
|---|---|---|---|---|
| **N–H stretching** | 3426, 3291 | 3432, 3338 | 3445, 3345 | Secondary amine vibration |
| **Ar–C–H stretching** | 3082 | — | — | Aromatic C–H |
| **C=O stretching** | 1647 | 1650 | 1651 | Acetyl carbonyl group |
| **C=C (aromatic)** | 1566, 1516 | 1582, 1510 | 1589, 1562 | Aromatic ring vibrations |
| **C–N stretching** | 1146 | 1170 | 1173 | Amine linkage |
| **C–H bending** | 1454, 1416 | 1450, 1365 | 1369 | Methyl/aromatic bending |
| **Out-of-plane C–H** | 1003, 617 | 820 | 822 | Aromatic substitution pattern |

As shown in **Figure II.9**, all compounds display closely related spectral profiles, confirming the preservation of the **ferrocenyl acetylaniline** framework across the series. Minor variations in band positions and intensities are observed and can be attributed to the different substitution patterns on the aromatic ring. **(Tlili et al., 2024)**

Broad absorption bands in the region 3445–3291 $cm^{-1}$ are assigned to N–H stretching vibrations, confirming the presence of secondary amine functionality formed during the nucleophilic substitution reaction. The slight shifts observed between the **derivatives** reflect variations in hydrogen bonding interactions and local electronic environments. **(Tlili et al., 2025)**

The strong and well-defined bands located at 1651–1647 $cm^{-1}$ correspond to the stretching vibration of the carbonyl **(C=O)** group of the acetyl substituent. The consistency of this band across all compounds confirms that the carbonyl functionality remains intact during synthesis.

Aromatic C=C stretching vibrations are observed in the region 1589–1510 $cm^{-1}$, providing clear evidence for the presence of the substituted benzene ring. Additionally, the bands detected between 1173–1146 $cm^{-1}$ are attributed to C–N stretching vibrations, confirming the successful formation of the **ferrocenyl**methyl–aniline linkage.

Particularly informative are the out-of-plane C–H bending vibrations observed between 820 and 617 $cm^{-1}$, which are highly sensitive to substitution patterns. The differences in these bands among the ortho, meta and para **derivatives** provide strong evidence for the positional variation of the acetyl group on the aromatic ring.

Overall, the FT-IR data provide clear confirmation of the successful synthesis of the target compounds. The observed spectral features are fully consistent with the proposed structures and align well with reported data for related **ferrocenyl** and substituted aniline systems. **(Khamouli et al., 2022)**

## 3. UV–Visible Spectral Analysis

The electronic absorption properties of the synthesised **ferrocenyl acetylaniline derivatives** were investigated using UV–visible spectroscopy in DMSO. The corresponding spectra are presented in **Figure II.10**, and the absorption maxima are summarised in **Table 3**.

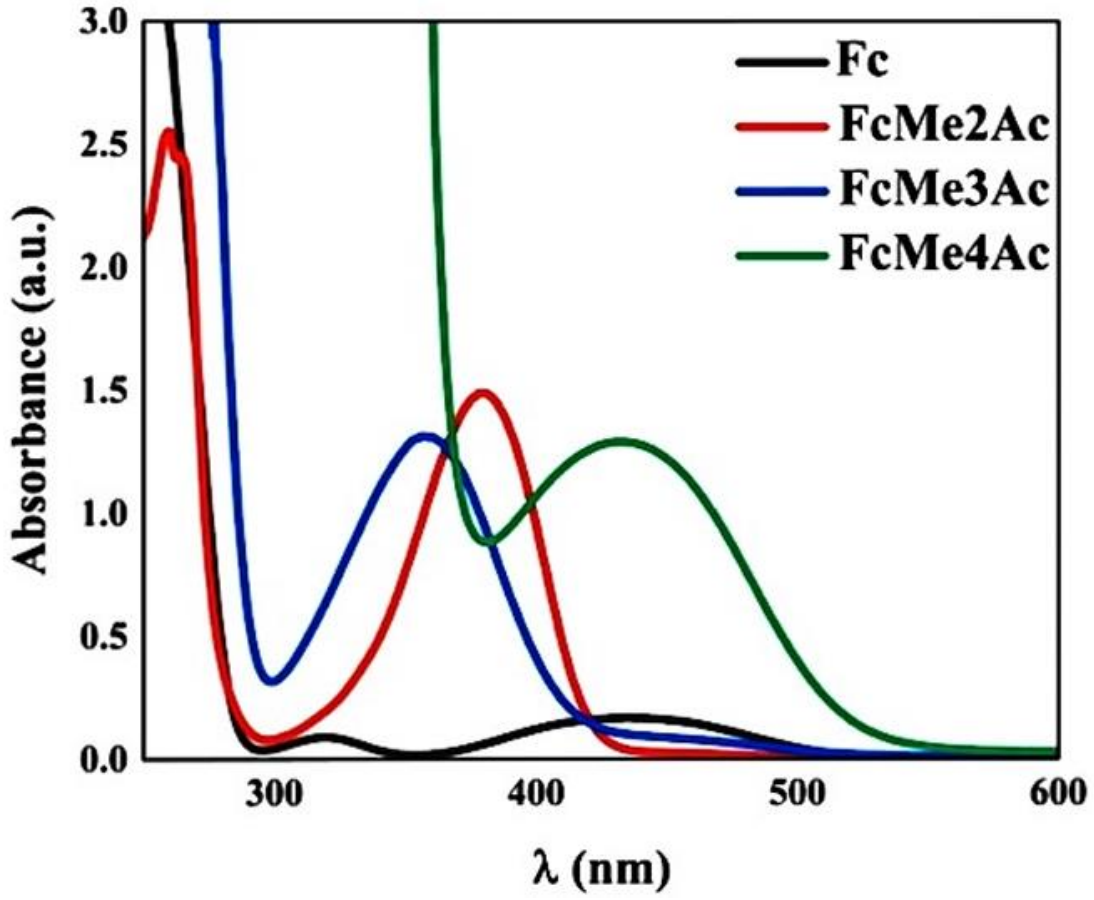


***Figure II.10.*** *UV–visible absorption spectra of the synthesised* ***ferrocenyl acetylaniline derivatives***.

**Table 3.** UV–visible absorption maxima **(λmax)** of the synthesised **ferrocenyl acetylaniline derivatives**.

| Compound | λmax (nm) | Assignment |
|---|---|---|
| **FcMe2Ac** | 259 | π → π* **(aromatic system)** |
| | 380 | d–d **($Fe^{2+}$ centre)** |
| **FcMe3Ac** | 268 | π → π* |
| | 402 | d–d transition |
| **FcMe4Ac** | 432 | d–d / charge transfer |

As illustrated in **Figure II.10**, all compounds exhibit characteristic absorption bands associated with both the aromatic system and the **ferrocenyl** moiety. Intense bands in the ultraviolet region **(259–268 nm)** are attributed to $\pi \rightarrow \pi^*$ transitions within the conjugated aromatic system, corresponding to electronic excitation within the benzene ring. **(Zouaghi et al., 2025)**

In the visible region, absorption bands between 380 and 432 nm are observed, corresponding to transitions involving the **ferrocenyl** iron centre. These transitions can be assigned to metal-centred d–d transitions and, in some cases, **ligand**-to-metal charge transfer **(LMCT)**, reflecting the interaction between the iron centre and the surrounding π-electron system. **(Zegheb et al., 2021)**

A pronounced bathochromic shift is observed from FcMe2Ac **(380 nm)** to FcMe4Ac **(432 nm)**, indicating an increase in electronic delocalisation in the para-substituted derivative. This behaviour arises from enhanced conjugation between the acetyl substituent and the aromatic system, which lowers the energy gap between **molecular** orbitals and facilitates lower-energy electronic transitions.

The meta derivative **(FcMe3Ac)** exhibits intermediate behaviour due to the absence of effective resonance interaction between substituents, limiting electron delocalisation. In contrast, the ortho derivative **(FcMe2Ac)**, although capable of resonance interaction, may experience steric effects that slightly distort **molecular** planarity and reduce conjugation efficiency.

These observations highlight the significant influence of substituent position on the electronic structure of **ferrocenyl derivatives**. Such variations in electronic distribution are expected to play a key role in modulating **molecular** recognition and interaction behaviour with biological targets **(Ben Amor et al., 2025)**

## 4. NMR Spectral Analysis

The structural elucidation of the synthesised **ferrocenyl acetylaniline derivatives** was comprehensively achieved using one-dimensional **($^{1}$H and $^{13}$C)** and two-dimensional **(HSQC and HMBC)** NMR techniques. These complementary analyses enabled precise assignment of all proton and carbon environments and provided unambiguous confirmation of the **molecular** structures. To facilitate interpretation, the spectra are presented individually for each compound, allowing direct correlation between spectral features and structural elements.

## 4.1. $^1$H NMR Analysis

The $^1$H NMR spectra of FcMe2Ac, FcMe3Ac and FcMe4Ac are presented in **Figure II.11**.

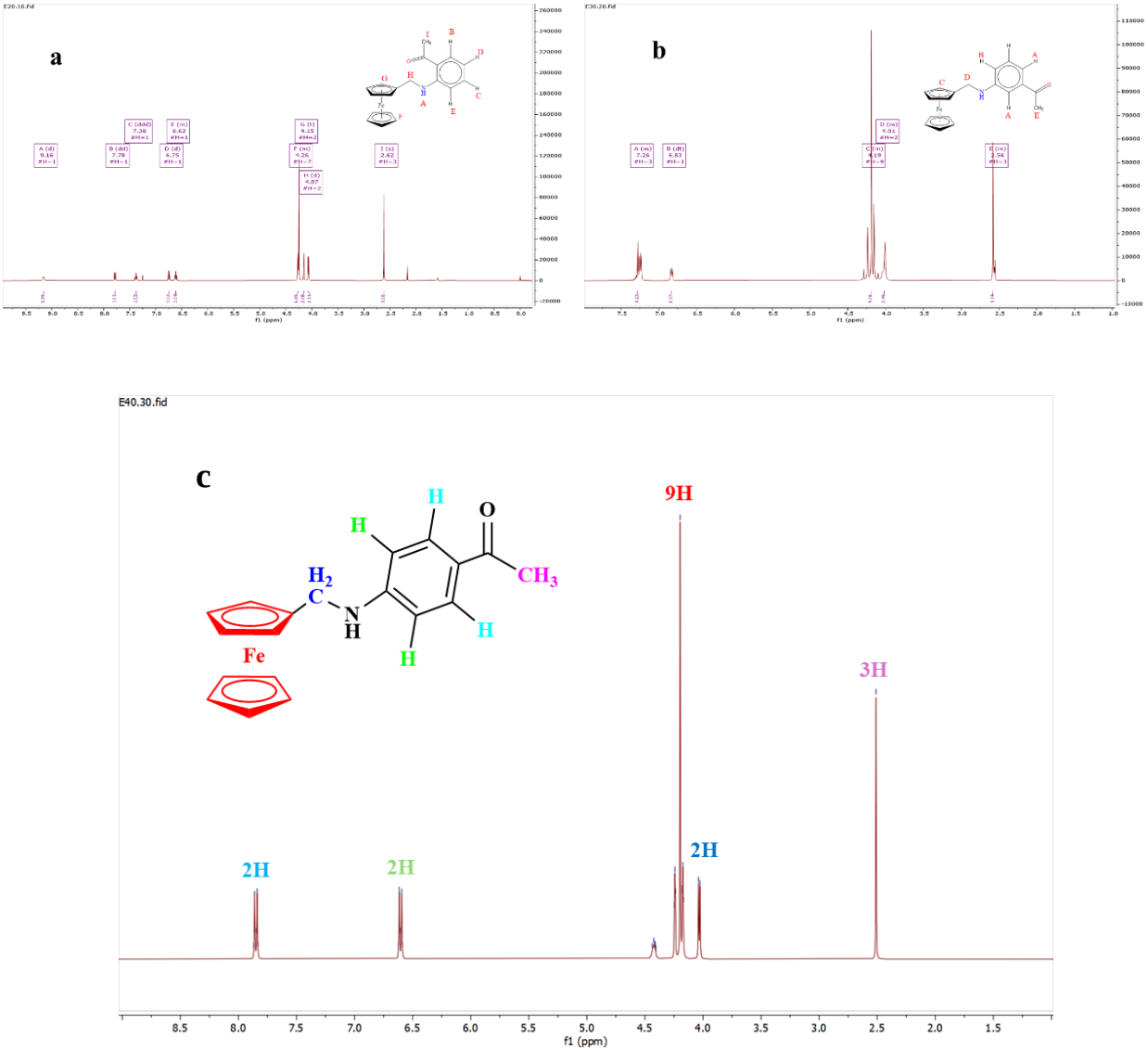


***Figure II.11.*** *$^1$H NMR spectra of the synthesised* ***ferrocenyl acetylaniline derivatives****: **(a)** FcMe2Ac, **(b)** FcMe3Ac, and **(c)** FcMe4Ac.*

As illustrated in **Figure II.11**, all compounds exhibit well-resolved signals consistent with the proposed **molecular** structures.

The methyl group of the acetyl functionality **(–$COCH_3$)** appears as a singlet in the region 2.35–2.60 ppm, confirming its isolated chemical environment. The methylene bridge **(–$CH_2$–N–)**, linking the **ferrocenyl** unit to the aromatic ring, is observed as a doublet at approximately 4.30 ppm, providing clear evidence for the formation of the C–N bond. **(Rebiai et al., 2014)**

The **ferrocenyl** moiety displays its characteristic spectral features. The unsubstituted cyclopentadienyl ring **($C_5H_5$)** appears as a sharp singlet around 4.15–4.20 ppm, reflecting its high symmetry. In contrast, the substituted cyclopentadienyl ring **($C_5H_4$)** gives rise to multiplet signals in the region 3.40–4.10 ppm, indicative of reduced symmetry upon substitution. This splitting pattern is a well-established signature of monosubstituted **ferrocenyl** systems.

Aromatic protons are detected between 6.6 and 7.8 ppm, exhibiting distinct splitting patterns depending on the substitution position. The ortho, meta and para isomers can be clearly differentiated based on their coupling patterns and signal multiplicity, reflecting differences in electronic distribution and proton–proton interactions within the aromatic ring.

The NH proton appears as a downfield singlet around 8.9–9.0 ppm for FcMe2Ac and FcMe3Ac, suggesting involvement in inter**molecular** or intra**molecular** hydrogen bonding. In FcMe4Ac, a slight upfield shift is observed, which may be attributed to enhanced electronic delocalisation in the para-substituted system, reducing deshielding effects. **(Ben Amor et al., 2025)**

## 4.2. $^{13}$C NMR Analysis

The $^{13}$C NMR spectra of the synthesised compounds are shown in **Figure II.12**.

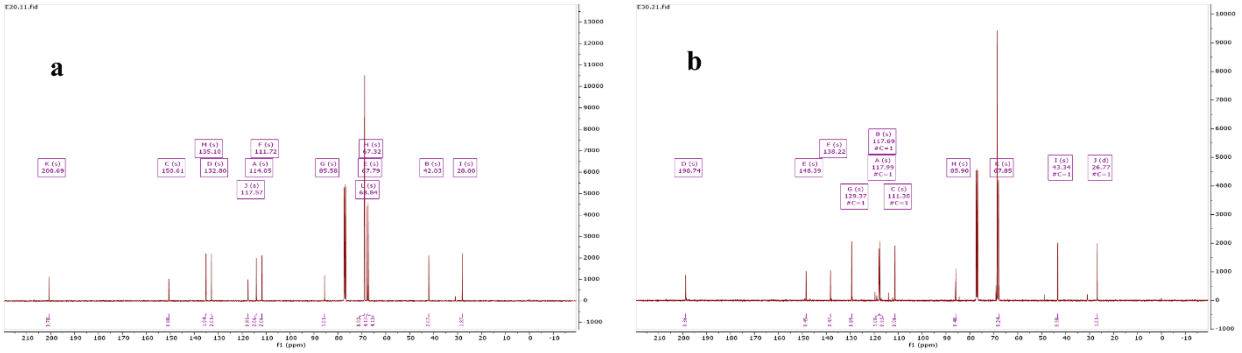

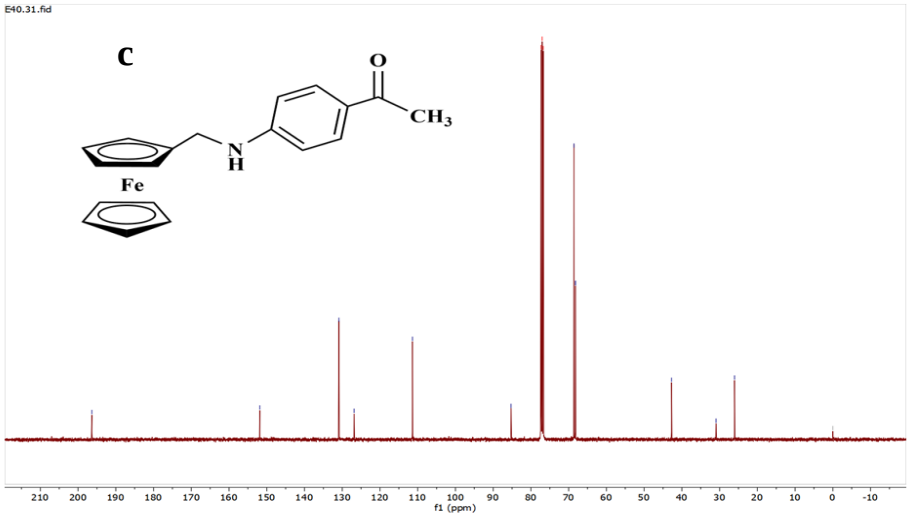


***Figure II.12.*** *$^{13}$C NMR spectra of the synthesised* ***ferrocenyl acetylaniline derivatives****:* ***(a)*** *FcMe2Ac,* ***(b)*** *FcMe3Ac, and* ***(c)*** *FcMe4Ac.*

As illustrated in **Figure II.12**, the spectra provide clear evidence for the carbon framework of the compounds.

The carbonyl carbon **(C=O)** is observed in the downfield region between 194 and 210 ppm, confirming the presence of the acetyl group. The variation in chemical shift among the three **derivatives** reflects differences in electronic environment due to substituent position.

The methylene carbon **($CH_2$–N)** appears consistently around 42–43 ppm, confirming the linkage between the **ferrocenyl** moiety and the aromatic system.

The **ferrocenyl** carbons are detected in the range 66–69 ppm, corresponding to the cyclopentadienyl rings. The ipso carbon bonded to the substituent appears slightly downfield due to its distinct electronic environment.

Aromatic carbons are distributed between 112 and 154 ppm, with slight variations depending on substitution pattern, which is consistent with substituted benzene **derivatives**. **(Khamouli et al., 2019)**

## 4.3. Two-Dimensional NMR Analysis (HSQC and HMBC)

Two-dimensional NMR spectroscopy was employed to achieve unambiguous structural assignment and to confirm the connectivity within the synthesised **ferrocenyl acetylaniline derivatives**. The HSQC and HMBC spectra are presented separately to allow a clear interpretation of both direct and long-range correlations.

The HSQC spectra of FcMe2Ac, FcMe3Ac and FcMe4Ac are shown in **Figure II.13**, while the corresponding HMBC spectra are presented in **Figure II.14**.

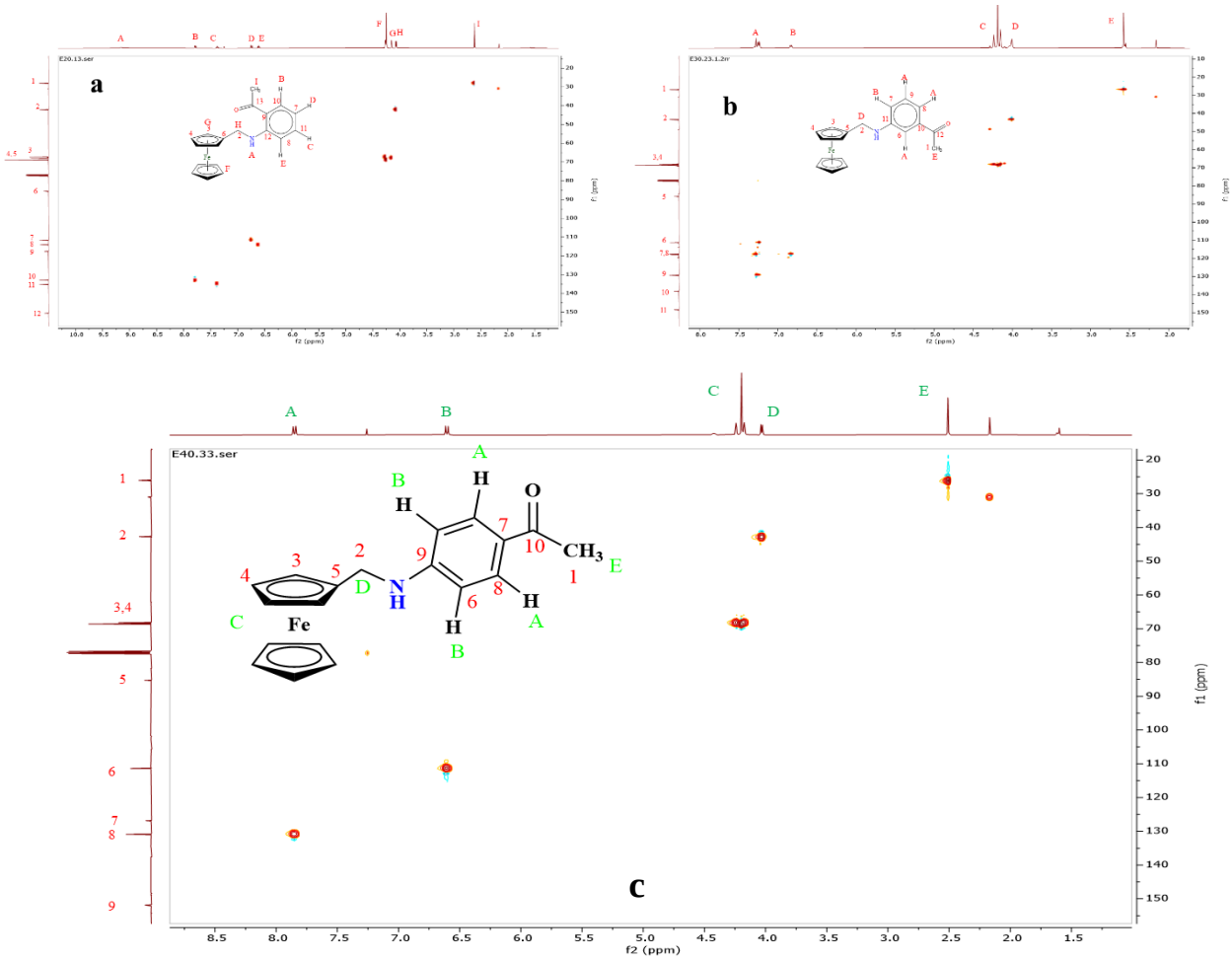


**Figure II.13.** *HSQC spectra of the synthesised* ***ferrocenyl acetylaniline derivatives****: **(a)** FcMe2Ac, **(b)** FcMe3Ac, and **(c)** FcMe4Ac.*

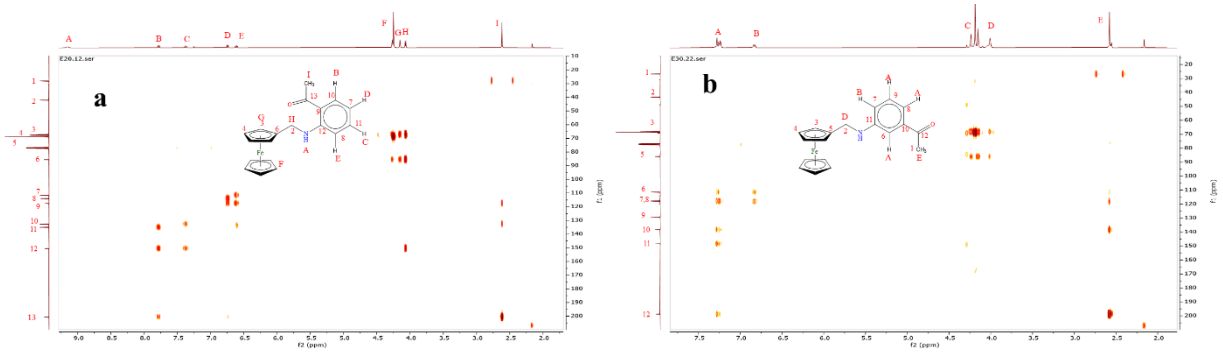

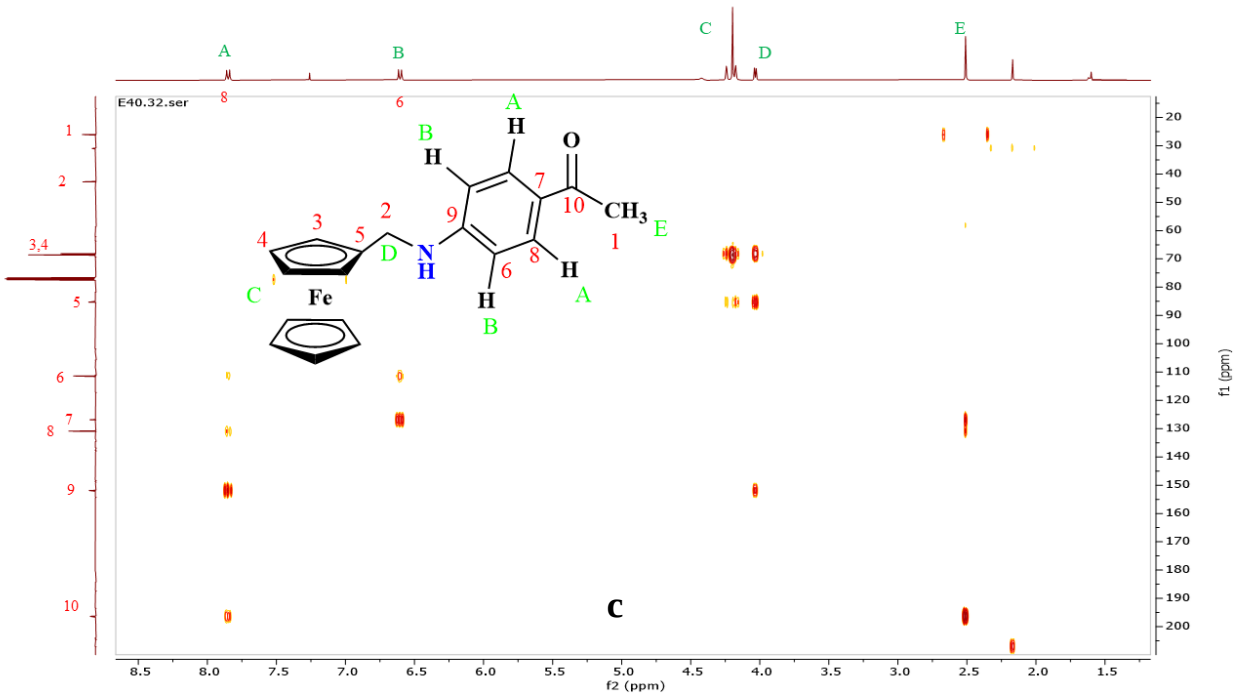


***Figure II.14.*** *HMBC spectra of the synthesised* ***ferrocenyl acetylaniline derivatives****:* ***(a)*** *FcMe2Ac,* ***(b)*** *FcMe3Ac, and* ***(c)*** *FcMe4Ac.*

As illustrated in **Figure II.13**, the HSQC spectra provide direct one-bond correlations between proton and carbon nuclei **($^1$JCH)**, allowing precise assignment of all protonated carbon atoms. The methylene protons **(–CH$_2$–N–)**, observed around 4.30 ppm in the $^1$H NMR spectra, show clear cross-peaks with their corresponding carbon signals at approximately 42–43 ppm, confirming the presence of the **ferrocenyl**methyl linkage.

Similarly, the signals corresponding to the cyclopentadienyl rings exhibit well-defined correlations. The unsubstituted Cp ring **(C$_5$H$_5$)** shows a single correlation pattern consistent with its symmetry, whereas the substituted Cp ring **(C$_5$H$_4$)** displays multiple correlations reflecting the loss of equivalence upon substitution. These observations are characteristic of monosubstituted **ferrocenyl** systems and further confirm the structural integrity of the organometallic core.

The aromatic proton signals also show distinct HSQC correlations with their corresponding carbon atoms in the region 112–140 ppm, enabling clear assignment of the benzene ring protons. The differences observed between the ortho, meta and para **derivatives** further support the positional variation of the acetyl substituent. **(Mouada et al., 2024) (Lanez et al., 2015)**

In contrast, the HMBC spectra **Figure II.14** provide long-range correlations **($^{2}$JCH and $^{3}$JCH)**, which are essential for confirming the connectivity between different fragments of the molecule. In particular, strong correlations are observed between the methylene protons **(–$CH_2$–N–)** and the aromatic carbons, confirming the formation of the C–N bond linking the **ferrocenyl** unit to the aniline moiety.

Additional long-range correlations between aromatic protons and the carbonyl carbon **(C=O)** are observed, allowing precise localisation of the acetyl group on the aromatic ring. These correlations are especially important for distinguishing between the regioisomers, as the HMBC patterns differ significantly depending on the substitution position **(ortho, meta or para)**.

Furthermore, correlations involving the **ferrocenyl** carbons provide additional confirmation of the substitution pattern on the cyclopentadienyl ring. The combined HSQC and HMBC data therefore establish a complete mapping of proton–carbon connectivity within the molecules. **(Bekkar et al., 2025) (Bekkar et al., 2025)**

Overall, the two-dimensional NMR analysis provides definitive structural confirmation of the synthesised **ferrocenyl acetylaniline derivatives**. The observed correlation patterns are fully consistent with the proposed structures and are in excellent agreement with literature reports on related **ferrocenyl** compounds, where HSQC and HMBC techniques are commonly used to validate substitution patterns and **molecular** connectivity.

## 5. Cyclic Voltammetry Characterization

### 5.1. Redox Properties and Voltammetric Response

The electrochemical properties of FcMe2Ac, FcMe3Ac and FcMe4Ac were investigated by **cyclic voltammetry** in DMSO **(1 mM)** containing 0.1 M $Bu_4NBF_4$ as supporting electrolyte, using $Hg/Hg_2Cl_2$ as reference electrode. Measurements were performed within a potential window of −0.60 to +0.60 V at a scan rate of 100 $mV \cdot s^{-1}$, with the $Fc/Fc^{+}$ **redox** couple used as an internal reference.

The corresponding voltammograms are presented in **Figure II.15**, where the responses of the substituted **derivatives** are compared with that of **ferrocene**.

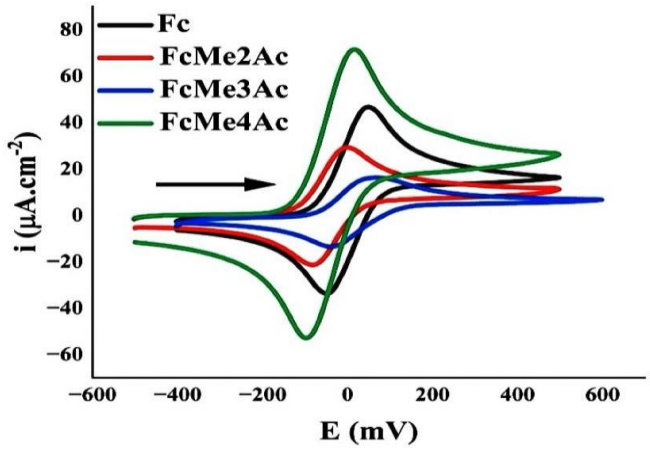


***Figure II.15.*** *Cyclic voltammograms of Fc, FcMe2Ac, FcMe3Ac and FcMe4Ac recorded in DMSO containing 0.1 M $Bu_4NBF_4$ at a scan rate of 100 $mV{\cdot}s^{-1}$* ***(referenced to $Fc^+$/Fc)***.

As shown in **Figure II.15**, all **derivatives** exhibit a single well-defined **redox** couple corresponding to the Fe**(II)**/Fe**(III)** transition, confirming that the **ferrocenyl** unit retains its electroactivity after functionalization. **(Lanez et al., n.d.)**

A systematic anodic shift in formal potential is observed following the order: FcMe2Ac **(43.9 mV)** < FcMe3Ac **(51.0 mV)** < FcMe4Ac **(57.5 mV)**

This trend reflects the influence of the **acetylaniline** substituent on the electronic environment of the **ferrocenyl** centre. The positive shift indicates a decrease in electron density at the iron centre, suggesting that oxidation becomes progressively less favourable. This behaviour can be attributed to the electron-withdrawing nature of the acetyl group, which modulates the electron-donating ability of the **ferrocenyl** moiety through inductive and resonance effects. **(Nacer and Lanez ,2013)**

The anodic-to-cathodic peak current ratios **(Ipa/Ipc ≈ 1)** indicate that the **redox** process is chemically reversible. However, the observed peak-to-peak separation **(ΔEp = 87.8–115 mV)** exceeds the theoretical value expected for an ideal reversible one-electron process **(59 mV)**, indicating a quasi-reversible electron transfer. **(Nacer and Lanez ,2013)**

This deviation suggests the presence of kinetic limitations, which may arise from:

- finite heterogeneous electron-transfer rates
- uncompensated ohmic resistance in the non-aqueous medium

- structural reorganisation accompanying oxidation of the **ferrocenyl** unit

## 5.2. Scan Rate Dependence and Mass Transport Regime

The influence of scan rate on the electrochemical response was examined in the range 100–500 mV·s⁻¹. The resulting voltammograms are shown in **Figure II.16**, while the dependence of anodic peak current on the square root of scan rate is presented in **Figure II.17**.

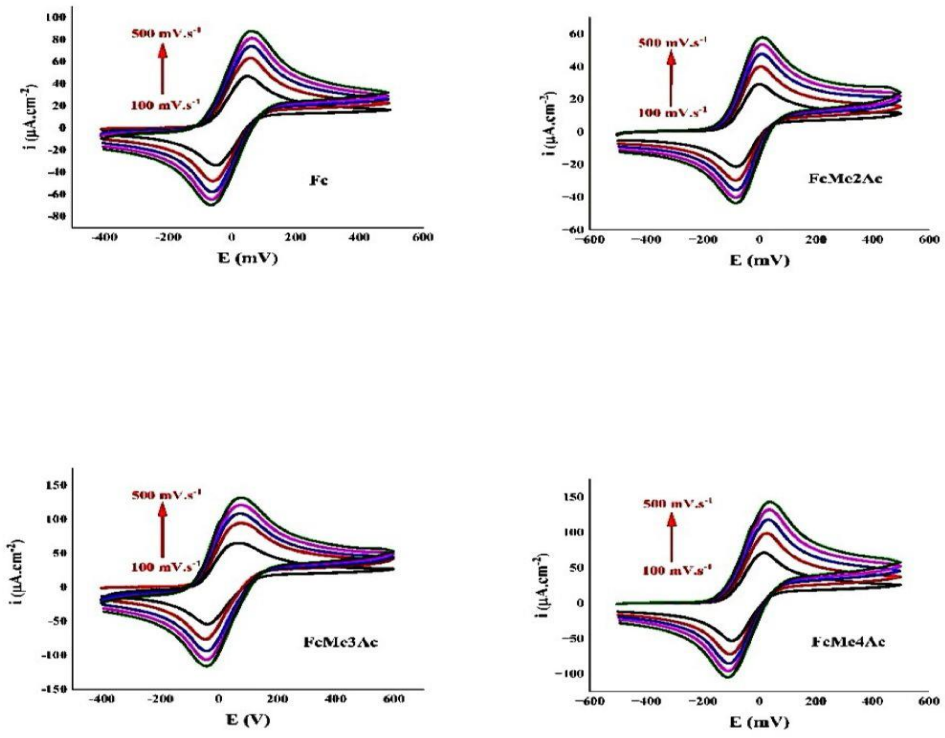


***Figure II.16.*** *Cyclic voltammograms of Fc, FcMe2Ac, FcMe3Ac and FcMe4Ac at different scan rates* ***(100–500 mV·s⁻¹)****.*

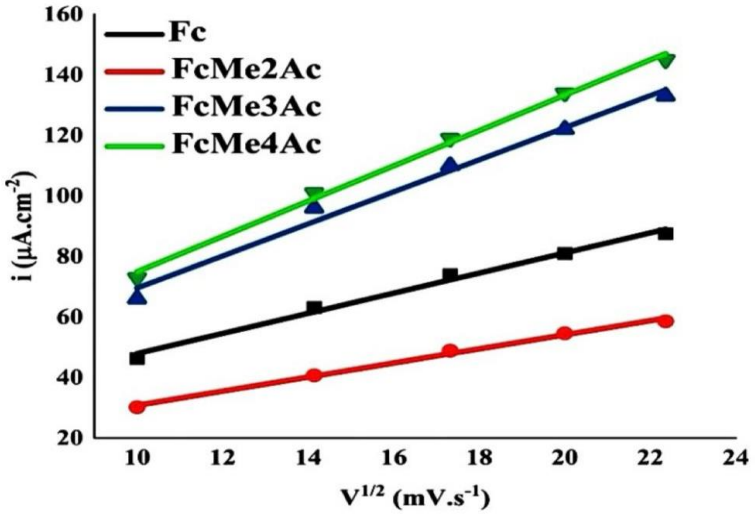


***Figure II.17.*** *Linear variation of anodic peak current* ***($i_{pa}$)*** *as a function of the square root of scan rate* ***($v^{1/2}$)*****.**

As illustrated in **Figure II.16**, increasing the scan rate results in a proportional increase in both anodic and cathodic peak currents, without significant distortion of peak shape. This behaviour indicates that the **redox** process is not governed by adsorption phenomena.

A linear relationship between anodic peak current **($i_{pa}$)** and $v^{1/2}$ is clearly observed in **Figure II.17** for all compounds. The corresponding linear regression equations **Table 4** exhibit high correlation coefficients **($R^2$ = 0.980–0.994)**, confirming excellent linearity. **(Khelef and Lanez 2015)**

The high $R^2$ values demonstrate that the experimental data closely follow the Randles–Ševčík model, thereby confirming that the electron transfer process is diffusion-controlled. Slight deviations from ideal linearity, particularly for FcMe3Ac **($R^2$ = 0.980)**, may reflect minor contributions from kinetic limitations or increased solution resistance. **(Zaiz & Lanez, 2015)**

## 5.3. Diffusion Coefficients and Transport Properties

The diffusion coefficients of the electroactive species were determined using the Randles–Ševčík **Equation 1** for a reversible system, which relates the peak current to the square root of the scan rate:

$$ip_a = 2.69\times10^5\left(\sqrt{n}\right)^3 SC\sqrt{D}\sqrt{v}$$

**Equation 1:** *where $i_p$ is the peak current **(A)**, $n$is the number of electrons transferred, $A$ is the electrode surface area **($cm^2$)**, $C$ is the concentration of the electroactive species **($mol.cm^{-3}$)**, $D$ is the diffusion coefficient **($cm^2 \cdot s^{-1}$)**, and $\nu$ is the scan rate **($V \cdot s^{-1}$)**.*

The diffusion coefficients **(D)** were calculated using the Randles–Ševčík equation, and the results are presented in **Table 4.**

**Table 4.** Diffusion coefficients and linear regression parameters obtained from Randles–Ševčík analysis.

| Compound | Equation | $R^2$ | $D \times 10^{-7}$ ($cm^2 \cdot s^{-1}$) |
|---|---|---|---|
| **Fc** | y = 3.321x + 14.727 | 0.987 | 6.952 |
| **FcMe2Ac** | y = 2.328x + 7.539 | 0.993 | 1.108 |
| **FcMe3Ac** | y = 5.298x + 16.578 | 0.980 | 5.738 |
| **FcMe4Ac** | y = 5.831x + 16.638 | 0.994 | 2.255 |

As shown in **Table 4**, the diffusion coefficients of the substituted **derivatives** are significantly lower than that of **ferrocene**. This decrease can be attributed to several physicochemical factors:

- Increased **molecular** volume, leading to reduced translational mobility
- Enhanced solute–solvent interactions in polar DMSO medium
- Greater structural complexity and conformational flexibility

FcMe2Ac exhibits the lowest diffusion coefficient **($1.11 \times 10^{-7}$ $cm^2 \cdot s^{-1}$)**, suggesting stronger inter**molecular** interactions and possibly a more hindered diffusion pathway. In contrast, FcMe3Ac retains a relatively higher diffusion coefficient, which may be associated with a more favourable **molecular** geometry and reduced steric constraints. **(Lanez & Hemmami, 2016) (Benyza et al., 2022)**

## 5.4. Electron Transfer Kinetics

The heterogeneous electron-transfer rate constants were estimated using Nicholson's method, which relates the peak-to-peak separation to the kinetic parameter Ψ and the standard rate constant as described in **Equation 2**:

$$\psi = \frac{K_s}{\sqrt{\pi D \frac{nFv}{RT}}}$$

**Equation 2:** *where $k_S$ is the standard heterogeneous electron-transfer rate constant* ***(cm.s⁻¹)****, D is the diffusion coefficient* ***(cm².s⁻¹)****, n is the number of electrons transferred, F is the Faraday constant* ***(96,500 C.mol⁻¹)****, ν is the scan rate* ***(V.s⁻¹)****, R is the gas constant* ***(8.314 J.mol⁻¹.K⁻¹)****, and T is the absolute temperature* ***(K)***.

The heterogeneous electron-transfer rate constants **($k_s$)** were estimated using Nicholson's method, and the results are summarised in **Table 5**.

**Table 5.** Nicholson kinetic parameters **(Ψ, ΔEp)** and heterogeneous electron-transfer rate constants **($k_s$)**.

| Compound | Ψ | ΔEp (mV) | $k_s \times 10^3$ (cm·s⁻¹) |
|---|---|---|---|
| **Fc** | 1.51 | 73 | 2.88 |
| **FcMe2Ac** | 0.323 | 124 | 0.62 |
| **FcMe3Ac** | 0.074 | 263 | 0.14 |
| **FcMe4Ac** | 0.100 | 223 | 0.19 |

The obtained kinetic parameters clearly indicate a decrease in electron-transfer rates upon substitution. The order: Fc > FcMe2Ac > FcMe4Ac > FcMe3Ac, reflects the increasing complexity of the **molecular** structure and its impact on electron-transfer dynamics**. (Lanez et al., 2024)**

The relatively high $k_s$ value for **ferrocene** confirms its well-known fast and reversible electron-transfer behaviour. In contrast, the substituted **derivatives** exhibit slower kinetics, which can be explained by:

- Increased steric hindrance, limiting effective interaction with the electrode surface
- Higher reorganisation energy associated with structural changes during oxidation
- Reduced electronic coupling between the **ferrocenyl** centre and the electrode

The particularly low $k_s$ value for FcMe3Ac suggests that the meta substitution pattern is least favourable for efficient electron transfer, likely due to suboptimal electronic communication within the molecule. **(Filote et al., 2022)**

# 6. In Vitro Biological Evaluation

The biological potential of the synthesised **ferrocenyl acetylaniline derivatives** was systematically investigated through complementary **antidiabetic** and anti-inflammatory assays, in order to evaluate their multifunctional therapeutic relevance. These assays were selected to probe two closely related pathological processes, namely **carbohydrate** metabolism dysregulation and inflammation, both of which are strongly interconnected in metabolic disorders.

The experimental approach combines **enzyme inhibition** studies, protein denaturation assays, and spectroscopic binding analyses, allowing a comprehensive evaluation of both activity and mechanism. Particular emphasis was placed on correlating the observed biological effects with structural features of the **ferrocenyl derivatives**, thereby establishing a detailed structure–activity relationship **(SAR)**.

## 6.1. Antidiabetic Activity

### 6.1.1. Enzyme Inhibition Studies

The inhibitory effects of FcMe2Ac, FcMe3Ac and FcMe4Ac against **carbohydrate**-hydrolysing enzymes were evaluated and compared with acarbose, a clinically used α-glucosidase inhibitor. The concentration–response curves **Figure II.18** clearly demonstrate that all compounds exhibit a progressive increase in inhibition with increasing concentration, confirming a typical dose-dependent behaviour.

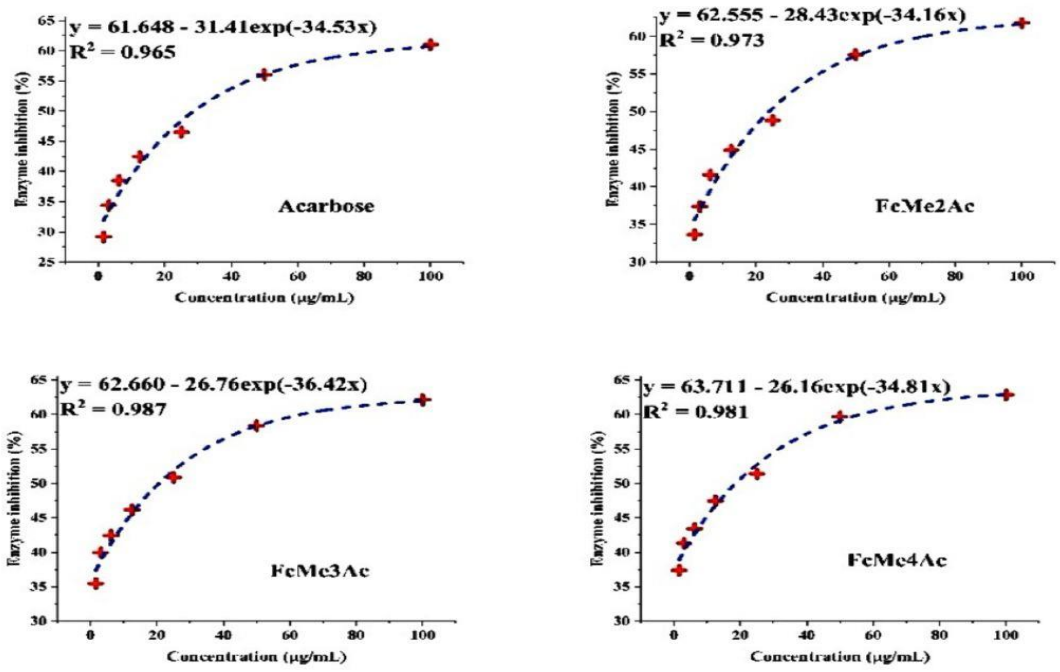


***Figure II.18.*** *Concentration–response curves for α-**amylase** inhibition by **ferrocenyl derivatives** and acarbose.*

The $IC_{50}$ values, obtained from non-linear regression fitting, are summarised in **Table 6**.

**Table 6.** $IC_{50}$ values for **enzyme inhibition**.

| Compound | Regression equation | $R^2$ | $IC_{50}$ (µg $mL^{-1}$) |
|---|---|---|---|
| **FcMe2Ac** | y = 62.55 − 28.43 exp**(−34.16x)** | 0.973 | 10.39 ± 0.31 |
| **FcMe3Ac** | y = 62.66 − 26.76 exp**(−36.42x)** | 0.987 | 8.93 ± 0.27 |
| **FcMe4Ac** | y = 63.71 − 26.16 exp**(−34.81x)** | 0.981 | 8.06 ± 0.24 |
| **Acarbose** | y = 61.65 − 31.41 exp**(−34.53x)** | 0.965 | 12.48 ± 0.37 |

The high correlation coefficients **($R^2$ = 0.965–0.987)** confirm the excellent fitting of the experimental data and validate the applied kinetic model. Importantly, all **ferrocenyl derivatives** exhibited significant inhibitory activity, with $IC_{50}$ values lower than that of acarbose under the same experimental conditions. **(Singirala et al. 2025)**

The observed activity order: FcMe4Ac > FcMe3Ac > FcMe2Ac > acarbose, strongly indicates that the **ferrocenyl** scaffold contributes positively to **enzyme inhibition**.

From a mechanistic perspective, inhibition of α-**amylase** and α-glucosidase involves interaction with catalytic residues responsible for glycosidic bond cleavage. The enhanced activity of FcMe4Ac can be attributed to several structural and electronic factors:

- Para substitution allows a more extended and planar **molecular** conformation, facilitating optimal accommodation within the enzyme active site.
- Improved electronic delocalisation enhances polarizability, promoting stronger inter**molecular** interactions.
- The **ferrocenyl** moiety, being highly lipophilic and **redox-**active, contributes to stabilising enzyme–**ligand complexes** through hydrophobic contacts and π-interactions.

In contrast, the reduced activity of FcMe2Ac may be associated with steric hindrance induced by ortho substitution, which can restrict proper orientation within the catalytic pocket. The meta derivative **(FcMe3Ac)** displays intermediate behaviour, consistent with its limited resonance interaction compared to the para isomer **(Cífková et al. 2025)**. These results suggest that **enzyme inhibition** is not solely governed by binding strength but also by the ability of the **ligand** to adopt a favourable conformation within the catalytic environment. **(Chajed et al. n.d.)**

### 6.1.2. Binding Constant and Thermodynamic Analysis

To gain further insight into the interaction mechanism, UV–visible titration experiments were performed, and the corresponding Benesi–Hildebrand plots are presented in **Figure II.19**.

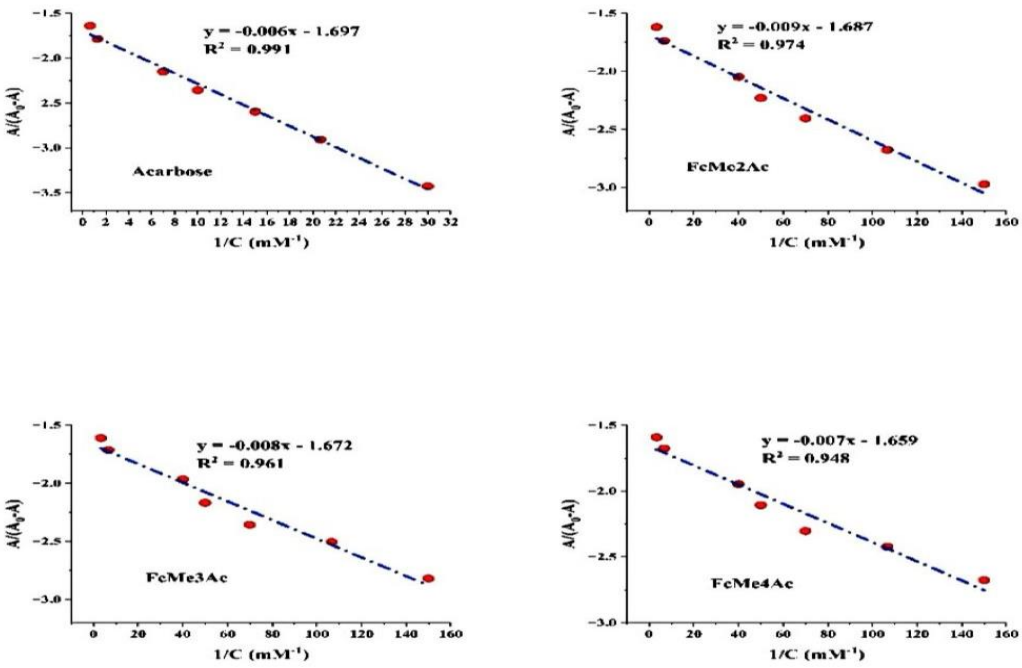


***Figure II.19.*** *Benesi–Hildebrand plots for interaction between* ***ferrocenyl derivatives*** *and target enzymes.*

The calculated binding constants **(K)** and thermodynamic parameters are summarised in **Table 7**.

**Table 7.** Binding constants and thermodynamic parameters for enzyme interaction.

| Compound | Equation | $R^2$ | K ($M^{-1}$) | ΔG (kJ $mol^{-1}$) |
|---|---|---|---|---|
| **FcMe2Ac** | y = −1.687 − 0.010x | 0.974 | $1.66 \times 10^6$ | −35.51 ± 0.85 |
| **FcMe3Ac** | y = −1.672 − 0.008x | 0.961 | $2.09 \times 10^6$ | −36.08 ± 0.90 |
| **FcMe4Ac** | y = −1.659 − 0.007x | 0.948 | $2.37 \times 10^6$ | −36.39 ± 0.92 |
| **Acarbose** | y = −1.697 − 0.006x | 0.991 | $2.83 \times 10^6$ | −36.83 ± 0.95 |

The excellent linearity confirms the validity of the applied model and supports the reliability of the calculated parameters.

All compounds exhibit high binding affinities **($10^6$ $M^{-1}$ range)**, indicating strong interaction with the enzyme. Although acarbose shows the highest binding constant, the **ferrocenyl derivatives** remain within the same order of magnitude, demonstrating comparable interaction capability. **(Piñeiro et al. 2025)**

The negative Gibbs free energy values confirm that all interactions are thermodynamically spontaneous. The slightly more negative ΔG values observed for FcMe4Ac indicate a more favourable binding process, which is consistent with its superior inhibitory activity.

The interaction mechanism likely involves a combination of:

- Hydrogen bonding with catalytic residues
- π–π stacking interactions with aromatic amino acids
- Hydrophobic interactions mediated by the **ferrocenyl** core

The strong correlation between $IC_{50}$ values and binding constants suggests that binding affinity is a key determinant of inhibitory activity, reinforcing the validity of the proposed mechanism. **(Aispuro-Pérez et al., 2025)**

## 6.2. Anti-Inflammatory Activity

### 6.2.1. Inhibition of BSA Denaturation

The anti-**inflammatory activity** was evaluated using the BSA denaturation assay, which mimics protein destabilisation processes occurring under inflammatory conditions. The inhibition profiles are shown in **Figure II.20**.

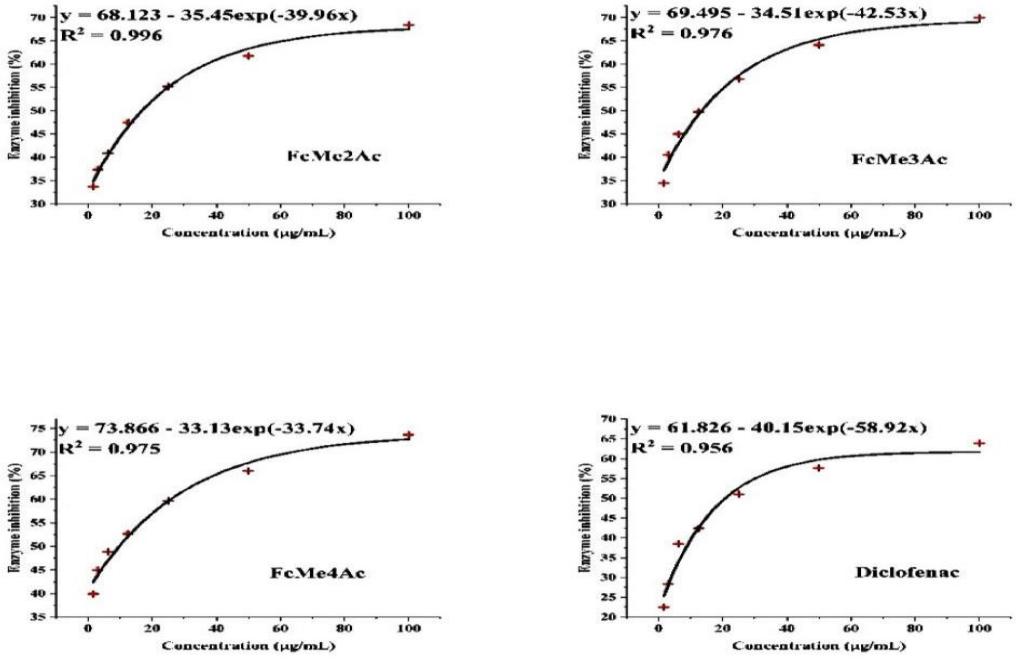


***Figure II.20.*** *Concentration-dependent inhibition of BSA denaturation by* ***ferrocenyl derivatives*** *and diclofenac.*

All compounds exhibited a sigmoidal dose–response behaviour, characteristic of protein stabilisation processes. The $IC_{50}$ values are summarised in **Table 8**.

**Table 8.** $IC_{50}$ values for inhibition of BSA denaturation.

| Compound | Regression equation | $R^2$ | $IC_{50}$ (µg $mL^{-1}$) |
|---|---|---|---|
| **FcMe2Ac** | y = 68.12 − 35.45 exp**(−39.96x)** | 0.996 | 7.29 ± 1.22 |
| **FcMe3Ac** | y = 69.50 − 34.51 exp**(−42.53x)** | 0.976 | 5.83 ± 0.85 |
| **FcMe4Ac** | y = 73.87 − 33.13 exp**(−33.74x)** | 0.975 | 4.22 ± 0.79 |
| **Diclofenac** | y = 61.83 − 40.15 exp**(−58.92x)** | 0.956 | 9.01 ± 0.78 |

The activity order: FcMe4Ac > FcMe3Ac > FcMe2Ac > diclofenac**,** indicates that all **ferrocenyl derivatives** exhibit superior protein stabilisation compared to the reference drug.

This behaviour can be interpreted in terms of protein–**ligand** interaction mechanisms. During thermal denaturation, proteins undergo conformational changes leading to loss of structure. The tested compounds appear to stabilise the native conformation by forming non-covalent interactions with the protein surface. **(Fahmy et al. 2025)**, **(Sargsyan et al. 2025)**
The enhanced activity of FcMe4Ac suggests:

- stronger interaction with hydrophobic domains of the protein
- improved electronic distribution facilitating binding
- optimal steric accessibility for interaction with key residues

### 6.2.2. Binding Interaction with BSA

The interaction between the compounds and BSA was further analysed spectroscopically, and the corresponding plots are presented in **Figure II.21**.

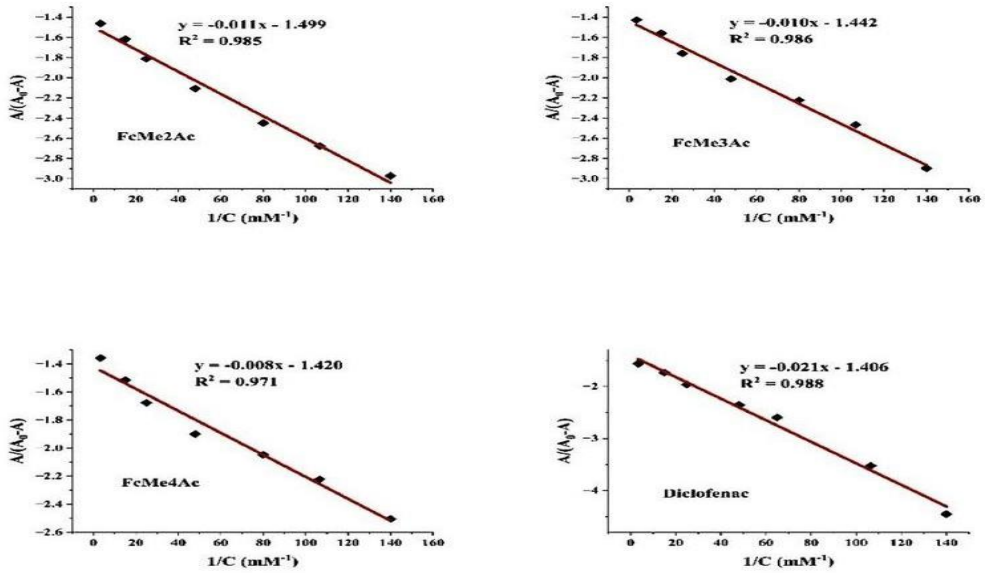


***Figure II.21.*** *Binding plots for interaction between* ***ferrocenyl derivatives*** *and BSA. The calculated parameters are summarised in* ***Table 9****.*

**Table 9.** Binding constants and thermodynamic parameters for BSA interaction**.**

| Compound | Equation | $R^2$ | K ($M^{-1}$) | ΔG (kJ $mol^{-1}$) |
|---|---|---|---|---|
| **FcMe2Ac** | y = −1.499 − 0.011x | 0.985 | $1.36 \times 10^6$ | −35.02 ± 3.45 |
| **FcMe3Ac** | y = −1.441 − 0.010x | 0.986 | $1.42 \times 10^6$ | −35.12 ± 4.66 |
| **FcMe4Ac** | y = −1.420 − 0.007x | 0.971 | $1.81 \times 10^6$ | −35.72 ± 2.22 |
| **Diclofenac** | y = −1.406 − 0.020x | 0.988 | $6.79 \times 10^5$ | −33.29 ± 4.31 |

The **ferrocenyl derivatives** exhibit significantly higher binding constants than diclofenac, confirming stronger affinity towards BSA. **(Bahsi et al. 2025)**

The interaction is spontaneous **(ΔG < 0)** and likely driven by:

- hydrophobic interactions
- π–π stacking
- electrostatic contributions

The higher affinity of FcMe4Ac confirms the formation of a more stable complex, which directly correlates with its superior anti-**inflammatory activity**. **(Chroho et al., 2022)**, **(Papada et al., 2023)**

## 6.3. Overall Structure–Activity Relationship

The combined analysis reveals a consistent trend across both biological assays: FcMe4Ac > FcMe3Ac > FcMe2Ac, This confirms that:

- para substitution enhances biological performance
- electronic delocalisation improves interaction capability
- steric hindrance reduces activity

The **ferrocenyl** core plays a central role by:

- enhancing lipophilicity
- promoting interaction with biological targets
- contributing to stabilisation of **ligand**–protein **complexes**

## 7. Density Functional Theory (DFT) Analysis

Density functional theory **(DFT)** calculations were performed to gain detailed insight into the electronic structure, reactivity and physicochemical properties of the synthesised **ferrocenyl acetylaniline derivatives**. These theoretical investigations provide a **molecular**-level interpretation of electronic distribution and complement the experimental findings, allowing a more comprehensive understanding of structure–property relationships. **(Boutarfaia et al., 2019)**

## 7.1. Frontier Molecular Orbitals and Electronic Structure

The frontier **molecular** orbitals **(HOMO and LUMO)** are key descriptors governing the reactivity of **molecular** systems, as they define electron-donating and electron-accepting capacities. The calculated orbital energies are summarised in **Table 6**, while their spatial distributions are presented in **Figure II.18.**

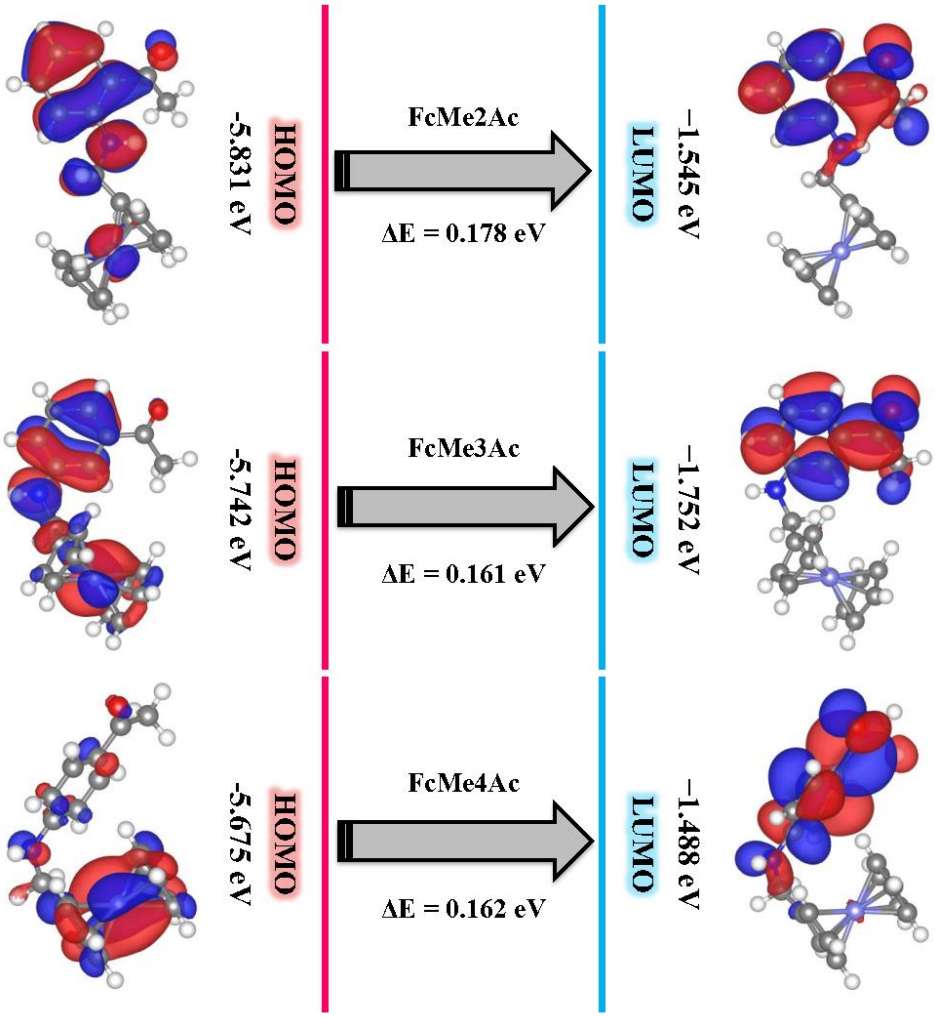


***Figure II.22.*** *Frontier* ***molecular*** *orbitals of* ***ferrocenyl acetylaniline derivatives****:* ***HOMO*** *and LUMO surfaces.*

**Table 10.** Frontier **molecular** orbital energies **(eV)** of the synthesised compounds.

| Compound | EHOMO (eV) | ELUMO (eV) | ΔE (eV) |
|---|---|---|---|
| **FcMe2Ac** | −5.8306 | −1.5453 | 4.285 |
| **FcMe3Ac** | −5.7421 | −1.7521 | 3.990 |
| **FcMe4Ac** | −5.6752 | −1.4882 | 4.187 |

The results reveal a gradual increase in **HOMO** energy from FcMe2Ac **(−5.8306 eV)** to FcMe4Ac **(−5.6752 eV)**, indicating an enhancement of electron-donating character across the

series. This trend reflects the influence of the substitution pattern on the electronic density of the **ferrocenyl** core, where improved conjugation promotes electron delocalisation.

The **HOMO**–LUMO energy gap **(ΔE)** ranges between 3.990 and 4.285 eV, suggesting that all compounds possess moderate chemical stability combined with sufficient electronic flexibility. Among the **derivatives**, FcMe3Ac exhibits the lowest energy gap **(3.990 eV)**, indicating increased softness and higher reactivity, whereas FcMe2Ac displays the highest gap, reflecting comparatively greater stability. **(Yahiaoui et al. 2023)**

The orbital distribution **Figure II.18** shows a clear donor–acceptor separation within the **molecular** framework. The **HOMO** is predominantly localised over the **ferrocenyl** moiety and partially extends towards the amine bridge, identifying this region as the principal electron donor. In contrast, the LUMO is mainly distributed over the aromatic ring and the carbonyl group, designating these sites as electron-accepting regions.

This spatial separation suggests an intra**molecular** charge-transfer character, whereby electron density is transferred from the **ferrocenyl** unit towards the aromatic substituent. Such donor–acceptor behaviour is particularly relevant for **molecular** recognition processes, as it facilitates electronic adaptation upon interaction with biological macromolecules. **(Kedadra et al., 2022)**

## 7.2. Global Reactivity Descriptors and Thermodynamic Parameters

To further quantify **molecular** reactivity, global descriptors derived from frontier orbital energies were calculated and are summarised in **Table 7**.

**Table 11.** Global reactivity descriptors and thermodynamic parameters of the synthesised **derivatives** at 298.15 K.

| Parameter | FcMe2Ac | FcMe3Ac | FcMe4Ac |
|---|---|---|---|
| **Hardness, η (eV)** | 2.143 | 1.995 | 2.094 |
| **Electronegativity, χ (eV)** | 3.688 | 3.747 | 3.582 |
| **Chemical potential, μ (eV)** | −3.688 | −3.747 | −3.582 |
| **Softness, S ($eV^{-1}$)** | 0.233 | 0.251 | 0.239 |
| **Electrophilicity, ω (eV)** | 3.174 | 3.519 | 3.064 |
| **Nucleophilicity, N** | 2.829 | 2.918 | 2.985 |

| | | | |
|---|---|---|---|
| **Dipole moment (D)** | 3.82 | 4.46 | 5.12 |
| **Polarizability (Å³)** | 38.5 | 42.7 | 47.3 |
| **Enthalpy (kJ·mol⁻¹)** | −1245.6 | −1388.2 | −1531.4 |
| **Entropy (J·mol⁻¹·K⁻¹)** | 412.5 | 448.9 | 486.7 |
| **Heat capacity (J·mol⁻¹·K⁻¹)** | 236.4 | 258.7 | 281.3 |

The hardness **(η)** values confirm that all compounds exhibit moderate stability, consistent with their **HOMO**–LUMO gaps. FcMe3Ac presents the lowest hardness **(1.995 eV)** and highest softness **(0.251 eV⁻¹)**, reinforcing its greater electronic flexibility and reactivity.

The electrophilicity index **(ω)** follows the order: FcMe3Ac > FcMe2Ac > FcMe4Ac, indicating that FcMe3Ac has the strongest electron-accepting capability. In contrast, FcMe4Ac exhibits the highest nucleophilicity index, suggesting enhanced electron-donating potential. This duality reflects the delicate balance between donor and acceptor characteristics within the series.

The negative values of chemical potential **(μ)** for all compounds indicate thermodynamic stability and a natural tendency towards charge redistribution. Additionally, a progressive increase in dipole moment from FcMe2Ac to FcMe4Ac is observed, reflecting enhanced **molecular** polarity and asymmetry. **(Khennoufa et al. 2021)**

Similarly, polarizability increases across the series, indicating that the electronic cloud becomes more easily deformable. This property is particularly important for inter**molecular** interactions, as it enhances the ability of the molecule to adapt to external electrostatic environments.

Thermodynamic parameters, including entropy and heat capacity, also show an increasing trend, suggesting greater **molecular** flexibility and a higher number of accessible vibrational states. This behaviour is consistent with increasing structural complexity and conformational freedom in the substituted **derivatives**. **(Meraghni et al., 2023)**

## 7.3. Molecular Electrostatic Potential (MEP) Analysis

The **molecular** electrostatic potential maps provide valuable insight into charge distribution and reactive sites. The calculated **MEP** surfaces are presented in **Figure II.19**.

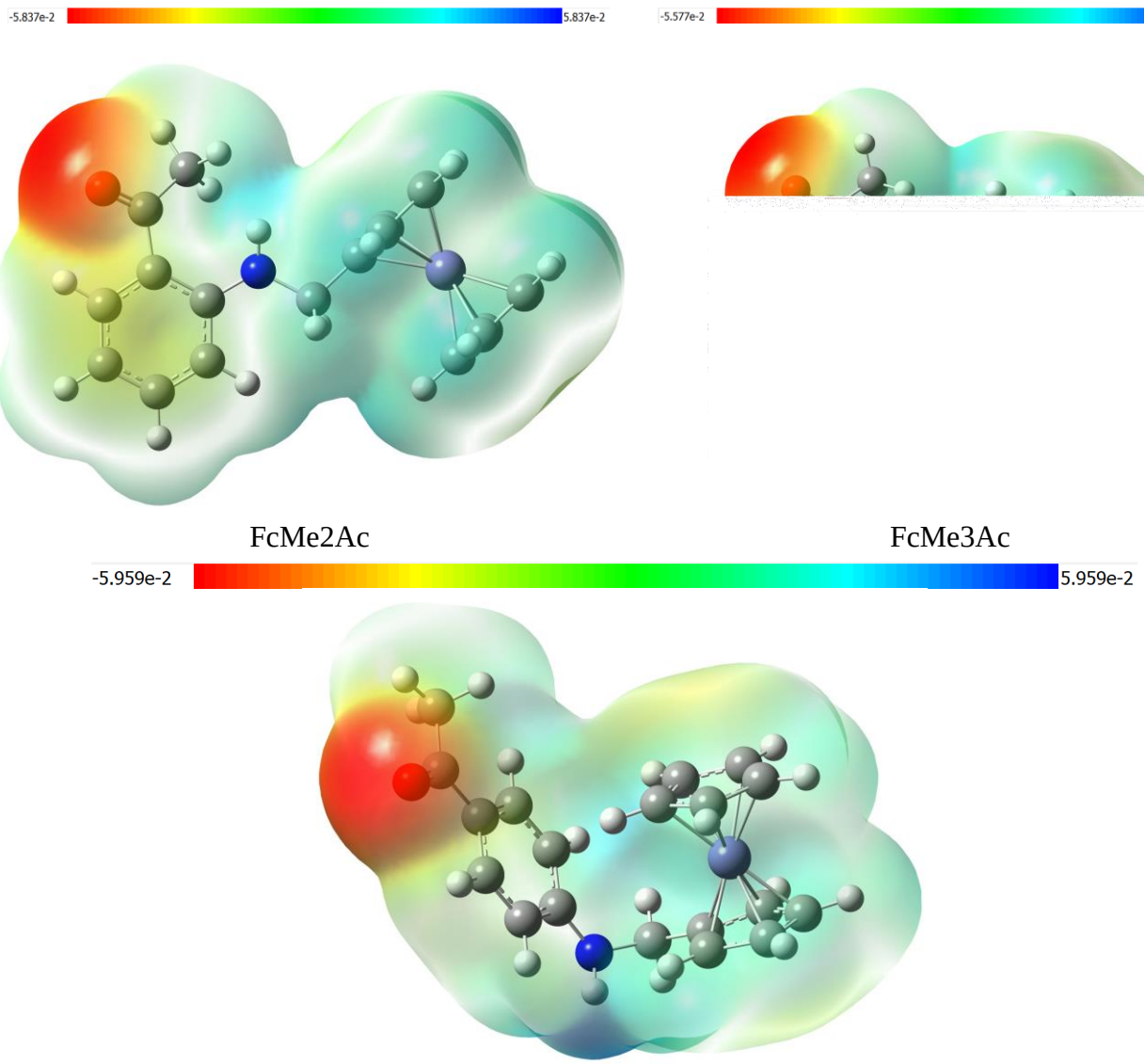


***Figure II.23.*** *Molecular electrostatic potential* ***(MEP)*** *maps of* ***ferrocenyl acetylaniline derivatives*** *showing charge distribution.*

The **MEP** analysis reveals that regions of highest negative potential are localised around the carbonyl oxygen atoms, indicating areas of high electron density and strong nucleophilic character. These regions are therefore likely to serve as preferential sites for inter**molecular** interactions, including hydrogen bonding and electrostatic interactions.

In contrast, positive electrostatic potential regions are primarily located around hydrogen atoms and partially over the **ferrocenyl** unit, corresponding to electron-deficient zones. **(Lanez et al. 2024)**

Although the overall electrostatic distribution remains similar across the three **derivatives**, subtle differences are observed, particularly in the para-substituted compound **(FcMe4Ac)**, which exhibits a more delocalised charge distribution. This enhanced delocalisation may contribute to improved interaction capabilities with biological targets. **(Nadjiba et al., 2018)**

## 7.4. Electron Localisation and Non-Covalent Interaction Analysis

To further investigate electronic behaviour, ELF, LOL and RDG analyses were performed. Representative maps are presented in **Figure II.20** and **II.21.**

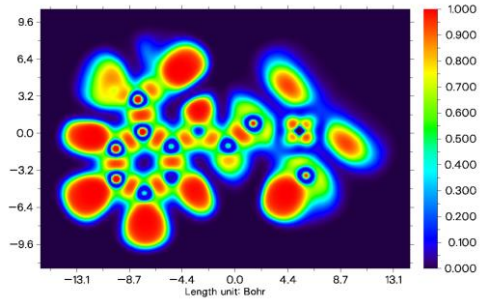


ELF_ FcMe2Ac

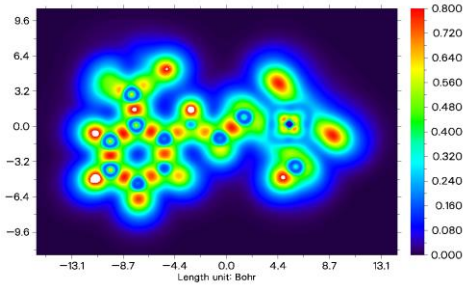


LOL_ FcMe2Ac

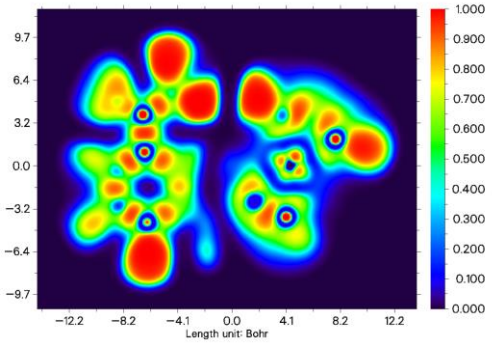


ELF_ FcMe3Ac

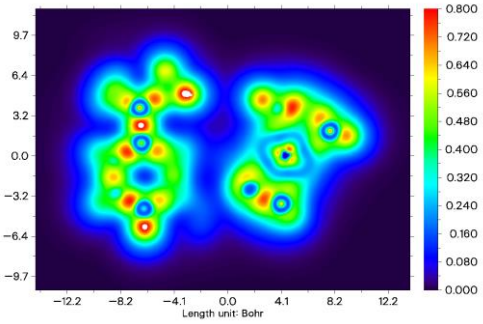


LOL_ FcMe3Ac

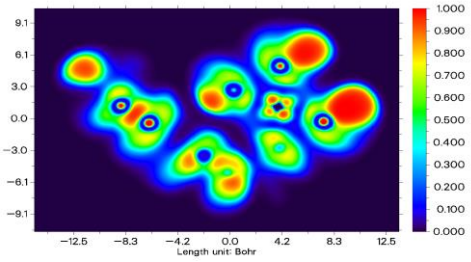


ELF_ FcMe4Ac

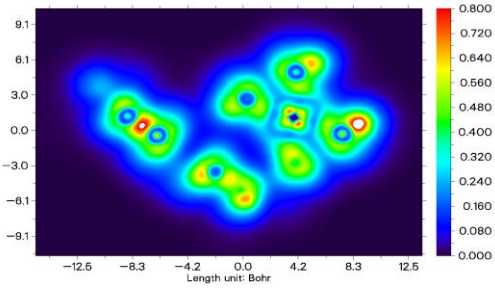


LOL_ FcMe4Ac

***Figure II.24.*** *Electron localisation* ***(ELF and LOL)*** *analyses of FcMeAc.*

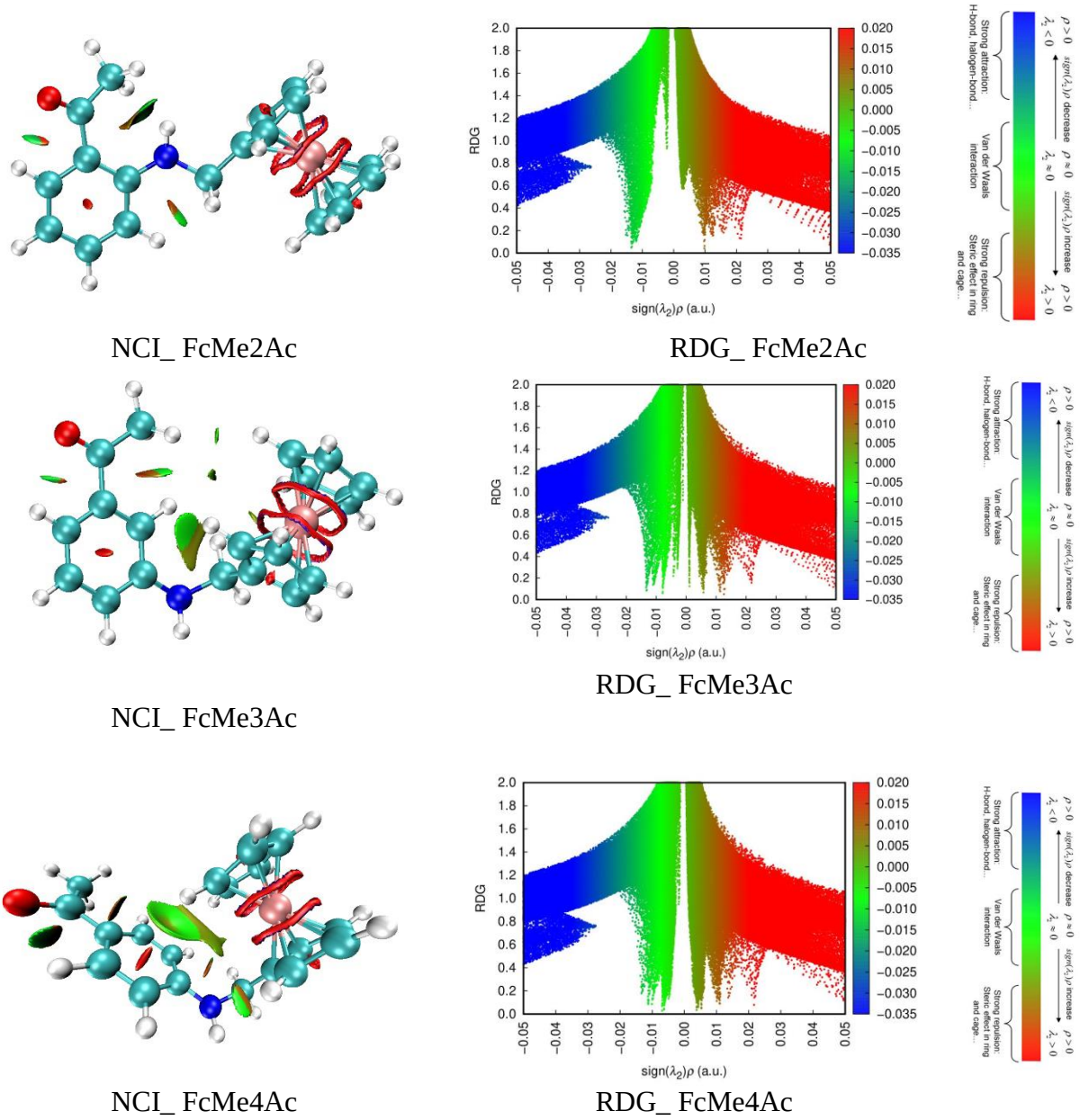


NCI_ FcMe2Ac RDG_ FcMe2Ac

NCI_ FcMe3Ac RDG_ FcMe3Ac

NCI_ FcMe4Ac RDG_ FcMe4Ac

***Figure II.25.*** *Non-covalent interaction* ***(RDG/NCI)*** *analyses of FcMeAc.*

The ELF and LOL maps clearly show strong electron localisation within the cyclopentadienyl rings and the aromatic system, reflecting extensive π-electron delocalisation. Localised electron density around nitrogen and oxygen atoms corresponds to lone-pair regions, which are important for inter**molecular** interactions.

The RDG analysis highlights weak non-covalent interactions, including van der Waals contacts and steric repulsion zones. These interactions contribute to the overall stability and conformational behaviour of the molecules.

The consistency of these features across the series indicates that the fundamental electronic structure of the **ferrocenyl** core is preserved, while substitution mainly modulates peripheral electronic properties. **(Zerrouk et al., 2024)**, **(Adaika et al., 2019)**

## 8. Molecular Docking Study

To further elucidate the **molecular** basis underlying the observed **antidiabetic** activity, **molecular docking** simulations were performed to investigate the interaction behaviour of the synthesised **ferrocenyl acetylaniline derivatives** within the active sites of α-**amylase (PDB ID: 1HNY)** and α-glucosidase **(PDB ID: 3TOP)**. These enzymes play a central role in **carbohydrate** digestion, and their inhibition represents a key therapeutic strategy for controlling postprandial hyperglycaemia.

The **docking** study aimed to evaluate binding affinity, identify dominant interaction forces, and rationalise the experimental inhibition results through a detailed structural analysis.

### 8.1. Docking Protocol Validation

Prior to analysing **ligand**–enzyme interactions, the **docking** protocol was validated through a re**docking** procedure of the co-crystallised **ligand** into the active site of the target enzymes. The superposition between the crystallographic and predicted binding conformations is presented in **Figure II.26.**

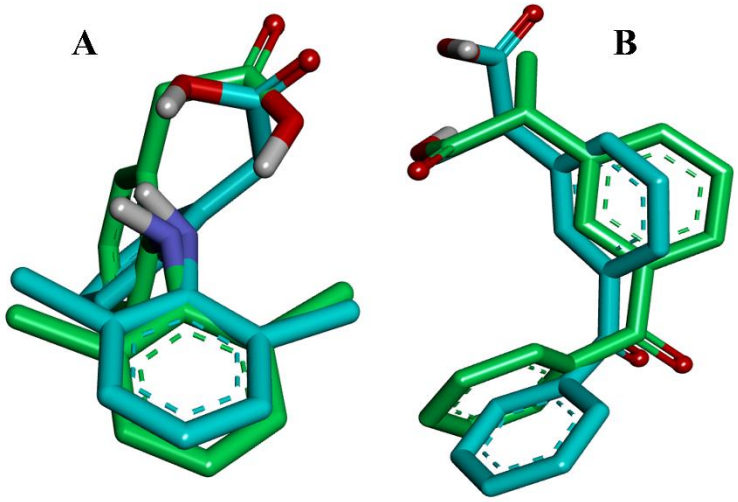


***Figure II.26.*** *Superposition of the co-crystallised* ***ligand*** *and the redocked pose within the active site of α-****amylase*** *and α-glucosidase* ***(validation of docking protocol)***.

The calculated RMSD value **(0.339 Å)** is significantly below the commonly accepted threshold of 2.0 Å, indicating excellent agreement between experimental and predicted binding modes. This confirms the reliability of the **docking** parameters, including grid definition and scoring function, and validates the protocol for subsequent interaction analysis.

Such a low RMSD value demonstrates that the adopted computational approach is highly accurate in reproducing the native binding orientation, thereby ensuring the robustness of the obtained **docking** results. **(Lanez et al., 2018)**

## 8.2. Binding Affinity and Energetic Analysis

The **molecular docking** results of the **ferrocenyl acetylaniline derivatives** against α-**amylase (1HNY)** and α-glucosidase **(3TOP)** are summarised in Tables 12 and 13, respectively. These results provide quantitative insight into the binding strength and energetic contributions governing **ligand**–enzyme interactions.

**Table 12.** Molecular **docking** results of **ferrocenyl acetylaniline derivatives** against α-**amylase (1HNY)**.

| Compound | Intermolecular Energy (kcal·mol⁻¹) | Internal Energy (kcal·mol⁻¹) | Torsional Energy (kcal·mol⁻¹) | Binding Energy (kcal·mol⁻¹) |
|---|---|---|---|---|
| **FcMe2Ac** | −7.96 | −0.58 | +0.74 | −7.34 |
| **FcMe3Ac** | −8.48 | −0.71 | +0.88 | −7.92 |
| **FcMe4Ac** | −9.42 | −0.83 | +0.96 | −8.58 |
| **Acarbose** | — | — | — | −7.65 |

**Table 13.** Molecular **docking** results of **ferrocenyl acetylaniline derivatives** against α-glucosidase **(3TOP)**.

| Compound | Intermolecular Energy (kcal·mol⁻¹) | Internal Energy (kcal·mol⁻¹) | Torsional Energy (kcal·mol⁻¹) | Binding Energy (kcal·mol⁻¹) |
|---|---|---|---|---|
| **FcMe2Ac** | −8.12 | −0.61 | +0.76 | −7.51 |
| **FcMe3Ac** | −8.73 | −0.74 | +0.91 | −8.07 |
| **FcMe4Ac** | −9.68 | −0.86 | +0.99 | −8.72 |

| | | | | |
|---|---|---|---|---|
| **Acarbose** | — | — | — | −8.01 |

The data presented in **Tables 12** and **13** clearly demonstrate that all **ferrocenyl derivatives** exhibit negative binding energies toward both α-**amylase** and α-glucosidase, confirming that the **ligand**–enzyme interactions are thermodynamically favourable and occur spontaneously.

For α-**amylase Table 12**, the binding affinity follows the order: FcMe4Ac **(−8.58)** > FcMe3Ac **(−7.92)** > FcMe2Ac **(−7.34)** > acarbose **(−7.65)**.

This trend indicates that FcMe4Ac binds more strongly than the reference drug under identical **docking** conditions, while FcMe3Ac exhibits comparable affinity, and FcMe2Ac shows slightly weaker interaction. These results are fully consistent with the in vitro $IC_{50}$ values, where FcMe4Ac demonstrated the highest inhibitory activity.

For α-glucosidase **Table 13**, a similar but more pronounced trend is observed: FcMe4Ac **(−8.72)** > FcMe3Ac **(−8.07)** > FcMe2Ac **(−7.51)** > acarbose **(−8.01)**

Interestingly, all compounds exhibit stronger binding affinities toward α-glucosidase compared to α-**amylase**. This suggests that the active site of α-glucosidase provides a more favourable environment for **ligand** accommodation, likely due to enhanced steric compatibility and the possibility of forming additional stabilising interactions. **(Khallouki et al. 2015)**

A detailed examination of the energetic components reveals that the inter**molecular** energy is the dominant contributor to the overall binding energy for both enzymes. This confirms that **ligand** stabilisation is mainly driven by non-covalent interactions, including van der Waals forces, electrostatic interactions and hydrogen bonding. The more negative inter**molecular** energy values observed for α-glucosidase **complexes** further support the presence of stronger and more favourable interactions within its catalytic pocket.

The internal energy values remain low and negative across all systems, indicating that **ligand** binding does not induce significant conformational strain. This reflects the ability of the **ferrocenyl derivatives** to adopt energetically favourable conformations within the enzyme active sites. Similarly, the torsional energy contributions are relatively small, suggesting that only minor rotational adjustments are required for optimal binding, which enhances overall interaction efficiency. **(Guaouguaou et al., 2020)**

## 8.3. Binding Mode and Interaction Analysis

The three-dimensional binding conformations of the most active compound **(FcMe4Ac)** within the active sites of α-**amylase (1HNY)** and α-glucosidase **(3TOP)** are illustrated in **Figure II.27.**

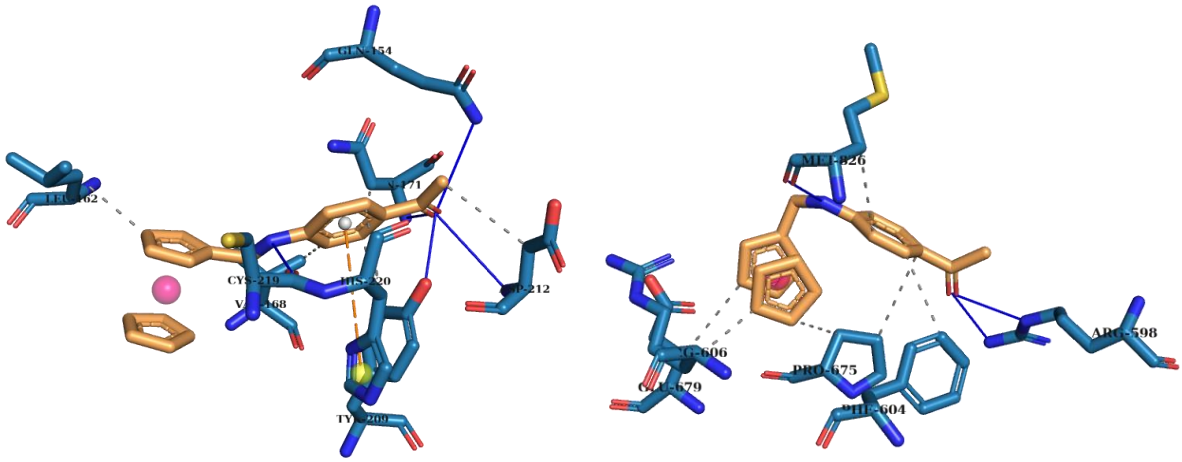


***Figure II.27.*** *Three-dimensional binding modes of FcMe4Ac within* ***(a)*** *α-**amylase (1HNY)** and* ***(b)*** *α-glucosidase **(3TOP)** active sites.*

The **docking** results reveal that all **ferrocenyl acetylaniline derivatives** are efficiently accommodated within the catalytic pockets of both enzymes, where the **ferrocenyl** moiety plays a central role in stabilising **ligand** binding through hydrophobic and π-related interactions. Despite structural similarities, distinct interaction patterns are observed between the two enzymes, reflecting differences in active site topology and residue composition. **(Jurowski and Krośniak 2025)**

For α-**amylase**, the **ligand**s are positioned within the catalytic groove, interacting with key residues involved in **carbohydrate** hydrolysis. The interaction profile is characterised by:

- Hydrophobic interactions with residues such as TRP59, TYR62, LEU165, and ILE235, contributing to **ligand** anchoring within the active site
- π–π stacking interactions between the aromatic ring of the **ligand** and residues such as TRP59 and TYR62, enhancing binding stability

- Hydrogen bonding interactions involving the carbonyl group and catalytic residues, particularly ASP197, GLU233, and ASP300, which are essential for enzymatic activity
- Van der Waals interactions that further stabilise the **ligand** within the binding pocket

In contrast, within α-glucosidase, the **ligand**s adopt a slightly deeper and more stabilised conformation, reflecting the larger and more flexible binding pocket of this enzyme. The interaction network includes:

- Extensive hydrophobic contacts with residues such as PHE525, TRP406, and TYR299, promoting strong **ligand** anchoring
- Enhanced π–π stacking interactions with aromatic residues, contributing significantly to binding affinity
- Hydrogen bonding interactions with catalytic residues such as ASP518 and ASP616, which play a key role in substrate recognition
- Additional electrostatic interactions, favouring stronger stabilisation compared to α-**amylase**

The comparative analysis clearly indicates that α-glucosidase provides a more favourable interaction environment, which is consistent with the more negative binding energies observed in **docking** studies. **(Bajad et al. 2025)**

Regarding **ligand**-specific behaviour:

- FcMe2Ac exhibits limited interaction capacity due to steric constraints associated with ortho substitution, leading to reduced accessibility within the active site and fewer stabilising interactions.
- FcMe3Ac demonstrates improved binding through increased interaction density, including additional hydrogen bonds and aromatic contacts.
- FcMe4Ac shows the most optimal binding configuration in both enzymes, characterised by:
    - Extensive hydrophobic interactions along the catalytic pocket
    - Strong and persistent hydrogen bonding with key catalytic residues
    - Pronounced π–π stacking interactions with aromatic residues
    - Optimal spatial orientation enabling maximum contact with the active site

This cooperative interaction network results in enhanced stabilisation of the **ligand**–enzyme complex and explains the superior binding affinity and inhibitory activity of FcMe4Ac observed in both in vitro and in silico studies. **(Gutiérrez-Grijalva et al., 2018)**

## 8.4. Structure–Interaction Relationship

The differences observed in binding affinity and interaction behaviour among the **ferrocenyl derivatives** can be rationalised based on structural and electronic factors.

The para-substituted derivative **(FcMe4Ac)** exhibits the most favourable interaction profile due to its extended and symmetrical **molecular** geometry, which allows optimal insertion into the catalytic pockets of both α-**amylase** and α-glucosidase. This structural configuration enhances steric complementarity and maximises contact with key residues, resulting in stronger binding interactions.

In addition, FcMe4Ac displays higher dipole moment and increased polarizability, which contribute to enhanced electrostatic and dispersion interactions within the enzyme environment. The improved electronic delocalisation across the **ferrocenyl** and aromatic moieties further facilitates efficient interaction with catalytic residues, particularly through π–π stacking and charge transfer interactions.

Conversely, the ortho-substituted derivative **(FcMe2Ac)** suffers from steric hindrance, which restricts its conformational flexibility and limits its ability to adopt an optimal binding orientation. This results in weaker interaction networks and reduced binding affinity.

The meta derivative **(FcMe3Ac)** exhibits intermediate behaviour, reflecting a balance between steric effects and electronic distribution. While it achieves better accommodation than FcMe2Ac, its interaction efficiency remains lower than that of FcMe4Ac due to less optimal alignment within the active site.

Importantly, the strong agreement between binding affinity **(docking)**, interaction profiles, and in vitro inhibitory activity **($IC_{50}$ values)** confirms that the biological performance of these compounds is directly governed by their ability to establish stable and extensive interactions within enzyme active sites.

Overall, these findings demonstrate that substitution pattern is a critical determinant of **ligand**–enzyme interaction efficiency, and they clearly identify FcMe4Ac as the most promising candidate for the inhibition of **carbohydrate**-hydrolysing enzymes. Its favourable structural,

electronic, and interaction properties highlight its potential as a lead scaffold for the development of novel **antidiabetic** agents. **(Mouada et al., 2019)**

## 9. Molecular Dynamics Simulation

Molecular dynamics **(MD)** simulations were performed to investigate the stability and dynamic behaviour of the most active compound **(FcMe4Ac)** in complex with α-**amylase (1HNY)** and α-glucosidase **(3TOP)**. These enzymatic systems provide a reliable framework for evaluating **ligand** binding within **carbohydrate**-hydrolysing enzymes under dynamic conditions relevant to **antidiabetic** activity.

### 9.1. System Stability: RMSD Analysis

The temporal evolution of backbone RMSD for both apo enzymes and FcMe4Ac-bound **complexes** is presented in **Figure II.28.**

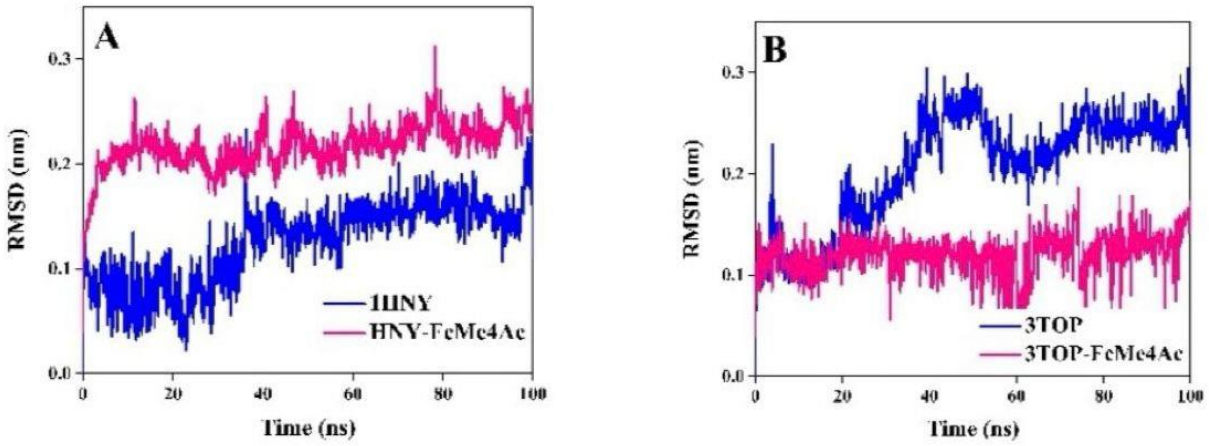


***Figure II.28.*** *RMSD evolution of* ***(a)*** *α-**amylase (1HNY)** and* ***(b)*** *α-glucosidase* ***(3TOP)*** *systems over 100 ns.*

The apo forms of both enzymes stabilise rapidly within ~0.10–0.15 nm after initial equilibration, confirming their intrinsic structural stability. Upon **ligand** binding, the RMSD values increase moderately and stabilise in the range of ~0.18–0.25 nm.

This slight increase reflects **ligand**-induced conformational adaptation within the catalytic pockets, particularly around residues directly involved in substrate recognition and catalysis.

Importantly, no large fluctuations or structural deviations are observed throughout the simulation period, indicating that the **complexes** remain stable.

Notably, the FcMe4Ac–α-glucosidase complex exhibits slightly lower RMSD fluctuations compared to α-**amylase**, suggesting a more stable binding environment, which is fully consistent with the stronger binding affinity observed in **docking** studies.

Overall, RMSD analysis confirms that FcMe4Ac forms stable and well-equilibrated **complexes** with both enzymes. **(Siles-Sánchez et al., 2024)**, **(Ghadge et al., 2025)**

## 9.2. Residue Flexibility: RMSF Analysis

The RMSF profiles for enzyme residues are presented in **Figure II.29.**

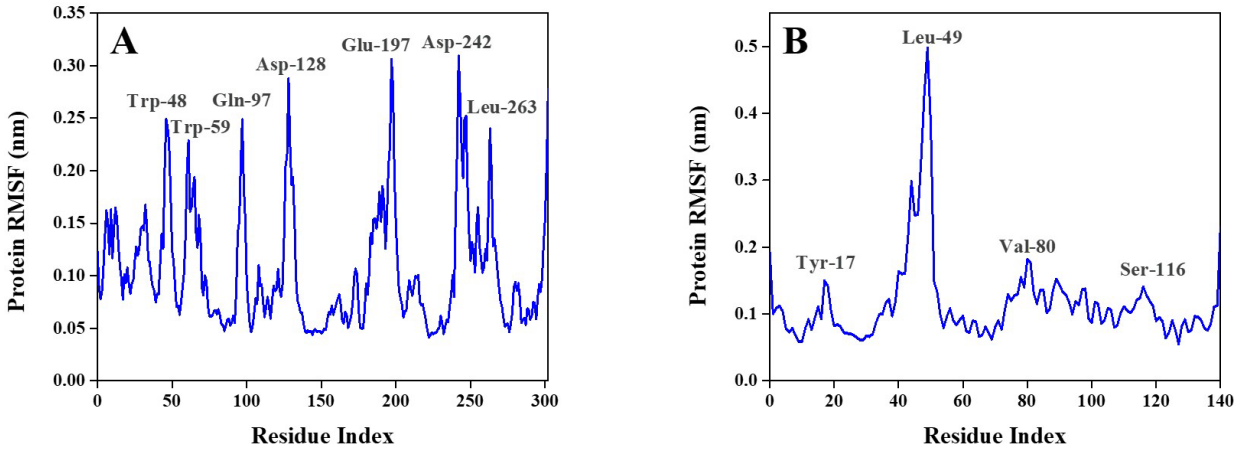


***Figure II.29.*** *RMSF profiles of* ***(a)*** *α-**amylase** and* ***(b)*** *α-glucosidase residues in complex with FcMe4Ac.*

Most residues exhibit low fluctuations **(<0.15 nm)**, indicating a rigid and stable protein backbone during simulation. Higher fluctuations are observed mainly in loop regions and solvent-exposed segments, which are inherently flexible.

Importantly, residues located within the catalytic sites show minimal fluctuations, confirming strong **ligand** stabilisation:

- α-**amylase**: ASP197, GLU233, ASP300
- α-glucosidase: ASP518, ASP616

The reduced mobility of these key catalytic residues indicates that FcMe4Ac effectively stabilises the active site architecture, thereby potentially inhibiting enzymatic activity. **(Stoyanova et al., 2025)**, **(Gadakh & Kulkarni, 2025)**

## 9.3. Ligand Stability: Ligand RMSF Analysis

The conformational stability of FcMe4Ac within both enzyme binding pockets is illustrated in **Figure II.30.**

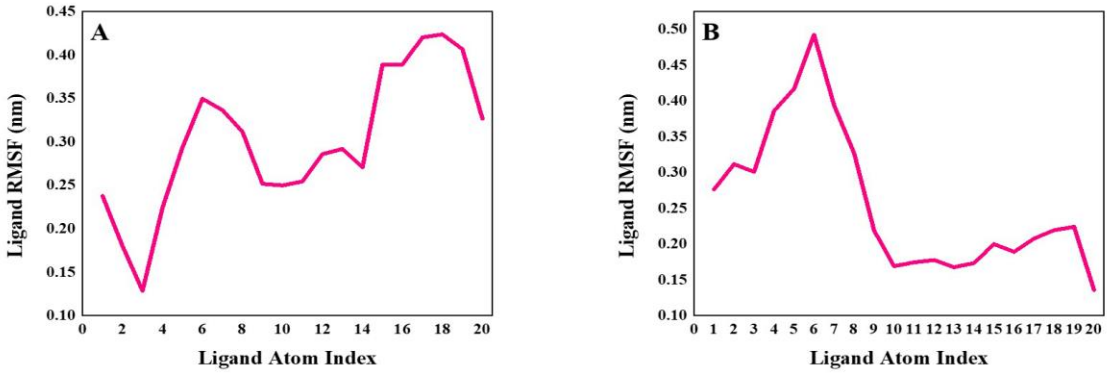


**Figure II.30.** *Ligand RMSF profile of FcMe4Ac in* ***(a)*** *α-**amylase** and* ***(b)*** *α-glucosidase **complexes**.*

FcMe4Ac exhibits moderate fluctuations **(~0.15–0.25 nm)**, primarily associated with peripheral substituents, while the **ferrocenyl** core remains highly stable throughout the simulation.

This behaviour indicates that:

- The **ferrocenyl** scaffold acts as a rigid anchoring unit
- Peripheral groups provide adaptive flexibility, facilitating optimal interactions

The slightly reduced fluctuations observed in the α-glucosidase complex further support a more confined and stable binding mode in this enzyme. **(Puspadewi et al., 2025)**

## 9.4. Interaction Profile Analysis

The interaction profiles during simulation are shown in **Figure II.31.**

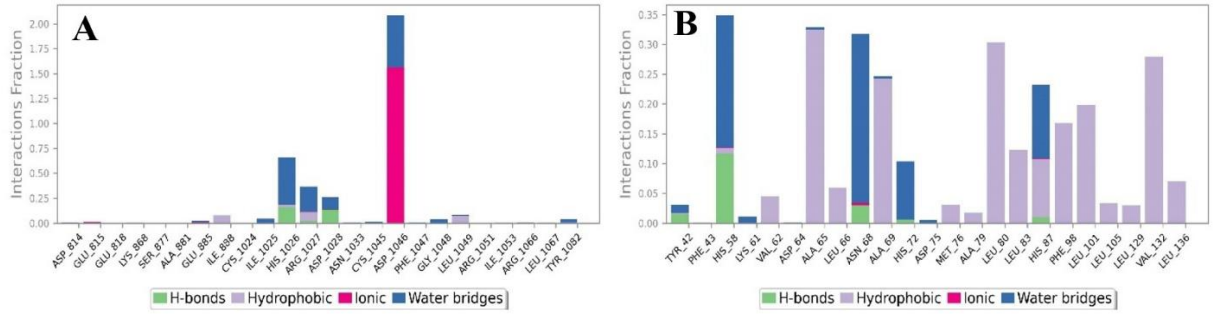

***Figure II.31.*** *Interaction fraction analysis showing hydrogen bonds, hydrophobic interactions, π–π stacking, and water bridges in* ***(a)*** *α-**amylase** and* ***(b)*** *α-glucosidase* ***complexes****.*

The stabilisation of the **complexes** is governed by a cooperative interaction network:

- Hydrophobic interactions with residues such as TRP59, TYR62 **(α-amylase)** and PHE525, TRP406 **(α-glucosidase)**
- π–π stacking interactions involving aromatic residues, enhancing binding strength
- Hydrogen bonding interactions with catalytic residues **(ASP197, GLU233, ASP300 for α-amylase; ASP518, ASP616 for α-glucosidase)**
- Water-mediated bridges, contributing to interaction persistence

The interaction network is more pronounced in α-glucosidase, explaining its stronger binding affinity and higher inhibitory potential. **(Sabiha et al., 2023)**, **(Muqaddas et al., 2016)**

## 9.5. Global Structural Properties (Rg, SASA, PSA)

The evolution of global structural parameters is presented in **Figure II.32.**

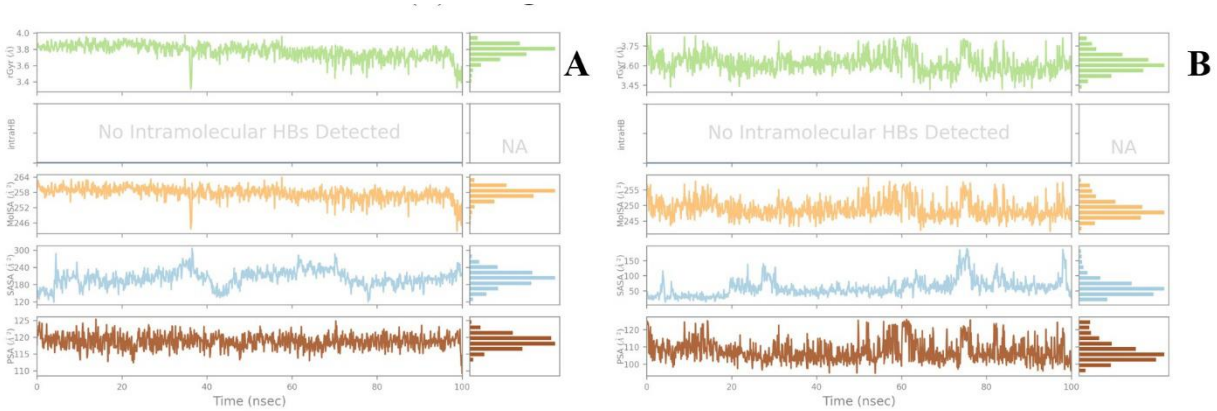


***Figure II.32.*** *Time evolution of radius of gyration* ***(Rg)****, solvent-accessible surface area* ***(SASA)****, and polar surface area* ***(PSA)*** *for enzyme–FcMe4Ac* ***complexes****.*

The radius of gyration **(Rg)** remains stable **(~2.2–2.5 nm)**, indicating that no unfolding or structural destabilisation occurs upon **ligand** binding. SASA values exhibit moderate fluctuations, reflecting normal solvent exposure without significant conformational disruption.

Similarly, PSA values remain nearly constant, suggesting that **ligand** binding does not significantly alter the global polarity of the enzymes.

These results confirm that FcMe4Ac binding preserves structural integrity while stabilising the catalytic environment, which is essential for effective **enzyme inhibition**. **(Juan et al., 2021)**, **(Sharifi-Rad et al., 2020)**

## 10. ADMET Prediction and Pharmacokinetic Evaluation

To complement the biological and computational investigations, the pharmacokinetic and toxicity profiles of the **ferrocenyl derivatives** were evaluated using in silico **ADMET** tools.

### 10.1. Drug-Likeness and Physicochemical Properties

The fundamental physicochemical parameters governing drug-likeness are summarised in **Table 14**.

**Table 14.** Predicted physicochemical properties and drug-likeness parameters of **ferrocenyl derivatives**.

| Parameter | FcMe2Ac | FcMe3Ac | FcMe4Ac |
|---|---|---|---|
| **Molecular weight ($g \cdot mol^{-1}$)** | 335.2 | 335.2 | 335.2 |
| **LogP (consensus)** | 3.12 | 3.28 | 3.45 |
| **Lipinski violations** | 0 | 0 | 0 |

All compounds comply with Lipinski's rule of five, indicating favourable oral bioavailability. Their moderate lipophilicity ensures a balance between solubility and membrane permeability, which is advantageous for enzyme-targeting **antidiabetic** agents. **(Guan et al., 2019)**

### 10.2. Absorption and Distribution Properties

The predicted absorption and distribution profiles are presented in **Table 15.**

**Table 15.** Predicted absorption and distribution properties of the studied compounds**.**

| Parameter | FcMe2Ac | FcMe3Ac | FcMe4Ac |
|---|---|---|---|
| **Gastrointestinal absorption** | High | High | High |
| **Blood–brain barrier permeability** | No | No | No |

All **derivatives** exhibit high gastrointestinal absorption, supporting their potential for oral administration. The absence of BBB permeability is advantageous for peripheral targets such as digestive enzymes, reducing the risk of central nervous system side effects. **(Xiong et al., 2021)**

## 10.3. Toxicological Profile

The toxicity predictions are summarised in **Table 16.**

**Table 16.** Predicted toxicity profiles of **ferrocenyl acetylaniline derivatives**.

| Parameter | FcMe2Ac | FcMe3Ac | FcMe4Ac |
|---|---|---|---|
| **Ames toxicity** | No | No | No |
| **Hepatotoxicity** | No | No | No |
| **Skin sensitisation** | Low risk | Low risk | Low risk |

The absence of mutagenicity and hepatotoxicity indicates a favourable safety profile, supporting further development. **(Dascalu et al., 2020)**

## 10.4. Structure–Property Relationship and Comparative Analysis

The **ADMET** results reveal a consistent trend:

- FcMe4Ac exhibits the highest lipophilicity and interaction potential.
- Increased substitution enhances electronic delocalisation and binding efficiency.
- All compounds maintain a balanced pharmacokinetic profile without toxicity risks.

Importantly, the agreement between:

- in vitro activity **($IC_{50}$)**
- **docking** affinity
- **MD** stability
- **ADMET** properties

strongly validates FcMe4Ac as the most promising candidate for both **antidiabetic** and <anti-inflammatory applications. **(Hodgson, 2001)**.

# CONCLUSION

## General Conclusion

The present work was devoted to the rational design, synthesis, comprehensive characterisation, and integrated biological and computational evaluation of a series of **ferrocenyl acetylaniline derivatives**, with particular emphasis on their potential as **antidiabetic** and anti-inflammatory agents. The multidisciplinary strategy adopted in this study enabled a coherent combination of experimental investigations and in silico approaches, providing a robust framework for establishing structure–property–activity relationships within this class of organometallic compounds.

The synthetic methodology allowed the efficient preparation of three regioisomeric **derivatives (FcMe2Ac, FcMe3Ac, and FcMe4Ac)** under mild and reproducible conditions. Structural elucidation was successfully achieved through complementary spectroscopic techniques, including FT-IR, UV–Visible spectroscopy, and one- and two-dimensional NMR analyses. The obtained spectral data confirmed the integrity of the **ferrocenyl** scaffold and validated the substitution patterns on the aromatic ring, demonstrating the reliability of the synthetic approach and the structural consistency of the prepared compounds.

Electrochemical studies revealed that all **derivatives** retain the characteristic quasi-reversible Fe**(II)**/Fe**(III) redox** behaviour of the **ferrocenyl** core. The observed anodic shifts in **redox** potentials across the series highlight the significant influence of **acetylaniline** substitution on the electronic environment of the iron centre. Furthermore, diffusion-controlled electron-transfer processes and variations in kinetic parameters confirmed that the electrochemical behaviour is strongly dependent on **molecular** structure, reflecting the sensitivity of the **ferrocenyl** system to substitution effects.

From a biological perspective, the in vitro investigations demonstrated that all compounds exhibit significant enzyme inhibitory activity against α-**amylase** and α-glucosidase, as well as pronounced anti-inflammatory potential through inhibition of protein denaturation. The results revealed a clear structure–activity relationship, with FcMe4Ac consistently showing the lowest $IC_{50}$ values in both **antidiabetic** and anti-inflammatory assays. The enhanced activity of this derivative can be attributed to its favourable structural configuration, which promotes improved interaction with enzyme active sites and stabilisation of protein structures.

Complementary spectroscopic binding studies further confirmed the strong affinity of the **ferrocenyl derivatives** toward biological targets, with high binding constants and negative Gibbs free energy values indicating spontaneous and stable **ligand**–protein interactions. The consistency between inhibition data and binding parameters highlights the direct relationship between binding strength and biological activity.

Density functional theory calculations provided deeper insight into the electronic structure and intrinsic reactivity of the compounds. Frontier **molecular** orbital analysis revealed a pronounced donor–acceptor character, with electron density primarily localised on the **ferrocenyl** unit and partially delocalised towards the aromatic system. Global reactivity descriptors, together with **MEP**, ELF, and RDG analyses, identified key reactive regions and confirmed that substitution pattern plays a decisive role in modulating electronic distribution, polarity, and inter**molecular** interaction potential.

Molecular **docking** studies against α-**amylase** and α-glucosidase demonstrated favourable binding affinities for all **derivatives**, governed by a combination of hydrophobic interactions, hydrogen bonding, and π–π stacking within the enzyme active sites. Among the series, FcMe4Ac consistently exhibited the strongest binding affinity, reflecting optimal steric complementarity, enhanced electronic delocalisation, and an extended interaction network within the catalytic pockets.

The stability of these interactions was further validated through **molecular** dynamics simulations, which confirmed the formation of stable and well-equilibrated **ligand**–enzyme **complexes**. In particular, FcMe4Ac displayed reduced structural fluctuations, enhanced conformational rigidity, and persistent interaction networks, especially within the α-glucosidase system. These findings indicate a strong and durable binding mode under dynamic conditions, reinforcing its superior inhibitory potential.

In addition, in silico **ADMET** analysis revealed that all **derivatives** possess favourable pharmacokinetic and safety profiles, including compliance with drug-likeness criteria, high predicted gastrointestinal absorption, and absence of mutagenic or hepatotoxic effects. The lack of blood–brain barrier permeability is advantageous for targeting peripheral enzymes involved in metabolic disorders, reducing the risk of central nervous system-related side effects.

Collectively, the results obtained in this study demonstrate that structural modification of **ferrocenyl derivatives** through **acetylaniline** substitution significantly influences their electronic properties, biological activity, interaction behaviour, and pharmacokinetic profile. The strong agreement between in vitro assays and computational predictions further validates the reliability of the integrated methodological approach.

Among the investigated compounds, FcMe4Ac emerges as the most promising candidate, combining optimal electronic characteristics, strong inhibitory activity against **carbohydrate**-hydrolysing enzymes, significant anti-inflammatory potential, high binding affinity, dynamic stability, and favourable **ADMET** properties. This derivative represents a valuable lead scaffold for further optimisation and development of multifunctional agents targeting metabolic and inflammatory disorders.

In conclusion, this work provides a comprehensive and scientifically rigorous contribution to the field of organometallic medicinal chemistry, highlighting the potential of **ferrocenyl derivatives** as versatile and effective scaffolds for the development of novel **antidiabetic** and anti-inflammatory agents, and paving the way for future experimental validation and clinical-oriented investigation.

# BIBLIOGRAPHIC REFERANCES

## Bibliographic References

**Adaika, A., Adaika, T., Lanez, T., & Lanez, E. (2019).** In Vitro and in Silico Evaluation of Anticancer Activity of N,N-Dimethylaminomethyl**ferrocene**. *Journal of Fundamental and Applied Sciences*, 11, 748–768. https://jfas.info/index.php/JFAS/article/view/289

**Adaika, A., Bekkar, Y., Youmbai, S., Bourougaa, L., Lanez, E., Ben Amor, M. L., Nesba, K., Lanez, T., & Bechki, L. (2025). synthesis**, Antioxidant, and Antidiabetic Potential of Ferrocenylmethylnucleobase Compounds: In Vitro, In Silico Molecular Docking, **DFT** Calculation, and Molecular Dynamic Simulations. *Appl. Organomet. Chem.*, 39, e7988.

**Aispuro-Pérez, A., Pedraza-Leyva, F. J., Ochoa-Acosta, A., Arias-Gastélum, M., Cárdenas-Torres, F. I., Amezquita-López, B. A., Terán, E., Aispuro-Hernández, E., Martínez-Téllez, M. Á., & Avena-Bustillos, R. J. (2025).** A Functional Beverage from Coffee and Olive Pomace: Polyphenol-Flavonoid Content, Antioxidant, Antihyperglycemic Properties, and Mouse Behavior. *Foods*, 14, 1331.

**Andersson, M. P., & Uvdal, P. (2005).** New scale factors for harmonic vibrational frequencies using the B3LYP density functional method with the triple-ζ basis set 6-311+ G **(d, p)**. *J. Phys. Chem. A*, 109, 2937–2941.

**Astruc, D. (2007).** *Organometallic Chemistry and Catalysis*. Springer Science & Business Media. https://doi.org/10.1007/978-3-540-46129-6

**Astruc, D. (2011).** Eur J Inorganic Chemistry. *Eur. J. Inorg. Chem.*, 2011, 2953–2964.

**Bajad, N. G., Sharma, K., Tapadia, M. G., Kumar, A., Krishnamurthy, S., & Singh, K. (2025).** Development of Donor–Acceptor Architecture-Based Potential Theranostic Fluorescent Probes for Alzheimer's Disease. *ACS Chem. Neurosci.*

**Banerjee, P., Eckert, A. O., Schrey, A. K., & Preissner, R. (2018).** ProTox-II: A webserver for the prediction of toxicity of chemicals. *Nucleic Acids Res.*, 46, W257–W263. https://doi.org/10.1093/nar/gky318

## Bibliographic Referances

**Bard, A. J., & Faulkner, L. R. (2001).** *Electrochemical Methods: Fundamentals and Applications* (2nd ed.). John Wiley & Sons.

**Bekkar, Y., Lanez, E., Lanez, T., Bourougaa, L., Adaika, A., Saada, Z., & Benine, A. (2025).** Antidiabetic Potential of Synthesized Ferrocenylmethylaniline Derivatives: Insights From In Vitro Studies, Molecular Docking, **ADMET**, **DFT** Calculations, and Molecular Dynamics Simulation. *Biotechnol. Appl. Biochem.*

**Bekkar, Y., Lanez, E., Lanez, T., Bourougaa, L., Adaika, A., Benine, A., & Saada, Z. (2025).** Combined In Vitro and In Silico analysis of **ferrocenyl**methylaniline **derivatives**: Antibacterial potential, **DFT** calculations, and **molecular** dynamics insights. *J. Organomet. Chem.*, 123618.

**Ben Amor, M. L., Lanez, E., Bekkar, Y., Adaika, A., Lanez, T., Nesba, K., & Bechki, L. (2025).** Evaluation of Ferrocenylmethylnucleobases Derivatives Interacting with DNA: Insights from Electrochemical, Spectroscopic, **DFT** Calculation, Molecular Docking and Molecular Dynamic Simulations. *Studia Universitatis Babes-Bolyai, Chemia*, 70.

**Ben Amor, M. L., Lanez, E., Bekkar, Y., Adaika, A., Lanez, T., Nesba, K., & Bechki, L. (2025).** Exploring the Interactions of Ferrocenylmethylnucleobase Derivatives With BSA and HHb: Insights From Electrochemical, Spectroscopic, **ADMET**, in Silico Docking, and **MD** Simulations. *ChemistrySelect*, 10, e202404678.

**Benamara, H., Lanez, T., & Lanez, E. (2020).** Bsa-binding studies of 2-and 4-**ferrocenyl**benzonitrile: Voltammetric, spectroscopic and **molecular docking** investigations. *Journal of Electrochemical Science and Engineering*, 10, 335–346. https://doi.org/10.5599/jese.861

**Benine, C., Boutlelis, D. A., Touhami, L. A., Lanez, E., Amara, D. G., Rim, G., Hanen, N., Zahnit, W., & Messaoudi, M. (2025).** Green synthesis, characterization, antioxidant, interaction with DNA/BSA, and investigation of cytotoxicity against MCF-7 cancer cells of zinc oxide nanoparticles using Hammada scoparia **(Pomel)** Iljin extract. *Int. J. Biol. Macromol.*, 295, 139709.

## Bibliographic Referances

**Benyza, N., Allouche, F., Dammak, S. W., Lanez, E., & Lanez, T. (2022).** Chemical Reactivity, Topological Analysis, and Second-Order Nonlinear Optical Responses of M3O@ Al12N12: A Quantum Chemical Study. *Russian Journal of Physical Chemistry A*, 96, 2909–2920.

**Boutarfaia, A., Bechki, L., Lanez, T., Lanez, E., & Kadri, M. (2019). synthesis**, Antioxidant Activity, and Determination of Binding Parameters of Meso-Tetra-4-Actophenyl-Porphyrin and its Palladium **(II)** Complex with Superoxide Anion Radicals. *Curr. Bioact. Compd.*, 16, 1063–1071. https://doi.org/10.2174/1573407215666191017105239

**Bouterfit, S., Ourari, A., & Villemin, D. (2013).** Electrochemical behavior of **ferrocene**/ferricenium couple in dichloromethane and in aqueous ethanol. *Recent Trends in Physical Chemistry: An International Journal*, 1**(1)**, 1-3.

**Chajed, Y. K., Somani, S. J., & Sherkar, R. (2020).** Synthesis, characterization and biological evaluation of some novel ferrocene derivatives. *International Journal of Modern Pharmaceutical Research*, *4*(3), 85–91.

**Chebbah, M., Lanez, E., Bouacida, S., Athmani, H., Ben Amor, M. L., Hafidi, R., & Bouchemma, A. (n.d.). synthesis**, Characterization, Structural Analysis, Hirshfeld Surface Studies, and Molecular Docking of 1, 3, 5-Tris **(P-Bromophenyl)**-1, 3, 5-Triazacyclohexane.

**Chroho, M., Bouymajane, A., Aazza, M., Oulad El Majdoub, Y., Cacciola, F., Mondello, L., Zair, T., & Bouissane, L. (2022).** Determination of the phenolic profile, and evaluation of biological activities of hydroethanolic extract from aerial parts of Origanum compactum from Morocco. *Molecules*, 27, 5189.

**Cífková, E., Neuerová, Z., & Lísa, M. (2025).** Reversed-phase liquid chromatography/mass spectrometry approach for **(un)** targeted analysis of polar to mid-polar metabolites. *Talanta*, 291, 127853.

**Cramer, C. J. (2013).** *Essentials of computational chemistry: theories and models* (2nd ed.). John Wiley & Sons.

## Bibliographic Referances


**Daina, A., Michielin, O., & Zoete, V. (2017).** SwissADME: A free web tool to evaluate pharmacokinetics and drug-likeness. *Scientific Reports*, 7, 42717.

**Dascalu, D., Larisa Roman, D., Filip, M., Ciorsac, A., & Isvoran, A. (2020).** Solubility and Admet Profiles of Short Oligomers of Lactic Acid. ***ADMET*** *DMPK*, 8, 425–436. https://doi.org/10.5599/admet.801

**Dong, J., Wang, N. N., Yao, Z. J., Zhang, L., Cheng, Y., Ouyang, D., Lu, A. P., & Cao, D. S. (2018).** Admetlab: A platform for systematic **ADMET** evaluation based on a comprehensively collected **ADMET** database. *J. Cheminform.*, 10, 1–11. https://doi.org/10.1186/s13321-018-0283-x

**El-Sayed, A., et al. (2022).** Density functional theory study of **molecular** reactivity. *Molecules*, 27**(3)**, 620.

**Fahmy, M. I., Sadek, M. A., Abdou, K., El-Dessouki, M., El-Shiekh, A., & Khalaf, S. S. (2025).** Orientin: a comprehensive review of a promising bioactive flavonoid. *Inflammopharmacology*, 1–16.

**Filote, C., Lanez, E., Popa, V. I., Lanez, T., & Volf, I. (2022).** Characterization and Bioactivity of Polysaccharides Separated through a **(Sequential)** Biorefinery Process from Fucus spiralis Brown Macroalgae. *Polymers **(Basel)***, 14, 4106. https://doi.org/10.3390/polym14194106

**Frisch, M. J., Trucks, G. W., Schlegel, H. B., Scuseria, G. E., Robb, M. A., Cheeseman, J. R., Scalmani, G., Barone, V., Mennucci, B., & Petersson, G. A. (2009).** *Gaussian 09*. Wallingford, CT: Gaussian.

**Gadakh, A. S., & Kulkarni, A. D. (2025).** In-vitro Anti-inflammatory Potential of Nelumbo nucifera Rhizomes. *Journal of Pharma Insights and Research*, 3, 17–22.

**Gagne, R. R., Koval, C. A., & Lisensky, G. C. (1980).** Ferrocene as an Internal Standard for Electrochemical Measurements. *Inorganic Chemistry*, 19**(9)**, 2854–2855.

## Bibliographic Referances

**Ghadge, S. R., Shimpi, P. H., Kumbhar, V. V., Khairnar, B. B., & Nikam, V. S. (2025).** Comprehensive evaluation of AChE inhibition by Eulophia ochreata extract utilizing in silico, ex vivo, and in vivo zebrafish models. *Brain Res.*, 1854, 149531.

**Guaouguaou, F., Ahl Bebaha, M. A., Yadlapalli, S., Taghzouti, K., & Es-Safi, N. E. (2020).** Structural characterization of bioactive compounds in Cotula cinerea extracts by ultra-high-performance liquid chromatography with photodiode array and high-resolution time-of-flight mass spectrometry detectors. *Rapid Communications in Mass Spectrometry*, 34, e8695.

**Guan, L., Yang, H., Cai, Y., Sun, L., Di, P., Li, W., Liu, G., & Tang, Y. (2019). ADMET**-score-a comprehensive scoring function for evaluation of chemical drug-likeness. *Medchemcomm*, 10, 148–157. https://doi.org/10.1039/C8**MD**00472B

**Gutiérrez-Grijalva, E. P., Picos-Salas, M. A., Leyva-López, N., Criollo-Mendoza, M. S., Vazquez-Olivo, G., & Heredia, J. B. (2018).** Flavonoids and Phenolic Acids from Oregano: Occurrence, Biological Activity and Health Benefits. *Plants*, 7. https://doi.org/10.3390/plants7010002

**Hanane, M., Lanez, T., Zafar, I., Afghan, M. S., & Zegheb, N. (2023).** N'-Ferrocenylmethyl-N'-phenylbenzohydrazide as a potential DNA binding compound: a combined experimental and computational study. *J. Coord. Chem.*, 76, 1984–1998. https://doi.org/10.1080/00958972.2023.2275247

**Hodgson, J. (2001). ADMET**—turning chemicals into drugs. Nature Biotechnology, 19(8), 722–726. https://doi.org/10.1038/90761

**Holub, K. V., Peregudov, A. S., & Voloshin, Y. Z. (2022).** Ferrocene in agriculture: from agrochemicals and soil remediation to selective chemosensors. *Chemical and Biological Technologies in Agriculture*, 9**(52)**.

**Huang, J., & Mackerell, A. D. (2013).** CHARMM36 all-atom additive protein force field: Validation based on comparison to NMR data. *J. Comput. Chem.*, 34, 2135–2145. https://doi.org/10.1002/jcc.23354

## Bibliographic Referances

**Jaouen, G., Vessières, A., & Top, S. (2015).** Ferrocifen type anti-cancer drugs. *Chemical Society Reviews*, 44, 8802–8817.

**Juan, C. A., Pérez de la Lastra, J. M., Plou, F. J., & Pérez-Lebeña, E. (2021).** The chemistry of reactive oxygen species **(ROS)** revisited: outlining their role in biological macromolecules **(DNA, lipids and proteins)** and induced pathologies. *Int. J. Mol. Sci.*, 22, 4642.

**Jurowski, K., & Krośniak, A. (2025).** ADME profile of AP-238-opioid designer drug **(CAS: 140924-11-4)**: first application of multi-in silico approach methodology for comprehensive prediction of ADME profile **(absorption, distribution, metabolism and excretion)** important for clinical toxicology a. *Chem. Biol. Interact.*, 111493.

**Karplus, M., & McCammon, J. A. (2002).** Molecular dynamics simulations of biomolecules. *Nature Structural Biology*, 9, 646–652.

**Kealy, T. J., & Pauson, P. L. (1951).** A new type of organo-iron compound. *Nature, 168*(4285), 1039–1040. https://doi.org/10.1038/1681039a0

**Kedadra, A., Lanez, T., Lanez, E., Adaika, A., & Zegheb, N. (2024).** In vitro antioxidant activity, QSAR, in silico toxicity prediction, **molecular docking** studies, and **molecular** dynamics of a series of N-**ferrocenyl**methylanilines as potent antioxidant agents. *J. Organomet. Chem.*, 123284.

**Kedadra, A., Lanez, T., Lanez, E., Hemmami, H., & Henni, M. (2022). synthesis** and antioxidant activity of six novel N-**ferrocenyl**methyl-N-**(nitrophenyl)**and-N-**(cyanophenyl)**-acetamides: Cyclic voltammetry and **molecular docking** studies. *Journal of Electrochemical Science and Engineering*, 12, 293–304. https://doi.org/10.5599/jese.1162

**Khallouki, F., Sellam, K., Koyun, R., Icarte, I., Alem, C., Elrhaffari, L., & Owen, R. W. (2015).** Phytoconstituents and in vitro evaluation of antioxidant capacities of Cotula cinerea **(Morocco)** methanol extracts. *Records of Natural Products*, 9, 572.

## Bibliographic Referances


**Khamouli, S., Belaidi, S., & Lanez, T. (2019).** Molecular **docking** and **ADMET** studies of amino-pyrimidine **derivatives** as mycobacterium tuberculosis Ser/Thr protein kinases B inhibitors. *Journal of Fundamental and Applied Sciences*, 11, 914–939.

**Khamouli, S., Belaidi, S., Ouassaf, M., Lanez, T., Belaaouad, S., & Chtita, S. (2022).** Multi-combined 3D-QSAR, **docking molecular** and **ADMET** prediction of 5-azaindazole **derivatives** as LRRK2 tyrosine kinase inhibitors. *J. Biomol. Struct. Dyn.*, 40, 1285–1298.

**Khand, I. U., Lanez, T., & Pauson, P. L. (1989).** Ferrocene **derivatives**. Part 24. **synthesis** of dihydro-2-pyrindines and dihydro-3 H-2-cyclopent [c] azepines by photolysis of their cyclopentadienyliron **derivatives**. *J. Chem. Soc. Perkin 1*, 2075–2078.

**Khennoufa, L., Bechki, L., Lanez, T., Lanez, E., & Zegheb, N. (2021).** Spectrophotometric, voltammetric and **molecular docking** studies of binding interaction of N-**ferrocenyl**methylnitroanilines with bovine serum albumin. *J. Mol. Struct.*, 1224, 129052. https://doi.org/10.1016/j.molstruc.2020.129052

**Kim, Y. M., Bio, S. H., Park, J. Y., Kim, J. Y., Rhee, H. I., & Lee, H. S. (2005).** Biological screening of $\alpha$-glucosidase with $\alpha$-amylase inhibitors from natural materials. *Bioscience, Biotechnology, and Biochemistry*, *69*(8), 1610–1614. https://doi.org/10.1271/bbb.69.1610

**Khelef, A., & Lanez, T. (2015).** In vitro assays of the antioxidant activities of **ferrocene derivatives** bearing amine, amide or hydrazine groups. 7, 318–323.

**Kumari, R., Kumar, R., & Lynn, A. (2014).** G-mmpbsa -A GROMACS tool for high-throughput MM-PBSA calculations. *J. Chem. Inf. Model.*, 54, 1951–1962. https://doi.org/10.1021/ci500020m

**Lanez, E., Bechki, L., & Lanez, T. (2019/2020).** Antioxidant Activities, Binding Parameters, and Electrochemical Behavior of Superoxide Anion Radicals Towards 1-Ferrocenylmethylthymine and 1-Ferrocenylmethylcytosine. *Curr. Phys. Chem.*, 10, 10–22. https://doi.org/10.2174/1877946809666190424143752

## Bibliographic Referances


**Lanez, E., Bechki, L., & Lanez, T. (2020).** Ferrocenylmethylnucleobases: **synthesis**, dft calculations, electrochemical and spectroscopic characterisation. *Chemistry and Chemical Technology*, 14, 146–153. https://doi.org/10.23939/chcht14.02.146

**Lanez, E., Bechki, L., & Lanez, T. (2019).** N6, 9-bis **(ferrocenylmethyl)** adenine: synthesis, cyclic voltammetric, spectroscopic characterization, and **DFT** calculations. *Scientific Study & Research. Chemistry & Chemical Engineering, Biotechnology, Food Industry*, 20, 509–519.

**Lanez, E., Bekkar, Y., Bourougaa, L., Benamor, M. L., Bouraoui, R., Boudebia, O., Adaika, A., Nesba, K., Chaoua, H., & Bechki, L. (2025).** Antidiabetic potential of mentha piperita essential oil: GC-MS profiling, in vitro, in vivo and in silico analyses. *J. Mol. Struct.*, 144239.

**Lanez, E., Benkhelifa, D., Cheriet, F. Z., Gori, K., Slimani, C., Kebache, S., Ouakouak, R., Abdellaoui, O., Djoughi, Y., & Benamor, M. L. (2025).** Theoretical Investigation of Mitomycin Derivatives as Dual Inhibitors of HER2 and ER-α: Prospects for Novel Breast Cancer Treatment Strategies. *Algerian Journal of Biosciences*, 6, 1–20.

**Lanez, E., Saidi, M., & Lanez, T. (2023).** Assessment of antioxidant and DPPH free radical scavenging activity of 1,2-dithiole-3-thione **derivatives** by using **cyclic voltammetry**, spectroscopic, and **molecular docking** studies. *Journal of Sulfur Chemistry*, 44, 542–558. https://doi.org/10.1080/17415993.2023.2200142

**Lanez, E., Zegheb, N., & Lanez, T. (2023).** In silico ADME, toxicological analysis, **molecular docking** studies and Molecular dynamics simulation of Afzelin with potential antibacterial effects against Staphylococcus aureus. *Turkish Computational and Theoretical Chemistry*, 7, 10–16. https://doi.org/10.33435/TCANDTC.1196422

**Lanez, E., Zerrouk, L., Bechki, L., Lanez, T., Adaika, A., Zegheb, N., & Nesba, K. (n.d.). synthesis**, **molecular docking**, drug-likeness analysis, and **ADMET** prediction of nickel and zinc tetraphenyl-porphyrin **complexes** as possible antioxidant agents. *Journal of the Chinese Chemical Society*.

## Bibliographic Referances


**Lanez, T., Benaicha, H., Lanez, E., & Saidi, M. (2018).** Electrochemical, spectroscopic and **molecular docking** studies of 4-methyl-5-**((phenylimino)**methyl)-3H- and 5-**(4-fluorophenyl)**-3H-1,2-dithiole-3-thione interacting with DNA. *Journal of Sulfur Chemistry*, 39, 76–88. https://doi.org/10.1080/17415993.2017.1391811

**Lanez, T., Feizi-Dehnayebi, M., & Lanez, E. (2024).** Assessment of the electrostatic binding of **ferrocenyl**methyl-nitroaniline **derivatives** to DNA: A combined experimental and theoretical study. *J. Mol. Struct.*, 138386.

**Lanez, T., & Hemmami, H. (2016).** Antioxidant Activities of N-**ferrocenyl**methyl-2- and -3-nitroaniline and Determination of their Binding Parameters with Superoxide Anion Radicals. *Curr. Pharm. Anal.*, 13, 110–116. https://doi.org/10.2174/1573412912666160831145524

**Lanez, T., Henni, M., & Hemmami, H. (2015).** Development of cyclic voltammetric method for the study of the interaction of antioxidant standards with superoxide anion radicals case of α-tocopherol. *Scientific Study and Research: Chemistry and Chemical Engineering, Biotechnology, Food Industry*, 16, 161–168.

**Lanez, T., & Henni, M. (2025).** Dual Anti-Inflammatory and Antidiabetic Potential of Ferrocenylmethylcyanophenyl Derivatives: Integrated In Vitro and In Silico Evaluation. *J. Organomet. Chem.*, 123956.

**Lanez, T., Lanez, M., Lanez, R., Lanez, E., & Talbi-Lanez, B. (2024).** Computational Screening of Novel Nitroimidazole Candidates: Targeting Key Enzymes of Oral Anaerobes for Anti-Parasitic Potential. *Curr. Drug Discov. Technol.*

**Laraoui, H., Lanez, E., Zegheb, N., Adaika, A., Lanez, T., & Benkhaled, M. (2023).** Anti-Diabetic Activity of Flavonol Glucosides From Fumana montana Pomel: In vitro Analysis, In Silico Docking, **ADMET** Prediction, and Molecular Dynamics Simulations. *ChemistrySelect*, 8, e202204512. https://doi.org/10.1002/slct.202204512

**Lu, T., & Chen, F. (2012).** Multiwfn: A multifunctional wavefunction analyzer. *J. Comput. Chem.*, 33, 580–592.

## Bibliographic Referances

**McDougall, G. J., Shpiro, F., Dobson, P., Smith, P., Blake, A., & Stewart, D. (2005).** Different polyphenolic components of soft fruits inhibit alpha-amylase and alpha-glucosidase. *Journal of Agricultural and Food Chemistry*, *53*(7), 2760–2766. https://doi.org/10.1021/jf0489926

**Meraghni, M., Lanez, T., Lanez, E., Bechki, L., & Kennoufa, A. (2023).** Experimental and theoretical study on corrosion inhibition of mild steel by meso-tetraphenyl-porphyrin **derivatives** in acid solution. *Journal of Electrochemical Science and Engineering*, 13, 217–229. https://doi.org/10.5599/jese.1400

**Mizushima, Y., & Kobayashi, M. (1968).** Interaction of anti-inflammatory drugs with serum proteins, especially with serum albumin. *Journal of Pharmacy and Pharmacology*, *20*(3), 169–173. https://doi.org/10.1111/j.2042-7158.1968.tb09718.x

**Mouada, H., Lanez, T., & Lanez, E. (2019).** Investigations of the binding parameters of the interaction of N'-**ferrocenyl**methyl-N'-phenylaceto-and propionohydrazide with DNA. *Journal of Fundamental and Applied Sciences*, 11, 875–882.

**Mouada, H., Lanez, T., & Zafar, I. (2024).** ROS scavenging, DNA binding and NADPH oxidase inhibition potential of N'-Ferrocenylmethyl-N'-phenylpropionohydrazide using **cyclic voltammetry** and **molecular docking**. *J. Organomet. Chem.*, 1007, 123026.

**Nacer, S. N., & Lanez, T. (2013).** Electrochemical properties of N'-**ferrocenyl**methyl-N'-phenylbenzohydrazide in aqueous and organic mediums. *International Letters of Chemistry, Physics and Astronomy*, 5, 76–85.

**Nadjiba, Z., Chérifa, B., Lanez, T., & Lanez, E. (2018).** In Silico Study on N-**ferrocenyl**methyl-N-phenylpropionohydrazide and N-**ferrocenyl**methyl-N-phenylbenzohydrazide as anticancer drugs for breast and prostate cancer. *International Journal of Pharmacology, Phytochemistry and Ethnomedicine*, 11, 17–25.

**Ouennoughi, Y., Karce, H. E., Aggoun, D., Lanez, T., Ruiz-Rosas, R., Bouzerafa, B., Ourari, A., & Morallon, E. (2017).** A novel ferrocenic copper **(II)** complex Salen-like, derived from 5-chloromethyl-2-hydroxyacetophenone and N-ferrocenmethylaniline: Design, spectral

approach and solvent effect towards electrochemical behavior of Fc+/Fc **redox** couple. *J. Organomet. Chem.*, 848, 344–351.

**Papada, E., Amerikanou, C., & Colone, M. (2023).** *Plant-Derived Natural Products and Their Biomedical Properties*. **MD**PI-Multidisciplinary Digital Publishing Institute.

**Patra, M., & Gasser, G. (2017).** The medicinal chemistry of **ferrocene** and its **derivatives**. *Nature Reviews Chemistry*, 1, 0066.

**Piñeiro, M., Manrique, S., J. Gómez, J. M., Rodriguez, P., Barrera, D., Caballero, M. A., Sosa, G., Vargas-Arana, A., Tapia, B., & Lima, B. (2025).** Biological activities of Usnea lethariiformis lichen extracts and UHPLC-ESI-QTOF-MS analysis of their secondary metabolites. *Front. Pharmacol.*, 15, 1508835.

**Puspadewi, R., Milanda, T., Muhaimin, M., & Chaerunisaa, A. Y. (2025).** Nanoparticle-Encapsulated Plant Polyphenols and Flavonoids as an Enhanced Delivery System for Anti-Acne Therapy. *Pharmaceuticals*, 18, 209.

**Rebiai, A., Lanez, T., & Belfar, M. L. (2014).** Total polyphenol contents, radical scavenging and **cyclic voltammetry** of Algerian propolis. *Int. J. Pharm. Pharm. Sci.*, 6, 395–400.

**Rose, P. W., Prlić, A., Altunkaya, A., Bi, C., Bradley, R. R., Christie, C. H., Di Costanzo, L., Duarte, J. M., Dutta, S., Feng, Z., Green, R. K., Goodsell, D. S., Hudson, B., Kalro, T., Lowe, R., Peisach, E., Randle, C., Rose, A. S., Shao, C., Tao, Y. P., Valasatava, M., Voigt, M., Westbrook, J. D., Woo, J., Yang, H., Young, J. Y., Zardecki, C., Berman, H. M., & Burley, S. K. (2017).** The RCSB protein data bank: Integrative view of protein, gene and 3D structural information. *Nucleic Acids Res.*, 45, D271–D281.

**Sabiha, M., Yanisse, S., Boudalia, M., Najem, A., Benhiba, F., Belfhaili, A., & Bouatia, M. (2023).** Promising Antioxidant, antibacterial and anticorrosive properties of an essential oil extract of Origanum majorana L. from Morocco. *Biointerface Res. Appl. Chem.*, 13, 1–27.

**Saleem, M., et al. (2021).** Ferrocene-based compounds as enzyme inhibitors and therapeutic agents. *European Journal of Medicinal Chemistry*, 211, 113054.

## Bibliographic Referances

**Sargsyan, T., Simonyan, H. M., Stepanyan, L., Tsaturyan, A., Vicidomini, C., Pastore, R., Guerra, G., & Roviello, G. N. (2025).** Neuroprotective Properties of Clove **(Syzygium aromaticum)**: State of the Art and Future Pharmaceutical Applications for Alzheimer's Disease. *Biomolecules*, 15, 452.

**Sharifi-Rad, M., Anil Kumar, N. V., Zucca, P., Varoni, E. M., Dini, L., Panzarini, E., Rajkovic, J., Tsouh Fokou, P. V., Azzini, E., & Peluso, I. (2020).** Lifestyle, oxidative stress, and antioxidants: back and forth in the pathophysiology of chronic diseases. *Front. Physiol.*, 11, 552535.

**Siles-Sánchez, M. de las N., Navarro del Hierro, J., Martín, D., Jaime, L., & Santoyo, S. (2024).** Supercritical antisolvent precipitation as a green technology to fractionate an Origanum majorana extract: Relationship between fractions cellular antioxidant activity and phytochemical composition. *Food Biosci.*, 59, 104103. https://doi.org/10.1016/j.fbio.2024.104103

**Singirala, K. S., Dubey, P. K., & Roy, S. (2025).** Extraction of Bioactive Compounds From Withania somnifera: The Biological Activities and Potential Application in the Food Industry: A Review. *Int. J. Food Sci.*, 2025, 9922626.

**Steffen, C., Thomas, K., Huniar, U., Hellweg, A., Rubner, O., & Schroer, A. (2010).** AutoDock4 and AutoDockTools4: Automated Docking with Selective Receptor Flexibility. *J. Comput. Chem.*, 31, 2967–2970.

**Stoyanova, M., Milusheva, M., Gledacheva, V., Todorova, M., Kircheva, N., Angelova, S., Stefanova, I., Pencheva, M., Vasileva, B., & Hristova-Panusheva, K. (2025).** Silver Nanoparticles with Mebeverine in IBS Treatment: **DFT** Analysis, Spasmolytic, and Anti-Inflammatory Effects. *Pharmaceutics*, 17, 561.

**Stepnicka , P. (Ed.). (2008).** *Ferrocenes: ligands, materials and biomolecules*. John Wiley & Sons. https://doi.org/10.1002/9780470511541

## Bibliographic Referances


**Tlili, M. L., Alia, F., Bahri, E., Beyat, T., Redouan, K., & Lanez, E. (2025).** In vivo evaluations of the **antidiabetic** and antioxidant effects of Olea europaea L. **(Chemlali variety)** leaves. *Acta Periodica Technologica*, 3.

**Tlili, M. L., Laib, I., Salemi, K., Chetehouna, I., BenMoussa, I., & Lanez, E. (2024).** Phytochemical Analysis and Evaluation of the Antioxidant, Anti-Inflammatory, Hemolytic, and Antibacterial Effects of Astragalus gombo **(L.)** Leaves. *Acta Chim. Slov.*, 71.

**Togni, A., & Hayashi, T. (1995).** *Ferrocenes: **Homo**geneous Catalysis, Organic **synthesis**, Materials Science*. Wiley-VCH.

**Togni, A. (1995).** Ferrocene chemistry: An overview. *Angewandte Chemie International Edition in English*, *34*(8), 890–893. https://doi.org/10.1002/anie.199508901

**Trott, O., & Olson, A. J. (2010).** AutoDock Vina: Improving the speed and accuracy of **docking**. *Journal of Computational Chemistry*, 31**(2)**, 455–461.

**Vanommeslaeghe, K., & MacKerell, A. D. (2012).** Automation of the CHARMM general force field **(CGenFF)** I: Bond perception and atom typing. *J. Chem. Inf. Model.*, 52, 3144–3154. https://doi.org/10.1021/ci300363c

**Vessières, A., Top, S., Beck, W., Hillard, E., & Jaouen, G. (2006).** Metal **complexes** in cancer therapy. *Dalton Transactions*, 529–541.

**Xiong, G., Wu, Z., Yi, J., Fu, L., Yang, Z., Hsieh, C., Yin, M., Zeng, X., Wu, C., & Lu, A. (2021). ADMET**lab 2.0: an integrated online platform for accurate and comprehensive predictions of **ADMET** properties. *Nucleic Acids Res.*, 49, W5–W14.

**Yahiaoui, A., Benyza, N., Messai, A., Lanez, T., & Lanez, E. (2023).** Voltammetric and **molecular docking** investigations of **ferrocenyl**methylaniline and its N-acetylated derivative interacting with DNA. *Journal of Electrochemical Science and Engineering*. https://doi.org/10.5599/jese.2061

## Bibliographic Referances

**Zaiz, T., & Lanez, T. (2015).** Corrosion inhibition of carbon steel XC70 in H2SO4 solution by **ferrocene** derivative 3-**(ferrocenylmethylamine)**benzonitrile. *Journal of Fundamental and Applied Sciences*, 4, 182. https://doi.org/10.4314/jfas.v4i2.8

**Zegheb, N., Boubekri, C., Lanez, T., Lanez, E., Küçükkılınç, T. T., Öz, E., Khennoufa, A., Khamouli, S., & Belaidi, S. (2021).** In Vitro and In Silico Determination of Some N-**ferrocenyl**methylaniline Derivatives as Anti-Proliferative Agents Against MCF-7 Human Breast Cancer Cell Lines. *Anticancer Agents Med. Chem.*, 22, 1426–1437. https://doi.org/10.2174/1871520621666210624141712

**Zerrouk, L., Bechki, L., Lanez, E., & Lanez, T. (2024). synthesis**, characterization, **cyclic voltammetry**, and **molecular docking** studies of the antioxidant activities of superoxide anion radicals towards meso-tetramethophenyl-porphyrin and meso-tetrabiphenyl-porphyrin. *Not. Sci. Biol.*, 16, 11823. https://doi.org/10.55779/nsb16211823

**Zouaghi, N., Lanez, E., Benamor, M. L., Nacer, S. N., Lanez, T., Bekkar, Y., Haddad, H., Al-Abdallat, K., Zihlif, M., & Al-Abdallat, Y. (2025).** Targeting Alzheimer's Disease via Phytochemicals from Artemisia campestris L.: GC/MS Analysis with an Integrated Computational Approach. *Food Biosci.*, 108128.

**Zubair, S., Badshah, A., Patujo, J., Khan, M., Raheel, A., & Shah, A. (2023).** New **ferrocene** integrated amphiphilic guanidines: **synthesis**, spectroscopic elucidation, **DFT** calculation and in vitro α-**amylase** and α-glucosidase inhibition combined with **molecular docking** studies. *Heliyon*, 9**(5)**, e16130.